SPECTROSCOPIC AND MAGNETIC STUDIES OF SOME OCTAHEDRAL AND SQUARE PLANAR FERROUS COMPLEXES

By

TSANG BIK TSIN

B.Sc., University of Hong Kong, 1970

A THESIS SUBMITTED IN PARTIAL FULFILMENT OF
THE REQUIREMENTS FOR THE DEGREE OF
DOCTOR OF PHILOSOPHY

in the Department
of
CHEMISTRY

We accept this thesis as conforming to the
required standard

THE UNIVERSITY OF BRITISH COLUMBIA

February, 1975

In presenting this thesis in partial fulfilment of the requirements for an advanced degree at the University of British Columbia, I agree that the Library shall make it freely available for reference and study. I further agree that permission for extensive copying of this thesis for scholarly purposes may be granted by the Head of my Department or by his representatives. It is understood that copying or publication of this thesis for financial gain shall not be allowed without my written permission.

Department of CHEMISTRY

The University of British Columbia
Vancouver 8, Canada

Date March 18, 1975

ABSTRACT

Three series of ferrous complexes have been prepared, and characterized with the aid of ^{57}Fe Mössbauer spectroscopy, magnetic susceptibility and electrical conductivity measurements, and various other spectroscopic techniques where appropriate.

The first series consists of four high-spin octahedral solvates of ferrous perchlorate, namely $Fe[(CH_3)_2SO]_6(ClO_4)_2$, $Fe[(C_6H_5)_2SO]_6(ClO_4)_2$, $Fe[(CH_2)_4SO]_6(ClO_4)_2$ and $Fe(C_5H_5NO)_6(ClO_4)_2$. Magnetic susceptibilities have been measured over the temperature range 80-320° K, and Mössbauer spectra over the range 4.2-330° K. Signs of the quadrupole coupling constants e^2qQ and values of the asymmetry parameters η were obtained from magnetic perturbation Mössbauer spectra. Analysis of the e^2qQ vs T data in terms of crystal field theory yields values for the axial and rhombic field splittings, and spin-orbit and spin-spin coupling constants. The values found are consistent with the susceptibility data. The $(CH_3)_2SO$ and $(C_6H_5)_2SO$ complexes are tetragonally distorted, with singlet $|xy\rangle$ ground states, while the other two are trigonally distorted, with ground states which are orbital doublets. The C_5H_5NO derivative shows slow spin-lattice relaxation below $\sim$ 30° K, and is the first example of such behaviour for an octahedrally coordinated Fe^{2+} ion. The Mössbauer spectrum of this complex at 4.2° K in a 10 kG applied field is treated in the spin Hamiltonian approximation and confirms slow relaxation.

Eleven new complexes of the chelating ligand 2-(2'-pyridyl)benzimidazole (pyben) have been synthesized. These are $Fe(pyben)_2(NCS)_2$ and $Fe(pyben)_3A_2 \cdot xH_2O$, where A = ClO_4^-, NO_3^-, NCS^-, Br^-, I^-, BF_4^-, $B(C_6H_5)_4^-$, $[Cr(NH_3)_2(NCS)_4]^-$ and x = 0, 1, 2 (but not all combinations). These compounds have been characterized by Mössbauer spectra (4.2-300° K), susceptibility measurements (80-320° K), solid state visible spectra (80-300° K), and conductance measurements (295° K). Most of the complexes are shown to exhibit $^5T_2$-$^1A_1$ spin crossover, the details of which are sensitive both to the nature of the anion and to the number of waters of crystallization. The latter effect is explained in terms of hydrogen bonding between water molecules and the imino hydrogen on the pyben ligand. From magnetic perturbation Mössbauer spectra it is deduced that the $Fe(pyben)_3^{2+}$ cation has a mer-octahedral structure in both spin states, indicating substantial inequivalence of the pyridine and imidazole nitrogens in pyben.

The final section of the thesis describes the synthesis and properties of two new ferrous porphyrins, Fe(OEP) and Fe(OTBP) (H_2OEP = octaethylporphyrin, H_2OTBP = octamethyltetrabenzporphyrin), and several of their adducts with amine bases and in one case tetrahydrofuran (THF). The complexes have been studied using Mössbauer, n.m.r., electronic and mass spectroscopic techniques as well as magnetic measurements. The square planar Fe(OEP) and Fe(OTBP) are high-spin compounds. Mössbauer parameters of these and related complexes are sensitive to the nature of the peripheral groups on the porphyrin, and can be correlated with changes in σ and π bonding properties of the ligands. Except for $Fe(OTBP)(THF)_2$, which has a $^5B_{2g}$ ground state, all other adducts obtained are diamagnetic. For Fe(OEP) at 4.2° K in applied

magnetic fields, the spin relaxation rate appears to be comparable to the Larmor precession frequency of the ^{57}Fe nucleus, whereas Fe(OTBP) is a fast-relaxing paramagnet under similar conditions. An apparently polymeric species $[Fe(OTBP)]_n$ can be obtained and is an electrical semiconductor. It is suggested that the polymeric structure involves Fe-Fe σ bonds.

ACKNOWLEDGEMENTS

I am extremely grateful to Dr. J.R. Sams for his invaluable guidance and help during the course of this investigation.

I would like to thank Dr. D. Dolphin for the octaethylporphyrin compound, Dr. J.B. Farmer for the use of the atomic absorption spectrophotometer, Dr. G.B. Porter for the use of the low temperature visible spectral cell, Dr. R.C. Thompson for the use of the Guoy balance and the A.C. conductance bridge.

I would like to thank Mr. Mark Vagg for all the modification work done on the magnetic perturbation Mössbauer apparatus.

I would also like to thank Mrs. Lia Sallos for processing most of the Mössbauer spectra, and Miss Jacqueline Garnett for the typing of this thesis.

Financial support from the National Research Council in the form of a postgraduate scholarship was greatly appreciated.

TABLE OF CONTENTS

LIST OF TABLES

LIST OF FIGURES

INTRODUCTION

This thesis is concerned with the preparation and characterization of three series of ferrous complexes. The principal techniques used for studying these complexes have been Mössbauer spectroscopy and magnetic susceptibility measurements, although extensive use has also been made of infrared and electronic spectra of the complexes, and in some cases of electrical conductance measurements and nuclear magnetic resonance spectra.

From the Mössbauer spectra one can obtain two chemically important parameters, namely the isomer shift and quadrupole splitting. (A more complete discussion is given in Chapter I). The former is related to the total s electron density at the nucleus, and is very useful for differentiating high-spin ($t_{2g}^4 e_g^2$) and low-spin ($t_{2g}^6 e_g^0$) ferrous complexes. High-spin Fe^{2+} systems typically have isomer shift values of about 1.5 mm s^{-1} (with respect to sodium nitroprusside)[1], while for low-spin Fe^{II}, isomer shifts are characteristically about 0.6 mm s^{-1}. Since one can usually measure this parameter with an accuracy of $\pm$ 0.02 mm s^{-1} or better, these two spin states are readily distinguishable.

The quadrupole splitting is related to the electric field gradient (efg) at the nucleus, established when the distribution of the surrounding electrons has lower than cubic symmetry. For low-spin ferrous compounds, quadrupole splittings are usually small and nearly independent of temperature. High-spin ferrous complexes on the other hand, tend to show splittings which are much larger in magnitude and

strongly temperature dependent.[1] In the latter case, detailed measurements of the quadrupole splitting over a wide range of temperatures (e.g., 4.2 - 300°K) enable one to estimate crystal field splitting parameters[2] as well as spin-orbit and spin-spin coupling constants.

The recently established technique of magnetic perturbation Mössbauer spectroscopy[3], in which the sample is subjected to a fairly large applied magnetic field, provides two further pieces of information about the efg. As discussed below, the efg is a 3 x 3 tensor which is symmetric and traceless, and which can be diagonalized by a proper choice of axes. The diagonal elements in the principal axis system are chosen such that $|V_{zz}| \geq |V_{yy}| \geq |V_{xx}|$, and the two independent parameters are taken to be V_{zz} and the asymmetry parameter $\eta = (V_{xx}-V_{yy})/V_{zz}$. A magnetically perturbed Mössbauer spectrum enables one to determine both the sign of V_{zz} and magnitude of $\eta(0\leq\eta\leq 1)$.[3] The former is determined by the shape of the charge distribution about the nucleus. A positive V_{zz} corresponds to an oblate charge distribution, and a negative V_{zz} to a prolate distribution. Moreover, if the asymmetry parameter is zero, then the efg is axially symmetric, i.e., $V_{xx} = V_{yy} = -\frac{1}{2}V_{zz}$, whereas a non-zero η indicates that all three principal axis directions are inequivalent.

In the first two chapters we discuss in detail the chemical information that can be obtained via Mössbauer spectroscopy, and describe the apparatus and experimental procedures employed in this study. In the final three chapters results of the spectroscopic and magnetic measurements on the three types of complexes studied are presented and discussed.

The first series of complexes, described in Chapter III, was first prepared by Reedijk and van der Kraan.[4] This consists of four high-spin complexes formed from ferrous perchlorate and the oxygen-donor Lewis bases dimethyl sulphoxide, diphenyl sulphoxide, tetramethylene sulphoxide, and pyridine-N-oxide. Mössbauer and magnetic susceptibility data obtained over a wide range of temperature are used to estimate the ground state splitting parameters for these compounds. At low temperatures, one of the complexes shows unusual behaviour, which can be attributed to slow spin-lattice relaxation.

Chapter IV describes a series of eleven new complexes. Ten of these can be written in the form $Fe(pyben)_3A_2 \cdot xH_2O$, where pyben is the bidentate chelating ligand 2-(2´-pyridyl)benzimidazole, A = ClO_4^-, NO_3^-, NCS^-, Br^-, I^-, BF_4^-, $B(C_6H_5)_4^-$, $[Cr(NH_3)_2(NCS)_4]^-$, and x=0, 1 or 2. The remaining compound is $Fe(pyben)_2(NCS)_2$. The tris(pyben) derivatives all exhibit high-spin - low-spin crossover behaviour, which is traced with the aid of Mössbauer spectroscopy and other physical techniques. The bonding and structure of the $Fe(pyben)_3^{2+}$ system in both high-spin and low-spin states is also discussed.

The final series of compounds, described in Chapter V, consists of two square planar ferrous porphyrins and some of their adducts with Lewis bases. The two porphyrins are octamethyltetrabenzporphyrin (OTBP) and octaethylporphyrin (OEP). The complexes in this series which have been prepared and characterized are: Fe(OTBP), $Fe(OTBP)(py)_2$, $Fe(OTBP)(THF)_2$, $Fe(OTBP)(3\text{-pic})_2$, $Fe(OTBP)(py)_4$, $Fe(OTBP)(4\text{-pic})_4$, $Fe(OTBP)(IQ)_4$, Fe(OEP) and $Fe(OEP)(py)_2$, where py = pyridine, THF = tetrahydrofuran, 3-pic = 3-picoline, 4-pic = 4-picoline, and IQ = isoquinoline.

CHAPTER I

THE MÖSSBAUER EFFECT

The Mössbauer effect, or nuclear gamma resonance, arises from the recoil-free emission and absorption of γ-rays by suitable nuclei. There are many isotopes for which the effect has been observed, but only a limited number of these have suitable nuclear parameters for the effect to be of practical interest. The most commonly studied of the Mössbauer nuclei are ^{57}Fe and ^{119}Sn. Since the work within this thesis is concerned entirely with iron systems, the Mössbauer process is illustrated here only for ^{57}Fe.

In the basic Mössbauer experiment, the energy of the γ-rays emitted by a radioactive source is modulated by applying a Doppler velocity to the source, and those γ-rays having the correct energies can be resonantly absorbed by absorber nuclei. The spectrum consists of a plot of the number of transmitted photons versus the photon energy (or Doppler velocity), and one or more peaks are observed where resonance occurs.

From a Mössbauer spectrum, two parameters can be obtained which are of special interest to chemists. These are the isomer shift (δ) and the quadrupole splitting (ΔE_Q). The former is related to the effective s electron density at the nucleus and the latter to the point group symmetry of the electronic environment around the nucleus arising from bonding or ionic effects. A typical spectrum for iron is shown in Figure I. The isomer shift denotes the position of the centroid of the

FIGURE I

A Typical ^{57}Fe Mössbauer Spectrum in the Absence of a Magnetic Field

FIGURE 1

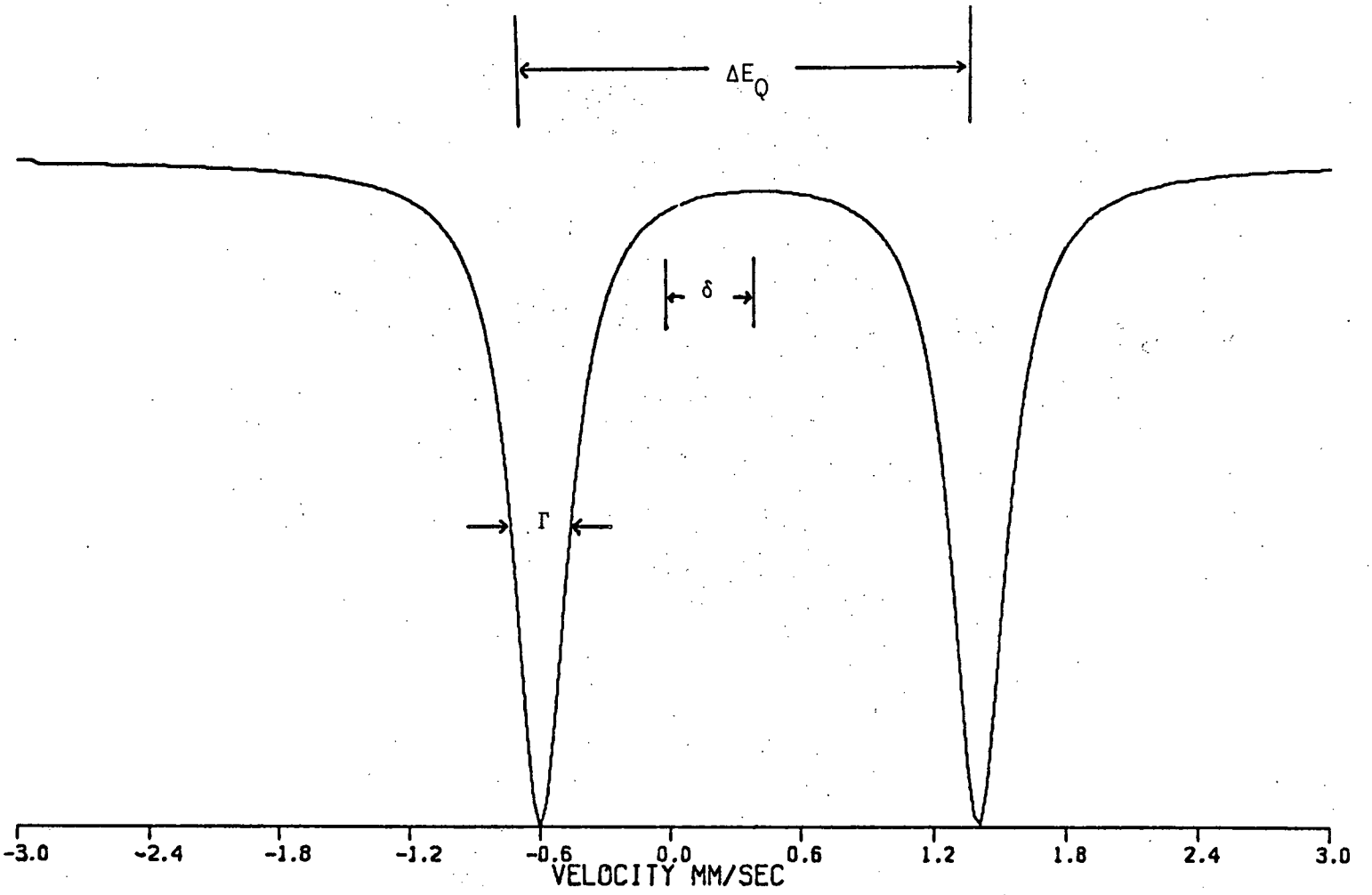

spectrum with respect to a standard absorber, and the quadrupole splitting is the magnitude of the separation of the two lines.

In order to understand the mechanisms by which the electronic environment affects the nucleus, it is profitable to look at the interactions which are responsible for the isomer shift and quadrupole splitting in a semi-classical picture.[5,6]

From classical electrostatics, a charge aggregate like the nucleus interacts with the electric potential field set up by electrons around it according to Coulomb's law.

$$\text{Energy} = H = \int_{\substack{\text{nuclear} \\ \text{volume}}} \rho(x,y,z)V(x,y,z)dv \qquad (1)$$

where $\rho(x,y,z)$ is the charge density function describing the nucleus, $V(x,y,z)$ the potential field set up by the surrounding electrons, and dv the differential volume element.

By the Taylor expansion of $V(x,y,z)$ around the nuclear centre of mass,

$$V(x,y,z) = V(0,0,0) + \sum_{\alpha=1}^{3} \left(\frac{\partial V}{\partial x_\alpha}\right)_o x_\alpha + \tfrac{1}{2} \sum_{\alpha,\beta=1}^{3} \left(\frac{\partial^2 V}{\partial x_\alpha \partial x_\beta}\right)_o x_\alpha x_\beta$$

$$+ \text{higher terms} \qquad (2)$$

Letting

$$V_\alpha = \left(\frac{\partial V}{\partial x_\alpha}\right)_o \qquad V_{\alpha\beta} = \left(\frac{\partial V}{\partial x_\alpha \partial x_\beta}\right)_o \qquad (3)$$

and substituting eqn.(2) into eqn.(1) we obtain

$$H = V(0,0,0)\int\rho(x,y,z)dv + \sum_{\alpha=1}^{3} V_\alpha\int\rho(x,y,z)x_\alpha dv$$

$$+ \tfrac{1}{2}\sum_{\alpha,\beta=1}^{3} V_{\alpha\beta}\int\rho(x,y,z)x_\alpha x_\beta dv + \text{higher terms} \qquad (4)$$

The first integral can be evaluated as

$$\int\rho(x,y,z)dv = Ze$$

where Ze is the total nuclear charge. The next three terms describe the interaction of the nuclear dipole with the electric field having components $V_\alpha(\alpha=1, 2, 3)$, and can be shown to vanish.[5] The next nine terms describe the interaction of the nuclear quadrupole moment $Q'_{\alpha\beta}$ with the electric field gradient (efg) tensor $V_{\alpha\beta}$, where

$$Q'_{\alpha\beta} = \int\rho(x,y,z)x_\alpha x_\beta dv \qquad (5)$$

With these substitutions, equation (4) becomes

$$H = V(0,0,0)\,Ze + \tfrac{1}{2}\sum_{\alpha,\beta=1}^{3} V_{\alpha\beta}\,Q'_{\alpha\beta} + \text{higher terms.} \qquad (6)$$

The leading term represents the electrostatic energy of a point nucleus, and is independent of whether the nucleus is in its excited state or

ground state. Since the Mössbauer transition measures energy differences between excited and ground nuclear states, this term can be neglected when considering the Mössbauer process. The higher order terms describe octapole, hexadecapole, etc. interactions, which can be shown to be negligible compared to the quadrupole interaction.[5]

With these simplifications, the only terms of interest are the quadrupolar terms $\frac{1}{2}\sum_{\alpha,\beta=1}^{3} V_{\alpha\beta}\, Q'_{\alpha\beta}$. Since $Q'_{\alpha\beta}$ is symmetric, it is expedient to define a new tensor that is both symmetric and traceless by[5]

$$Q_{\alpha\beta} = 3Q'_{\alpha\beta} - \delta_{\alpha\beta} \sum_{e=1}^{3} Q'_{ee} \tag{7}$$

where $\delta_{\alpha\beta} = 1$ if $\alpha = \beta$

$\delta_{\alpha\beta} = 0$ if $\alpha \neq \beta$

whence

$$H = \frac{1}{6}\sum_{\alpha,\beta=1}^{3} V_{\alpha\beta}\, Q_{\alpha\beta} + \frac{1}{6}\left(\sum_{e=1}^{3} Q'_{ee}\right)\left(\sum_{j=1}^{3} V_{jj}\right) \tag{8}$$

The first nine terms are responsible for the quadrupole splitting while the second group of terms is responsible for the isomer shift and will be discussed first.

Isomer Shift

By definition,

$$\sum_{e=1}^{3} Q'_{ee} = \int \rho(x,y,z) r^2 dv \tag{9}$$

where $r^2 = x^2 + y^2 + z^2$, and from electrostatics

$$\sum_{j=1}^{3} V_{jj} = -4\pi\sigma \tag{10}$$

where σ is the electronic charge density at the nuclear centre of mass. Since only s electrons have a finite charge density at that point[6]

$$\sum_{j=1}^{3} V_{jj} = 4\pi e |\psi(o)|^2 \tag{11}$$

where $\psi(o)$ is the value of the wavefunction of s electrons at that point. Hence,

$$H_{I.S.} = \frac{1}{6}\left(\sum_{e=1}^{3} Q'_{ee}\right)\left(\sum_{j=1}^{3} V_{jj}\right) = \frac{2}{3}\pi e|\psi(o)|^2 \int \rho(x,y,z) r^2 dv \tag{12}$$

For a source nucleus in the presence of s electrons both the ground state and excited state energies (E_e and E_g) will be shifted upward by the term $H_{I.S.}$. Thus the energy of the γ photon will be given by

$$\varepsilon_{\gamma_s} = (E_e + H^{EXCITED}_{I.S.}) - (E_g + H^{GROUND}_{I.S.})$$

$$= \varepsilon_o + (\tfrac{2}{3}\pi e^2 Z)|\psi_s(o)|^2(\langle r^2\rangle_e - \langle r^2\rangle_g) \qquad (13)$$

where

$$\langle r^2\rangle = \frac{\int \rho(x,y,z) r^2 dv}{\int \rho(x,y,z) dv}$$

and $\varepsilon_o = E_e - E_g$. Similarly, for an absorber nucleus

$$\varepsilon_{\gamma_a} = \varepsilon_o + (\tfrac{2}{3}\pi e^2 Z)|\psi_a(o)|^2(\langle r^2\rangle_e - \langle r^2\rangle_g) \qquad (14)$$

The energy difference between source and absorber is the isomer shift:

$$\varepsilon_{\gamma_a} - \varepsilon_{\gamma_s} = \delta = \tfrac{2}{3}\pi\, e^2 Z[\langle r^2\rangle_e - \langle r^2\rangle_g][|\psi_a(o)|^2 - |\psi_s(o)|^2] \qquad (15)$$

According to this formula, it is observed that δ arises from two factors. The first is a nuclear factor, $\frac{2}{3}\pi\, e^2 Z[\langle r^2\rangle_e - \langle r^2\rangle_g]$, and is fixed for ^{57}Fe. The magnitude of this quantity is not accurately known, however, its sign follows from the sign of $[\langle r^2\rangle_e - \langle r^2\rangle_g]$, which is known to be negative for the 14.4 keV Mössbauer transition[1] in ^{57}Fe. The second factor arises from the s electron charge density at the nucleus. If in a series of experiments, $|\psi_s(o)|^2$ is kept constant (i.e. the same source is used for all experiments), or if a fixed

standard is used to calibrate the isomer shift, then δ will be proportional to the s electron density at the absorber nucleus. In the case of ^{57}Fe, since $[\langle r^2\rangle_e - \langle r^2\rangle_g]$ is negative, an increase in s electron density at the absorber nucleus leads to a decrease in isomer shift. It is well known that p and d electrons can exert screening effects on the s electrons, so that changes in p and d orbital occupancy will influence the isomer shift by altering the effective s electron density at the nucleus. This screening effect can best be illustrated in the case of high-spin iron compounds. $Fe^{3+}(d^5)$ salts have isomer shifts (relative to sodium nitroprusside) in the range 0.3 to 0.7 mm s^{-1}, while $Fe^{2+}(d^6)$ salts have isomer shifts in the range 1.4 to 1.7 mm s^{-1}. The presence of the extra d electron screens the s electron density at the nucleus and thus increases the isomer shift.

Quadrupole Splitting

The quantum mechanical equivalent $\mathcal{H}_{Q.S.}$ of the term

$$H_{Q.S.} = \frac{1}{6} \sum_{\alpha,\beta=1}^{3} Q_{\alpha\beta} V_{\alpha\beta} \tag{16}$$

can be constructed using the usual correspondence[7]

$$\hat{Q}_{\alpha\beta} = \int \rho(x,y,z) \, [3x_\alpha x_\beta - \delta_{\alpha\beta} r^2] dv$$

$$= \int \rho(x,y,z) \left\{ C\left[\frac{3}{2} (\hat{I}_\alpha \hat{I}_\beta + \hat{I}_\beta \hat{I}_\alpha) - \delta_{\alpha\beta} I(I+1)\right] \right\} dv \tag{17}$$

where $\hat{I}_\alpha$, $\hat{I}_\beta$ are nuclear spin angular momentum operators. C is a constant within an angular momentum manifold[7].

Thus

$$\mathcal{H}_{Q.S.} = \frac{1}{6} \sum_{\alpha,\beta=1}^{3} \left[\int \rho(x,y,z)(3x_\alpha x_\beta - \delta_{\alpha\beta} r^2)dv\right] V_{\alpha\beta}$$

$$= \frac{1}{6} \sum_{\alpha,\beta=1}^{3} \left(\int \rho(x,y,z)Cdv\right)\left[\frac{3}{2}(\hat{I}_\alpha \hat{I}_\beta + \hat{I}_\beta \hat{I}_\alpha) - \delta_{\alpha\beta} I(I+1)\right] V_{\alpha\beta}$$

$$= \frac{1}{6} \sum_{\alpha,\beta=1}^{3} C'\left[\frac{3}{2}(\hat{I}_\alpha \hat{I}_\beta + \hat{I}_\beta \hat{I}_\alpha) - \delta_{\alpha\beta} I(I+1)\right] V_{\alpha\beta} \qquad (18)$$

If an "electric quadrupole moment" Q is defined such that

$$eQ = \langle II|\hat{Q}_{zz}|II\rangle \qquad (19)$$

then

$$eQ = C'(\langle II|3\hat{I}_z^2 - I(I+1)|II\rangle)$$

$$= C'[3I^2 - I(I+1)] \qquad (20)$$

whence

$$C' = \frac{eQ}{I(2I-1)} \qquad (21)$$

and

$$\mathcal{H}_{Q.S.} = \frac{eQ}{6I(2I-1)} \sum_{\alpha,\beta=1}^{3} [\tfrac{3}{2}(\hat{I}_\alpha \hat{I}_\beta + \hat{I}_\beta \hat{I}_\alpha) - \delta_{\alpha\beta} I(I+1)] V_{\alpha\beta} \tag{22}$$

Using the notation[5]

$$I_\pm = I_x \pm iI_y$$

$$V_o = V_{zz}$$

$$V_{\pm 1} = V_{xz} \pm iV_{yz}$$

$$V_{\pm 1} = \tfrac{1}{2}(V_{xx} - V_{yy}) \pm iV_{xy} \tag{23}$$

and

$$B = \frac{eQ}{4I(2I-1)}$$

we have

$$\mathcal{H}_{QS.} = B[(3\hat{I}_z^2 - I(I+1)]\, V_o + (\hat{I}_+ \hat{I}_z + \hat{I}_z \hat{I}_+) V_{-1}$$

$$+ (\hat{I}_- \hat{I}_z + \hat{I}_z \hat{I}_-) V_1 + \hat{I}_+^2\, V_{-2} + \hat{I}_-^2\, V_2] \tag{24}$$

Since $V_{\alpha\beta}$ is symmetric and has vanishing trace, it is possible to choose a principal axis system whereby $V_{\alpha\beta} = 0$ for $\alpha \neq \beta$. Further, one can choose the axis system such that

$$|V_{zz}| \geq |V_{yy}| \geq |V_{xx}| \tag{25}$$

and eqn.(24) can be written as

$$\mathcal{H}_{Q.S.} = B\left\{[3\hat{I}_z^2 - I(I+1)]V_{zz} + \tfrac{1}{2}(\hat{I}_+^2 + \hat{I}_-^2)(V_{xx} - V_{yy})\right\}$$

$$= BV_{zz}\left\{[3\hat{I}_z^2 - I(I+1)] + \frac{\eta}{2}(\hat{I}_+^2 + \hat{I}_-^2)\right\} \qquad (26)$$

where $\eta = \dfrac{V_{xx} - V_{yy}}{V_{zz}}$ $\qquad (0 \leq \eta \leq 1)$

η is called the asymmetry parameter.

The above Hamiltonian is valid in general. In the ^{57}Fe case, the Mössbauer transition involves a nuclear spin $I = \frac{3}{2}$ excited state and $I = \frac{1}{2}$ ground state. Since nuclear states with $I < 1$ do not have a quadrupole moment, only the excited state is affected by this Hamiltonian. The eignvalue matrix can then be set up for the $I = \frac{3}{2}$ case [3]:

$$\left\langle \tfrac{3}{2}m \middle| \mathcal{H}_{Q.S.} \middle| \tfrac{3}{2}m' \right\rangle = \begin{array}{c} \\ \frac{3}{2} \\ \frac{1}{2} \\ -\frac{1}{2} \\ -\frac{3}{2} \end{array} \begin{array}{c} \begin{array}{cccc} \frac{3}{2} & \frac{1}{2} & -\frac{1}{2} & -\frac{3}{2} \end{array} \\ \begin{bmatrix} 3 & 0 & \sqrt{3}\,\eta & 0 \\ 0 & -3 & 0 & \sqrt{3}\,\eta \\ \sqrt{3}\,\eta & 0 & -3 & 0 \\ 0 & \sqrt{3}\,\eta & 0 & 3 \end{bmatrix} \end{array} (BV_{zz}) \qquad (27)$$

On diagonalizing this matrix a pair of doubly degenerate eigenfunctions is obtained with energies[3]

$$E = \pm \; 3 \; B \; V_{zz} \left[1 + \eta^2/_3\right]^{\frac{1}{2}} \tag{28}$$

The energy difference between these two levels is the quadrupole splitting:

$$\Delta E_Q = 6 \; B \; V_{zz}\left[1 + \eta^2/3\right]^{\frac{1}{2}}$$

$$= \tfrac{1}{2}e^2Qq\left[1 + \eta^2/3\right]^{\frac{1}{2}} \tag{29}$$

where $eq = V_{zz}$, the z component of efg.

Again, eqn.(28), like eqn.(15), contains two factors, one nuclear and the other electronic. The nuclear factor involves the quadrupole moment Q which is estimated for ^{57}Fe to be about 0.2 barn[8]. The electronic factor involves efg components that arise from electrons surrounding the nucleus.

For a pure quadrupole interaction the Mössbauer transition will give rise to a spectrum consisting of two lines separated by ΔE_Q. In the usual case of a randomly oriented polycrystalline absorber, the line intensities are equal, as shown in Figure 2(a). Under these conditions one cannot determine which of the two lines arises from the $|\pm\frac{1}{2}\rangle_g \rightarrow |\pm\frac{1}{2}\rangle_e$ nuclear spin transition and which from the $|\pm\frac{1}{2}\rangle_g \rightarrow |\pm\frac{3}{2}\rangle_e$ transition. (The relative energies of the excited

FIGURE 2

Approximate Energy Level Diagram for an ^{57}Fe Nucleus, Showing the Effects of an Axially Symmetric efg and an Applied Magnetic Field at an Angle θ to the z Axis of the efg.

$$A = \frac{e^2qQ}{12}$$

$$\alpha = g_l \beta_n H_{ext}$$

$$\beta = g_o \beta_n H_{ext}$$

FIGURE 2

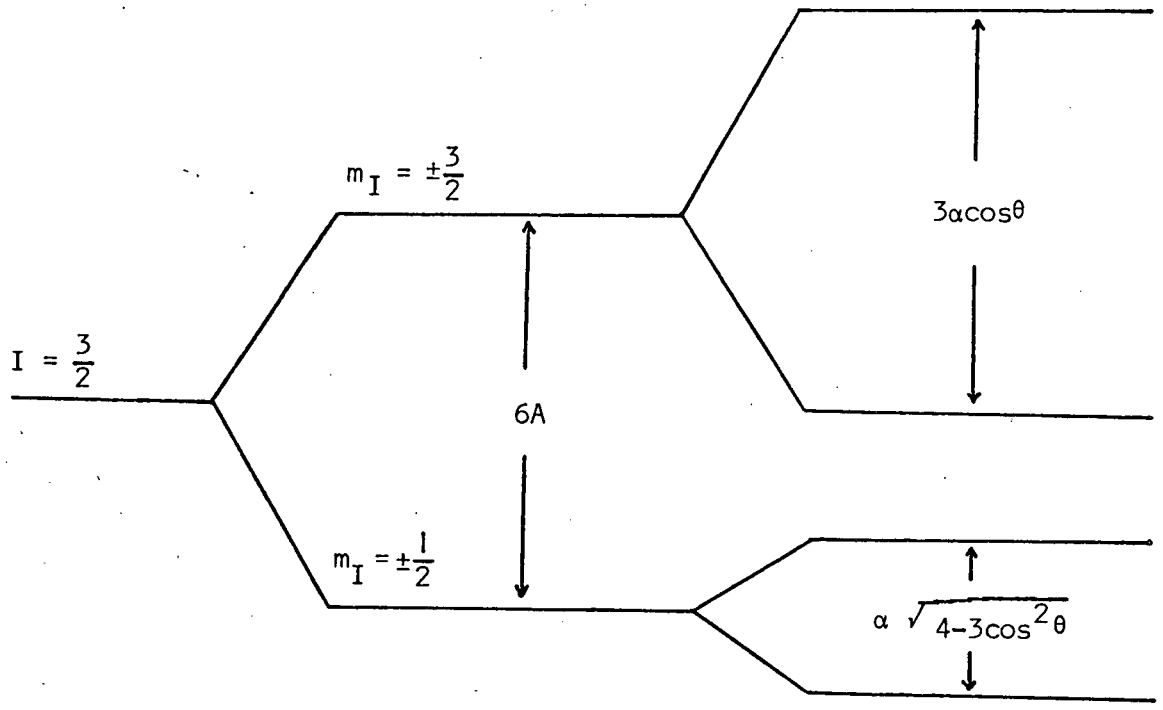

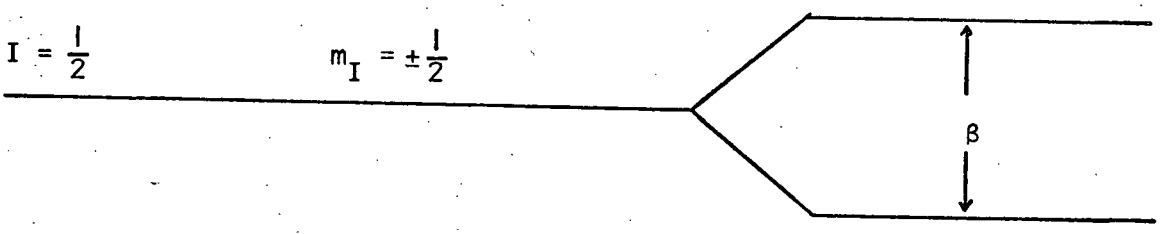

$\Delta E_Q = 0$

$\Delta E_Q > 0$
$\eta = 0$

$\Delta E_Q > 0$ $H_{ext} > 0$
$\eta = 0$

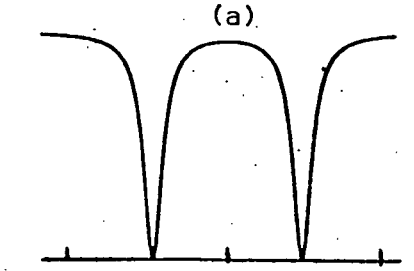

Typical Spectrum of ^{57}Fe
$\Delta E_Q = +2.0$ mm s^{-1}
$\eta = 0$

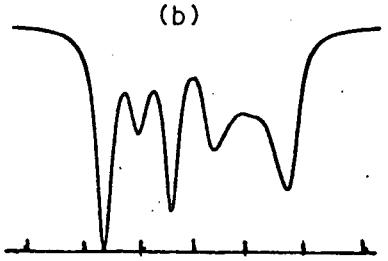

Typical Spectrum of ^{57}Fe
$\Delta E_Q = +2.0$ mm s^{-1}
$H_{ext} = 30$ kG
longitudinal
$\eta = 0$

state sub-levels depend on the sign of V_{zz} : if $V_{zz} > 0$ the $|\pm \frac{3}{2}>_e$ state lies higher in energy, and the $|\pm \frac{1}{2}>_e$ state is higher if $V_{zz} <0.$) Thus, neither the sign of V_{zz} nor the value of η can be deduced in this case, but only the magnitude of ΔE_Q, so that one does not obtain the full information potentially available from the quadrupole interaction.

In order to relate the efg to the chemical environment of the nucleus, the source of the efg is now examined. The contribution to the efg at the nucleus can be separated into two terms: (1) the lattice contribution ($eq_{LATTICE}$) due to charges on the ligands and neighbouring ions in the crystal; (2) the valence contribution ($eq_{VALENCE}$) arising from an asymmetric distribution of electrons in bonding and non-bonding orbitals. The electrons in the valence shell will usually make the major contribution to the second term, although inner shell electrons which acquire a non-spherical distribution due to induced polarization effects can also contribute. Thus one can write eq as[9]

$$eq = (1 - \gamma_\infty)eq_{LATTICE} + (1 - R)eq_{VALENCE} \tag{30}$$

where $R(0.2>R>-0.2)$ and $\gamma_\infty(-7>\gamma_\infty>-100)$ are Sternheimer factors accounting for the induced polarization of inner core electrons,

$$eq_{LATTICE} = \sum_i eq_i \frac{(3\cos^2\theta_i - 1)}{r_i^3} \tag{31}$$

and

$$eq_{VALENCE} = - \sum_j ep_j \left\langle \frac{(3\cos^2\theta_j - 1)}{r_j^3} \right\rangle \qquad (32)$$

Here q_i is the charge on the ith ion having polar coordinates θ_i, r_i (approximating the ions as point charges), p_j the population of the jth valence shell orbital, and $\langle(3\cos^2\theta_j - 1)/r_j^3\rangle$ the expectation value of this population over the electron coordinates θ_j, r_j, the summations being taken over all ions i and all valence orbitals j. The numerical values of $q_{VALENCE}$ for various atomic orbitals can be obtained from the angular parts of the wavefunctions[9], and are given in Table I.

It is generally assumed[9] that the valence term makes the major contibution to the efg for ferrous complexes, owing to the r^{-3} dependence. From Table I it can also be seen that if either a p or d shell is empty, half-filled or completely filled it will not contribute to the efg. In the case of high-spin Fe^{2+} ions with little covalency, the efg arises primarily because there is one d electron in addition to the spherically symmetric half-filled 3d shell. Since both V_{zz} and η will depend on which d orbital this extra electron occupies, it is important to know both these parameters.

TABLE I

Values of $q_{VALENCE}$ and η for various atomic orbitals[a]

Orbital	$q_{VALENCE}$[b]	η
p_x	$+\frac{2}{5}\langle r^{-3}\rangle$	-3
p_y	$+\frac{2}{5}\langle r^{-3}\rangle$	+3
p_z	$-\frac{4}{5}\langle r^{-3}\rangle$	0
$d_{x^2-y^2}$	$+\frac{4}{7}\langle r^{-3}\rangle$	0
d_{z^2}	$-\frac{4}{7}\langle r^{-3}\rangle$	0
d_{xy}	$+\frac{4}{7}\langle r^{-3}\rangle$	0
d_{xz}	$-\frac{2}{7}\langle r^{-3}\rangle$	+3
d_{yz}	$-\frac{2}{7}\langle r^{-3}\rangle$	-3
s	0	0

[a] Taken from Ref. 1, p.59.

[b] $\langle r^{-3}\rangle$ is the expectation value of $1/r^3$ for the appropriate radial function.

Combined quadrupole and magnetic interaction

In order to determine the value of η and the sign of V_{zz}, a magnetic perturbation experiment may be carried out in which an external magnetic field (usually 10-50 kG in magnitude) is applied to the absorber. This applied field lifts the remaining degeneracy of the m_I nuclear spin substates via the nuclear Zeeman effect. A general treatment has been developed for the case of diamagnetic compounds[3] and will be discussed first.

The Hamiltonian describing the interaction of the nuclear magnetic moment $\underline{\mu}$ with an effective magnetic field $\underline{H}$ at the nucleus (which for a diamagnet will equal the applied field) is[3]

$$\mathcal{H}_{Mag} = -\underline{\mu}\cdot\underline{H} = -g\beta_n \hat{\underline{I}}\cdot\underline{H} \tag{33}$$

where g is the gyromagnetic ratio and β_n the nuclear magneton. The total Hamiltonian will be a combination of magnetic and quadrupole terms. In the efg principal axis system, this can be written as

$$\mathcal{H} = \mathcal{H}_{Q.S.} + \mathcal{H}_{Mag} = \frac{e^2qQ}{4I(2I-1)}\left[3\hat{I}_z^2 - I(I+1) + \frac{\eta}{2}(\hat{I}_+^2 + \hat{I}_-^2)\right]$$

$$- g\beta_n H(\hat{I}_x\sin\theta\cos\phi + \hat{I}_y\sin\theta\sin\phi + \hat{I}_z\cos\theta) \tag{34}$$

where H is the magnitude of $\underline{H}$, and θ, ϕ the polar angles of $\underline{H}$ with respect to the z axis of the efg.

The $I = \frac{1}{2}$ ground state of ^{57}Fe has zero quadrupole moment so that for this state $\mathcal{H} = \mathcal{H}_{Mag}$ and one has[3]

$$\langle \tfrac{1}{2}m' | \mathcal{H}_{Mag} | \tfrac{1}{2}m \rangle = \begin{array}{c} \\ \tfrac{1}{2} \\ -\tfrac{1}{2} \end{array} \begin{array}{c} \begin{array}{cc} \tfrac{1}{2} & -\tfrac{1}{2} \end{array} \\ \begin{bmatrix} -\frac{1}{2}g_o\beta_n H\cos\theta & -\frac{1}{2}g_o\beta_n H\sin\theta e^{-i\phi} \\ -\frac{1}{2}g_o\beta_n H\sin\theta e^{i\phi} & \frac{1}{2}g_o\beta_n H\cos\theta \end{bmatrix} \end{array} \tag{35}$$

This can be diagonalized to give the eigenvalues

$$E = \pm\tfrac{1}{2} g_o \beta_n H \tag{36}$$

where g_o is the ground state gyromagnetic ratio, and eigenfunctions

$$|-\rangle = -\sin\frac{\theta}{2}\, e^{-i\phi} |\tfrac{1}{2}, \tfrac{1}{2}\rangle + \cos\frac{\theta}{2}\, |\tfrac{1}{2}, -\tfrac{1}{2}\rangle$$

$$|+\rangle = \cos\frac{\theta}{2}\, |\tfrac{1}{2}, \tfrac{1}{2}\rangle + \sin\frac{\theta}{2}\, e^{i\phi} |\tfrac{1}{2}, -\tfrac{1}{2}\rangle \tag{37}$$

For the excited state the matrix elements are

$$\langle \tfrac{3}{2} m' \,|\, \mathcal{H} \,|\, \tfrac{3}{2} m \rangle =$$

$$\begin{array}{c} \\ \frac{3}{2} \\ \frac{1}{2} \\ -\frac{1}{2} \\ -\frac{3}{2} \end{array} \begin{array}{c} \begin{array}{cccc} \frac{3}{2} & \frac{1}{2} & -\frac{1}{2} & -\frac{3}{2} \end{array} \\ \begin{bmatrix} 3A + \frac{3}{2}\alpha\cos\theta & \sqrt{\frac{3}{2}}\alpha\sin\theta e^{-i\phi} & \sqrt{3}\eta A & 0 \\ \sqrt{\frac{3}{2}}\alpha\sin\theta e^{i\phi} & -3A + \frac{1}{2}\alpha\cos\theta & \alpha\sin\theta e^{-i\phi} & \sqrt{3}\eta A \\ \sqrt{3}\eta A & \alpha\sin\theta e^{i\phi} & -3A - \frac{1}{2}\alpha\cos\theta & \sqrt{\frac{3}{2}}\alpha\sin\theta e^{-i\phi} \\ 0 & \sqrt{3}\eta A & \sqrt{\frac{3}{2}}\alpha\sin\theta e^{i\phi} & 3A - \frac{3}{2}\alpha\cos\theta \end{bmatrix} \end{array} \tag{38}$$

Where $A = \frac{e^2qQ}{12}$, $\alpha = -g_I\beta_n H$ and g_I is the gyromagnetic ratio of the excited state. Solutions to this matrix can be obtained for any given e^2qQ, η, H, θ and ϕ by computer diagonalization.

In order to compute a theoretical spectrum, transition probabilities connecting the various substates have to be calculated. To do this one must know the eigenvectors in terms of the basis kets for both ground and excited states, and the Clebsch-Gordan coupling coefficients[10] for the appropriate transtions. Then one must sum over the relative amounts of left- and right-handed circularly polarized γ-photons available. This intensity problem has been treated by Collins and Travis[3], and the calculations are discussed in Appendix I.

The result for an ^{57}Fe compound with axially symmetric efg (i.e., η=0) is the appearance of a characteristic triplet-doublet pattern as in Figure 2(b). For a positive V_{zz} the triplet lies at lower energy, whereas the doublet lies at lower energy for a negative V_{zz}. As η increases from zero the spectrum becomes more symmetrical, and when $\eta = 1$ a symmetric triplet-triplet pattern is observed. Thus, by generating theoretical spectra and comparing them with experimental ones, the sign of V_{zz} and an estimate of the η value can be obtained.

For paramagnetic systems the picture is far more complicated, and several different situations may arise. Johnson[11] has examined the problem in detail for a case where the relaxation rate of the electronic states is very fast compared to the Larmor precession frequency of the nucleus. The effective field at the nucleus, H_{eff}, can be expressed in this case by[11]

$$H_{eff} = H_{ext} + \frac{\langle S \rangle}{S} H_n^{\circ} \tag{39}$$

where $\langle S \rangle$ is the average of the total electronic spin S and H_n° the saturation value of the internal field H_n. The magnetization can be related to the susceptibility χ by

$$\langle S \rangle / S = \chi H_{ext} / N\mu \tag{40}$$

where μ is the magnetic moment and N Avogadro's number. (Properly, both H_n and χ are tensor quantities, but this does not alter the qualitative picture given here.) Since the susceptibility is small at high temperatures, the magnetization $\langle S \rangle$ induced by a moderate applied field ($\lesssim$ 50 kG) under these circumstances will be small, and $H_{eff} \simeq H_{ext}$. Thus in this case the paramagnetic system behaves in essentially the same way as a diamagnetic one, and the treatment given above will still be valid.

On the other hand, at 4.2°K (the temperature at which magnetic perturbation measurements are normally made) χ will be large and H_{eff} can be very much larger than the applied field. In addition, since H_n is an anisotropic tensor, H_{eff} and H_{ext} will in general not be collinear. Thus, Mössbauer spectra obtained under these conditions can have very diverse appearances depending on the detailed electronic structure of the complex, and it is often impossible to determine the sign of V_{zz} from such a measurement.

Further difficulties can arise if the spin relaxation is not fast compared to the nuclear Larmor frequency, since in this case $\langle S \rangle$ may be non-zero even in the absence of an applied field.

For the simpler high-spin ferric case, since Fe^{3+} is an S-state ion, the ground state is just a Kramers' doublet and the problem of varying relaxation rates has been given an adequate theoretical treatment[12-14]. For high-spin ferrous systems the situation is further complicated by the existence of several types of orbital ground states. There has been a very recent attempt to treat an eight-coordinate high-spin ferrous complex having an orbital singlet ground state, in both the fast and slow relaxation limits[15]. However, the theory for the case of intermediate relaxation rates has not been extended to include ferrous systems thus far.

CHAPTER II

EXPERIMENTAL TECHNIQUES

Analyses

Microanalyses of C, H, N were performed by Mr. P. Borda of this Department and by Drs. F. and E. Pascher, Microanalytical Laboratory, Bonn, Germany. The iron analyses were carried out with the aid of a Perkin-Elmer 305A atomic absorption spectrophotometer.

Infrared Spectra

Infrared spectra of solid samples were recorded either with nujol mulls between caesium iodide plates or with KBr pellets, using a Perkin-Elmer 457 grating spectrometer over the range 4000-250 cm^{-1}.

Molar Conductances

Molar conductances in methanol were measured using an A.C. conductance bridge. The measurements were made in a 25° oil bath, and the A.C. bridge frequency was set at 1000 Hz.

Electronic Spectra

The electronic spectra were recorded on a Cary Model 14 spectrophotometer. KBr pellets were used for solids while spectra of solutions were obtained in 1 cm standard quartz optical cells. In order to obtain variable temperature data, a brass liquid nitrogen dewar fitted with glass windows was used. The temperature variation was achieved by

passing controlled amounts of cold (79°K) nitrogen vapour into the inner chamber of the dewar. Temperatures were measured with a copper-constantan thermocouple attached to the copper sample holder inside the dewar.

Magnetic Measurements

Magnetic susceptibilities of powder samples were measured with a variable temperature Gouy balance over the temperature range 80-320°K. All measurements were made at two field strengths. Calibration of the apparatus was achieved using mercury tetrathiocyanatocobaltate(II). Pascal's constants were used to correct for diamagnetism[16].

Mössbauer Spectra

The Mössbauer spectrometer consisted of an Austin Science Associates S-3 drive unit and K3-K linear motor, a Reuter-Stokes RSG-61 proportional counter (Xe - CO_2 fill gas at two atmospheres pressure), and a Nuclear-Chicago model 24-2 400-word multichannel analyser operating in multiscaler mode. Also included (Nuclear-Chicago modules) were a model 40-9B high voltage power supply, a model 23805 preamplifier, a model 33-15 amplifier-single-channel analyser, a model 23-4 analog-to-digital converter, and a model 021308 time-base generator. A schematic diagram of a typical Mössbauer spectrometer is shown in Figure 3.

All spectra in zero applied field were obtained in transmission geometry using a 25 mCi $^{57}Co(Cu)$ source which was maintained at ambient temperature. Carefully powdered samples, contained in a copper cell with Mylar windows of cross-sectional area 2.5 cm^2, were mounted in a Janis Model DT-6 variable temperature cryostat. The cryostat was fitted with a Cryogenic Research Model TC-101 automatic temperature controller,

FIGURE 3

Schematic Diagram of a Typical Mössbauer Spectrometer

FIGURE 3

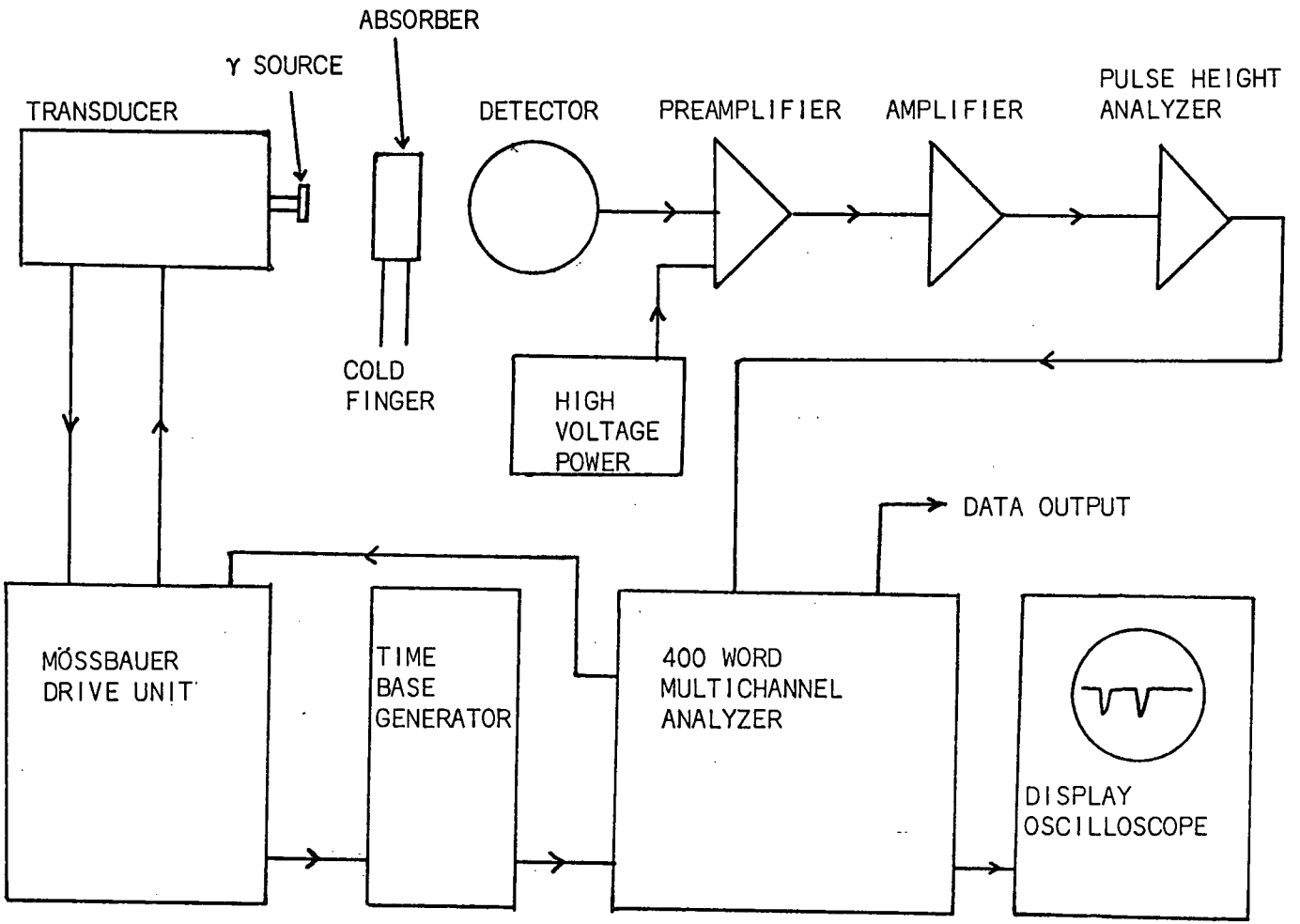
ABSORBER
γ SOURCE
TRANSDUCER
DETECTOR
PREAMPLIFIER
AMPLIFIER
PULSE HEIGHT ANALYZER
COLD FINGER
HIGH VOLTAGE POWER
DATA OUTPUT
MÖSSBAUER DRIVE UNIT
TIME BASE GENERATOR
400 WORD MULTICHANNEL ANALYZER
DISPLAY OSCILLOSCOPE

by means of which the temperature could be set and maintained constant to within ± 0.02° throughout the data acquisition time. Temperatures were measured with calibrated Ge and Pt resistance thermometers. The design of the cryostat (see Figure 4) is such that the sample is cooled by exchange gas and is not in direct contact with the liquid helium bath. Thus the lowest sample temperature which could be achieved in this system was approximately 8°K.

For spectra recorded above room temperature, the samples were mounted at the top of a solid copper rod, which was wrapped with heating tape powered through a variable transformer. Temperatures were monitored with a copper-constantan thermocouple and were found to vary by less than ± 0.5° during a run.

Mössbauer measurements in applied longitudinal magnetic fields of up to 50 kG were carried out in a Janis Model 11MDT helium cryostat fitted with a Westinghouse superconducting solenoid. The vertically mounted ^{57}Co(Cu) source was driven, via a long thin-walled stainless steel drive rod, by an Austin Science Associates K-3 linear motor (Figure 5). The copper sample cell was fitted into a copper ring located at the centre of the applied field. This ring was equipped with a heater and a copper-constantan thermocouple. To obtain spectra with the absorber at 4.2°K, thermal contact with the liquid helium reservoir was provided by filling the inner vacuum space shown in Figure 5 with helium exchange gas at a pressure slightly less than one atmosphere. For paramagnetic samples it was necessary in many cases to record magnetic perturbation spectra with the absorber at a temperature of 200°K or higher, as discussed in Chapter I. In order to heat the samples to high temperatures while maintaining the superconducting solenoid at 4.2°K, the sample

FIGURE 4

Schematic Diagram of the Apparatus Employed for Obtaining Variable Temperature Mössbauer Spectra

FIGURE 4

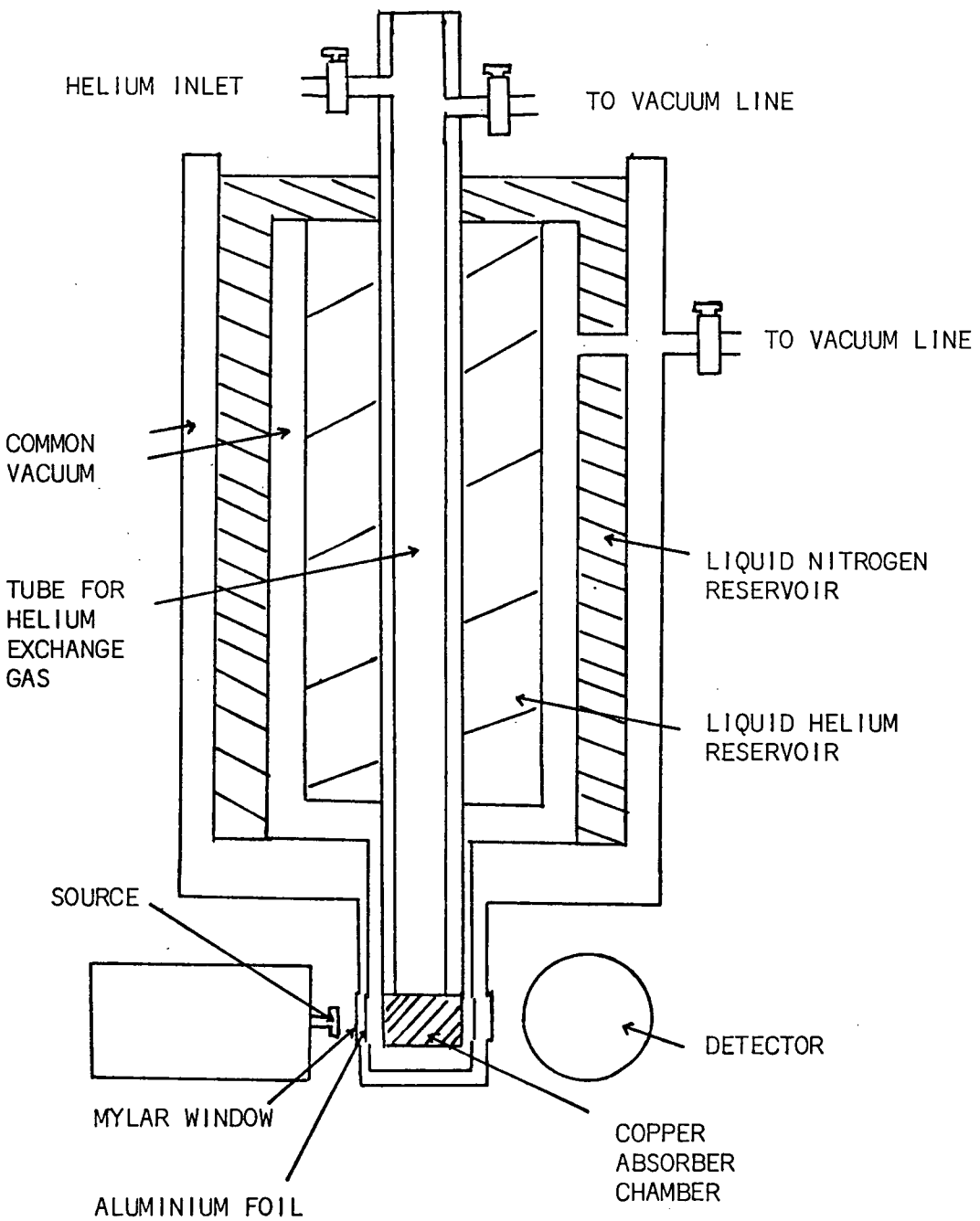
HELIUM INLET
TO VACUUM LINE
TO VACUUM LINE
COMMON VACUUM
TUBE FOR HELIUM EXCHANGE GAS
LIQUID NITROGEN RESERVOIR
LIQUID HELIUM RESERVOIR
SOURCE
DETECTOR
MYLAR WINDOW
ALUMINIUM FOIL
COPPER ABSORBER CHAMBER

FIGURE 5

Schematic Diagram of the Magnetic Perturbation Apparatus

FIGURE 5

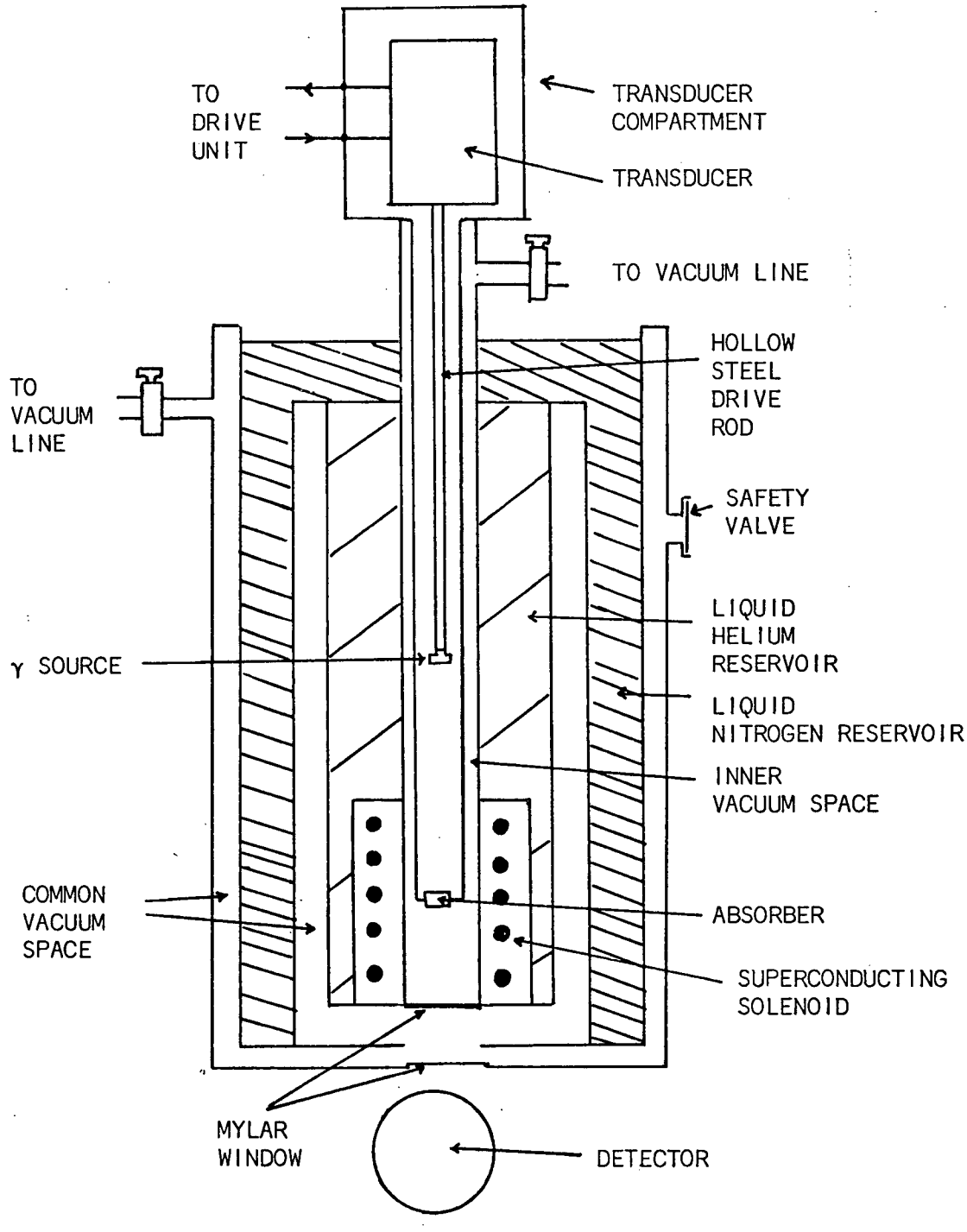
TO
DRIVE
UNIT
TRANSDUCER
COMPARTMENT
TRANSDUCER
TO VACUUM LINE
HOLLOW
STEEL
DRIVE
ROD
TO
VACUUM
LINE
SAFETY
VALVE
LIQUID
HELIUM
RESERVOIR
γ SOURCE
LIQUID
NITROGEN RESERVOIR
INNER
VACUUM SPACE
COMMON
VACUUM
SPACE
ABSORBER
SUPERCONDUCTING
SOLENOID
MYLAR
WINDOW
DETECTOR

chamber was evacuated to a pressure of less than 10^{-5} torr. After transfer of liquid helium to the system, cryopumping was sufficient to prevent excessive heat transfer from the sample to the solenoid helium bath. The temperature of the sample was then monitored throughout the experiment with the thermocouple and was found to vary by less than ± 2° during a run.

Calibration of the Doppler velocity scale was affected after each experiment with either a disodium pentacyanonitrosylferrate (II) absorber (for low velocities), or a metallic iron foil absorber (for high velocities). Isomer shifts are quoted relative to the centroid of the disodium pentacyanonitrosylferrate(II) (sodium nitroprusside) spectrum.

For spectra obtained in the absence of an applied field, the data points were least-squares fitted to Lorentzian components using a programme based on one originally supplied by the National Bureau of Standards. In this programme the positions, widths and intensities of the Mössbauer lines are treated as unconstrained fitting parameters. For some of the spectra discussed in Chapter IV which consisted of two strong and two weak absorptions, it was not possible to fit the weak lines using unconstrained parameters. In these cases four-line fits could be obtained by constraining the widths of the two weak lines.

Theoretical magnetic perturbation spectra used for comparison with the experimental spectra were generated by a programme supplied by Dr. G. Lang[17]. The magnitude and sign of the quadrupole coupling constant e^2qQ, and the magnitudes of the asymmetry parameter, linewidth and external magnetic field are used as adjustable parameters in this programme.

N.M.R. Spectra

Proton nuclear magnetic resonance spectra were run on a Varian T-60 spectrometer with chemical shifts given in ppm downfield from internal TMS standard.

Mass Spectra

Mass spectra were measured with an AEI MS-9 spectrometer.

CHAPTER III

ELECTRONIC GROUND STATES OF FOUR HIGH-SPIN FERROUS COMPLEXES

Introduction

In general, quadrupole splittings $|\Delta E_Q|$ in octahedral high-spin ferrous complexes show a continuous variation with temperature[1,18]. However, $Fe(H_2O)_6(ClO_4)_2$ was reported to show anomalous behaviour in its Mössbauer spectrum[19]. At 110°K $|\Delta E_Q|$ = 3.4 mm s^{-1}, at 295°K the splitting was only 1.4 mm s^{-1}, and between 220-250°K four lines were visible in the spectrum. These results were interpreted[19] in terms of a tetragonal distortion with axial compression and an $|xy\rangle$ orbital ground state at low temperature, with a phase transition leading to axial elongation and a doubly degenerate $|xz\rangle$, $|yz\rangle$ ground state at high temperature. A subsequent study of this compound using magnetic perturbation techniques[20] indicated that the quadrupole coupling constant e^2qQ was negative at 5°K, so that the low-temperature ground state is $|z^2\rangle$ rather than $|xy\rangle$, and the distortion is trigonal rather than tetragonal. However, the predicted[19] sign reversal was confirmed[20], e^2qQ being positive at 296°K.

Reedijk and van der Kraan[21] have published Mössbauer data (at room temperature only) for five solvates of ferrous perchlorate of the type $FeL_6(ClO_4)_2$, where L was either a sulphoxide ligand or pyridine-N-oxide. These data were interesting in that for four of the five complexes $|\Delta E_Q|$* was about 1.5 mm s^{-1}, similar to the value found for

---

*The values given for ΔE_Q in Table II of ref. 21 are in fact $\frac{1}{2}|\Delta E_Q|$.[22] Accordingly, these values have been multiplied by two in this thesis.

the hexahydrate at the same temperature. On the other hand, for the dimethylsulphoxide derivative $|\Delta E_Q|$ was reported to be 2.56 mm s^{-1}. Reedijk and van der Kraan[21] suggested that the small splitting of about 1.5 mm s^{-1} indicated 'hardly distorted' octahedral cations, whilst the larger value for the $(CH_3)_2SO$ complex showed a greater distortion in this case. However, since distortions of comparable magnitude will produce a quadrupolesplitting for an orbital singlet ground state which is roughly twice that for a doublet state, the alternative explanation of a different orbital ground state in the $(CH_3)_2SO$ derivative seemed to be equally plausible.

A more extensive investigation of such ferrous solvates was thus of interest for several reasons. Firstly, there was the possibility that at low temperatures one might observe phase transitions of the type reported[19] for $Fe(H_2O)_6(ClO_4)_2$. Secondly, a detailed study of the temperature dependence of $|\Delta E_Q|$ in these derivatives, together with determinations of the signs of the efg's at iron, would enable one to deduce the orbital ground states and to estimate the crystal field splitting parameters. Thirdly, since crystal field parameters can also be estimated from the temperature dependence of the magnetic susceptibility, it was of interest to compare the results of two independent evaluations of these parameters.

This Chapter describes the results of detailed magnetic susceptibility and ^{57}Fe Mössbauer measurements (the former between 80-300°K, the latter between 4.2-340°K) on four octahedral complexes of the type $FeL_6(ClO_4)_2$, where L = $(CH_3)_2SO$ (DMSO), $(C_6H_5)_2SO$ (DPSO), $(CH_2)_4SO$ (TMSO), and C_5H_5NO (PyNO).

Preparation of the Complexes

All chemicals used in the preparation of the complexes were of reagent grade and were used without further purification. The commercial sources of these chemicals are:

Ferrous perchlorate hexahydrate	- Alfa Inorganics Inc.
Dimethyl sulphoxide	- Fisher Scientific Co.
Diphenyl sulphoxide	- Eastman Kodak Co.
Tetramethylene sulphoxide Pyridine-N-oxide Ethyl orthoformate	- Aldrich Chemical Co.

All four compounds were prepared by the same procedure[21] and all operations were carried out under an atmosphere of dry nitrogen: 1.81 gms (5.0 mmol) of ferrous perchlorate hexahydrate was dissolved in 15 ml of 100% ethanol, and 20 ml of ethyl orthoformate was added. The solution turned brown immediately. A solution of the ligand (35 mmol) in 100% ethanol (25 ml) was added slowly with stirring. The precipitate which formed was filtered through a sintered glass funnel, washed with dry diethyl ether several times, and dried *in vacuo*.

Results and Discussion

Analytical and I.R. data for the complexes are given in Table II. Only the structurally relevant I.R. bands have been listed, and agreement with previously published data[23-26] is generally good. In all four compounds only the ν_3 and ν_4 bands of the ClO_4^- ion are observed, showing

that the anions retain tetrahedral symmetry and ruling out the possibility of iron-perchlorate coordination. The E-O stretching frequencies (E = S, N) are some 30-60 cm^{-1} lower in the complexes than in the free ligands, which indicates that the ligand molecules are coordinated to iron through the oxygen atoms[27]. For the PyNO complex ν(Fe-O) is seen at 307 cm^{-1}, and this band appears at about 400 cm^{-1} in the sulphoxide derivatives. There is some uncertainty about the position of ν(Fe-O) in $Fe(DPSO)_6^{2+}$. Prabhakaran and Patel[26] have assigned this stretch to a weak band at 430 cm^{-1}, whereas for the other three complexes studied here ν(Fe-O) appears as a strong absorption. However, the only other band in the 600-250 cm^{-1} region in $Fe(DPSO)_6^{2+}$ not attributable to a ligand mode is a strong band at 260 cm^{-1}, which seems too low in comparison with ν(Fe-O) for the other sulphoxide complexes. The assignment of ν(Sn-O) in DPSO adducts with diorganotin halides also appears to be uncertain[28].

Data for the effective magnetic moments μ_{eff} appear in Table III, and clearly indicate that the four complexes are high-spin (S=2). All values fall in the rather narrow range 5.30-5.54 B.M., and there is little variation amongst the four solvates. This suggests, contrary to the conclusions of Reedijk and van der Kraan[21], that the magnitudes of the axial distortions in all the complexes are quite similar. Although the μ_{eff} values do not have a pronounced temperature dependence, it can be seen that for the DMSO and DPSO derivatives μ_{eff} decreases smoothly with decreasing temperature, whilst the values for the TMSO and PyNO complexes increase initially before showing a slight decline at low temperature. As will be seen below, this difference in the behaviour of μ_{eff} as a function of temperature presumably arises from the fact that the two pairs of complexes (DMSO and DPSO on the one hand, TMSO and PyNO on

TABLE II

Analytical Data and Important Ir Bands for $FeL_6(ClO_4)_2$ Complexes

L	-------% Calcd.-----				------% found-------				ν(E-O)[a,b] (cm^{-1})	ν(Fe-O)[b] (cm^{-1})	ClO_4^- bands[b] (cm^{-1})
	C	H	N	Cl	C	H	N	Cl			
$(CH_3)_2SO$	19.90	4.98	0	9.83	19.79	4.94	0	9.76	990 vs, br	431s 410s	1085 vs, br 616 vs
$(C_6H_5)_2SO$	58.85	4.09	0	4.84	58.68	3.88	0	-	981 vs, br	419 w (?)	1082 vs, br 614 vs
$(CH_2)_4SO$	32.79	5.46	0	8.07	32.55	5.48	0	-	964 vs, br	393s	1084 vs, br 619 vs
C_5H_5NO	43.67	3.64	10.20	8.60	43.45	3.45	10.34	8.40	1217s	307s	1090 vs, br 617 vs

a E = S or N

b s = strong, w = weak, v = very, br = broad

TABLE III

Effective Magnetic Moments μ_{eff} of the $FeL_6(ClO_4)_2$ Complexes

T(°K)	μ_{eff}(B.M.)
FE(DMSO)6(CLO4)2	
80.4	5.30
97.0	5.33
112.0	5.31
125.1	5.34
140.1	5.32
153.5	5.35
165.5	5.35
180.4	5.36
196.5	5.36
213.0	5.38
229.9	5.38
246.6	5.38
262.3	5.38
278.1	5.39
295.0	5.40
309.5	5.42
FE(DPSO)6(CLO4)2	
81.0	5.32
92.2	5.33
111.3	5.34
132.0	5.32
153.6	5.33
174.0	5.36
193.0	5.34
209.7	5.37
227.7	5.38
249.8	5.38
272.1	5.38
300.4	5.41

T(°K)	μ_{eff}(B.M.)
FE(TMSO)6(CLO4)2	
80.7	5.39
103.8	5.42
123.9	5.43
143.9	5.45
165.2	5.45
186.6	5.44
205.7	5.45
224.0	5.47
244.1	5.47
263.3	5.45
284.8	5.45
307.2	5.41
FE(PYNO)6(CLO4)2	
81.2	5.51
90.2	5.55
109.6	5.54
129.1	5.52
151.9	5.53
173.7	5.52
192.0	5.51
214.2	5.50
237.1	5.46
256.7	5.44
280.5	5.42
302.6	5.41

the other) have different orbital ground states.

Mössbauer isomer shifts and quadrupole splittings, together with spectral linewidths, are listed in Table IV. Results for the DMSO, TMSO, and PyNO complexes are in only moderately good agreement with those of Reedijk and van der Kraan[21]. (The DPSO derivative was not reported in ref. 21.) In particular, the 'room temperature' $|\Delta E_Q|$ values reported by these authors[21] are between 0.08 and 0.16 mm sec^{-1} smaller than values at 295°K listed in Table IV. The present measurements were repeated on several different samples of each compound and the results were accurately reproducible.

The δ values in Table IV lie within the range normally observed for octahedral S=2 ferrous complexes[1] and show little variation amongst the four solvates. This implies that the extent of covalency of the Fe-O bonds is probably very similar in all these derivatives. The temperature dependence of the δ values can be attributed to a second-order Doppler shift[29] and will not be considered further.

The quadrupole splitting data show marked differences, both in temperature dependence and in the magnitude at a given temperature. At 295°K the TMSO and PyNO complexes have splittings of 1.64 mm s^{-1}, whereas for the other two derivatives the splittings are about 2.7 mm s^{-1}. The latter complexes also show a more pronounced temperature dependence of $|\Delta E_Q|$, and it is clear that on the basis of Mössbauer data the four compounds divide into the same two pairs as noted above in connection with the magnetic moments.

In no case was a clear four-line spectrum observed, and there is no indication in any of these complexes of the type of phase transition reported[19] for $Fe(H_2O)_6(ClO_4)_2$. However, at about 100°K, the lines of

TABLE IV

^{57}Fe Mössbauer Parameters for the $FeL_6(ClO_4)_2$ Complexes

T(°K)	δ(mm s^{-1})	ΔE_Q(mm s^{-1})	Γ_1(mm s^{-1})	Γ_2(mm s^{-1})
FE(DMSO)6(CLO4)2				
7.9	1.64	3.22	.28	.28
15.0	1.64	3.19	.27	.26
40.0	1.63	3.20	.26	.26
60.0	1.63	3.19	.25	.25
81.8	1.63	3.19	.27	.27
82.5	1.63	3.18	.28	.28
100.0	1.63	3.17	.27	.27
105.0	1.63	3.17	.27	.27
115.1	1.63	3.17	.26	.26
131.0	1.61	3.15	.26	.26
160.0	1.60	3.12	.26	.26
190.1	1.58	3.08	.25	.25
220.0	1.57	3.02	.27	.25
250.0	1.55	2.92	.25	.24
273.0	1.54	2.86	.26	.24
295.5	1.52	2.71	.23	.23
FE(DPSO)6(CLO4)2				
8.8	1.63	3.37	.27	.28
30.0	1.63	3.36	.26	.28
60.0	1.63	3.36	.28	.29
82.7	1.62	3.38	.28	.29
85.0	1.63	3.37	.28	.29
95.1	1.62	3.37	.28	.29
114.7	1.61	3.34	.27	.29
145.0	1.60	3.28	.28	.28
175.0	1.59	3.19	.27	.28
205.0	1.58	3.10	.25	.26
235.0	1.56	2.99	.25	.25
265.0	1.55	2.87	.23	.24
294.8	1.51	2.68	.23	.24
315.5	1.50	2.58	.29	.30
331.0	1.49	2.50	.32	.33

TABLE IV
(Continued)

T(°K)	δ(mm s^{-1})	ΔE_Q(mm s^{-1})	Γ_1(mm s^{-1})	Γ_2(mm s^{-1})
FE(TMSO)6(CLO4)2				
8.6	1.61	2.34	.48	.51
15.0	1.62	2.36	.52	.54
25.0	1.61	2.33	.49	.50
40.0	1.61	2.31	.53	.50
60.0	1.61	2.28	.47	.49
80.8	1.59	2.15	.43	.39
87.1	1.60	2.05	.29	.27
100.1	1.60	1.97	.27	.27
107.0	1.60	1.93	.27	.27
130.0	1.58	1.91	.25	.23
140.2	1.58	1.87	.25	.23
170.0	1.57	1.84	.28	.26
210.0	1.56	1.80	.30	.27
250.0	1.52	1.74	.27	.25
295.1	1.50	1.65	.25	.25
FE(PYNO)6(CLO4)2				
8.2	1.56	1.92	.40	.55
9.0	1.56	1.91	.38	.57
11.0	1.57	1.93	.38	.55
15.0	1.57	1.91	.37	.53
20.0	1.56	1.90	.33	.43
25.0	1.56	1.90	.31	.35
30.1	1.56	1.89	.29	.31
40.0	1.55	1.87	.28	.28
65.0	1.55	1.85	.28	.28
81.0	1.55	1.82	.27	.27
83.7	1.55	1.81	.27	.25
100.0	1.54	1.79	.26	.25
115.0	1.54	1.78	.26	.25
130.2	1.53	1.76	.28	.27
159.9	1.52	1.74	.24	.24
190.0	1.50	1.71	.24	.24
220.0	1.48	1.68	.25	.24
250.0	1.47	1.67	.24	.24
273.1	1.46	1.66	.23	.23
294.9	1.44	1.64	.23	.23
318.5	1.43	1.63	.32	.30
333.6	1.41	1.62	.32	.30

the TMSO spectrum start to broaden, and at the same time $|\Delta E_Q|$ increases from 1.97 mm s^{-1} at 100°K to about 2.3 mm s^{-1} at 60°K, staying at that value on further cooling. The reason for this phenomenon is not clear. It is possible that below 100°K the TMSO spectrum is in fact a four line spectrum. This could arise from two non-equivalent iron sites having slightly different electric field gradients. Unlike $Fe(H_2O)_6(ClO_4)_2$, however, the broadened spectrum does not resolve into two narrow lines again even at temperatures as low as 8°K, which might suggest an incomplete phase change. The PyNO compound also shows line broadening, but only below about 30°K, and in this case the broadened spectrum becomes highly asymmetric. This effect is attributed to slow spin-lattice relaxation and will be discussed in detail in the last section of this Chapter.

Orbital Ground States of the Complexes

An octahedral crystal field splits the ferrous 3d orbitals into triply degenerate t_{2g} and double degenerate e_g subsets, with the triplet lying lower by an energy 10Dq. If the fourfold axis C_4 is taken as the quantization axis (see Figure 6), the d orbitals transform as follows:

$$e_g = |x^2-y^2>, \quad |z^2>$$

$$t_{2g} = |xy>, \quad |xz>, \quad |yz>$$

On the other hand, if one of the C_3 axes (lying along the [1,1,1] directions of the octahedron) is taken to be the axis of quantization, then in terms of the real d orbitals one has instead[30]:

FIGURE 6

Quantization Axes for an Octahedral Crystal Field

FIGURE 6

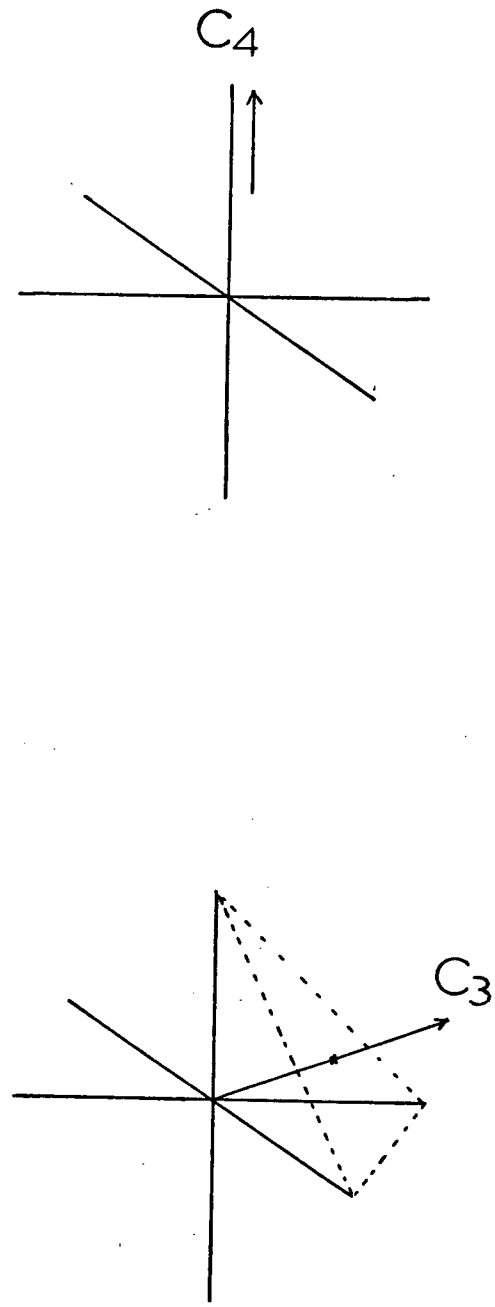

$$e_g = \sqrt{\tfrac{1}{3}}\,|x^2-y^2\rangle + \sqrt{\tfrac{2}{3}}\,|xz\rangle$$

$$\sqrt{\tfrac{1}{3}}\,|xy\rangle - \sqrt{\tfrac{2}{3}}\,|yz\rangle$$

$$|z^2\rangle$$

$$t_{2g} = \sqrt{\tfrac{2}{3}}\,|x^2-y^2\rangle - \sqrt{\tfrac{1}{3}}\,|xz\rangle$$

$$\sqrt{\tfrac{2}{3}}\,|xy\rangle + \sqrt{\tfrac{1}{3}}\,|yz\rangle$$

An axial field partially lifts the degeneracy of the t_{2g} orbitals[30], splitting them into a doublet and a singlet separated by 3Ds. In the tetragonal (C_4) case the singlet is $|xy\rangle$, and in the trigonal case it is $|z^2\rangle$.* In both instances, if the singlet lies lower the distortion corresponds to a compression along the quantization axis, whereas a doublet ground term corresponds to an elongation along this axis. If there is also a rhombic field, the remaining spatial degeneracy of the t_{2g} orbitals is removed, the doublet being split by 12Dr. Each of the 3d wavefunctions also has a five-fold spin degeneracy which will be split by the spin-orbit coupling. For the moment this last feature will be ignored, and only the orbital parts of the states considered.

---

* For a tetragonal field the e_g orbitals are also split, but they remain degenerate in the case of a trigonal field.

The contribution to the efg from a single electron in each of the d orbitals has been given in Table I. From this table one can see that for similar values of Ds an orbitally nondegenerate ground state (either $|xy\rangle$ or $|z^2\rangle$) should produce an appreciably larger quadrupole splitting than that for a doublet state. It is possible, of course, for an orbital singlet ground term to produce only a small $|\Delta E_Q|$ at room temperature if $|3Ds|/k$ is not much larger than 300°K, since this would provide significant thermal population of the doublet. However, $|\Delta E_Q|$ would then be expected to show a very pronounced increase on lowering the temperature, as the electron is progressively localized in the singlet. Finally, since an efg of $\frac{4}{7} e \langle r^{-3} \rangle$ is expected to yield a quadrupole splitting of about 4 mm s^{-1} (details are given in the next section), experimental $|\Delta E_Q|$ values substantially greater than 2 mm s^{-1} are only consistent with a singlet ground state.

From this discussion and the data in Table IV it is clear that for both the $Fe(DMSO)_6^{2+}$ and $Fe(DPSO)_6^{2+}$ complexes the ground state must be an orbital singlet, whereas $Fe(TMSO)_6^{2+}$ and $Fe(PyNO)_6^{2+}$ have doublet ground states. To identify these states more precisely we must know the signs of V_{zz}, the principal component of the efg tensor. For a paramagnetic complex, however, there are certain difficulties associated with the usual magnetic perturbation method[31,32] for determining the sign of V_{zz}. As discussed in Chapter I, the effective magnetic field H_{eff} at the nucleus, measured by the Mössbauer spectrum, can be very different from H_{ext} if the measurement is made at low temperature. The situation is further complicated by the facts that (a) both the magnetization and hyperfine field tensors are anisotropic for high-spin Fe^{2+}, and (b) for a

polycrystalline sample the magnitude of the splittings is an average over all possible orientations of H_{ext} relative to the z axis of the efg[11].

These difficulties can be overcome by maintaining the specimen at high temperature so that the magnetization <S> produced by the applied field is negligible and $H_{eff} \cong H_{ext}$. The situation is then similar to that for a diamagnetic complex[32], where the line of the quadrupole doublet which arises from the $|\pm\frac{1}{2}\rangle_g \rightarrow |\pm\frac{1}{2}\rangle_e$ nuclear spin transitions splits into an apparent triplet, and that from the $|\pm\frac{1}{2}\rangle_g \rightarrow |\pm{}^{3}/_{2}\rangle_e$ transitions splits into a doublet. To ensure that the results would be unambiguous, determinations of the sign of V_{zz} in all four complexes were made with the samples at 210°K or higher in applied fields of 35-50 kG.

In each case it was found that $V_{zz}>0$. This is an important and surprising result because it shows there are two fundamentally different types of distortions from octahedral symmetry in these solvates. For the DMSO and DPSO complexes the ground state is $|xy\rangle$ and the distortion is a compression along the tetragonal C_4 axis. For the TMSO and PyNO derivatives the ground state is essentially the doublet

$$(\sqrt{\tfrac{2}{3}}\,|x^2-y^2\rangle - \sqrt{\tfrac{1}{3}}\,|xz\rangle),\ (\sqrt{\tfrac{2}{3}}\,|xy\rangle + \sqrt{\tfrac{1}{3}}\,|yz\rangle),\ \text{and the}$$

distortion corresponds to an elongation along the trigonal C_3 axis.

The reasons for the occurrence of two distinct types of distortions in these complexes are not completely clear, but may well arise from different steric requirements of the ligands. The most obvious difference is that both TMSO and PyNO contain heterocyclic rings which are only two bonds removed from the Fe^{2+} ion in the complexes, whereas DMSO

and DPSO do not. Since Fe-O-N and Fe-O-S bond angles are both expected to be roughly 120°,[33-35] the presence of six rings of substantial size in close proximity to the central ion should produce considerable steric crowding. Molecular models suggest that this is indeed so. DMSO is of course the least bulky of the four ligands, but even for the DPSO complex, since the phenyl rings are one bond (about 1.8 Å) farther away from the ferrous ion than are the heterocycles in the PyNO and TMSO derivatives, the structure appears to be less crowded. It is worth noting here that the X-ray crystal structure of $(CH_3)_2SnCl_2 \cdot 2PyNO$[33] shows the PyNO groups to be <u>trans</u>, whereas the DMSO ligands are <u>cis</u> in $(CH_3)_2SnCl_2 \cdot 2DMSO$[34].

Crystal Field, Spin-Orbit and Spin-Spin Splitting Parameters

Both Ingalls[18] and Gibb[36] have treated the effects of crystalline fields and spin-orbit coupling on the quadrupole splitting in octahedral Fe^{2+} systems, and we have followed these authors in general outline. The effect of the non-cubic part of the crystal field is treated in terms of the perturbation Hamiltonian

$$\mathcal{H} = V_T + V_R + V_{SO} + V_{SS} \qquad (41)$$

where V_T is the axial (tetragonal or trigonal) field term, V_R the rhombic term, V_{SO} the spin-orbit coupling, and V_{SS} the intraionic spin-spin coupling. The last term was omitted by both Ingalls[18] and Gibb[36]. Its inclusion significantly improves agreement between calculated ΔE_Q values and the low-temperature data in the 8-40°K region. In fact,

for the range of axial distortions encountered here, omission of V_{SS} from the Hamiltonian causes $|\Delta E_Q|$ to decrease rather than increase as the temperature is lowered below ~80°K, contrary to what is observed experimentally.

In operator notation, eqn. (41) can be written as[30]

$$\mathcal{H} = Ds(\hat{L}_z^2 - 2) + Dr(\hat{L}_+^2 + \hat{L}_-^2) - \lambda[\hat{L}_z\hat{S}_z + \tfrac{1}{2}(\hat{L}_+\hat{S}_- + \hat{L}_-\hat{S}_+)] - D\sigma(\hat{S}_z^2 - 2) \qquad (42)$$

where the $\hat{L}_\pm$ and $\hat{S}_\pm$ are respectively orbital and spin angular momentum shift operators, Ds and Dr the axial and rhombic field parameters, λ and $D\sigma$ the spin-orbit and spin-spin coupling constants.

In order to choose the basis functions on which this Hamiltonian acts, one considers first the ^5D ground state term of the free Fe^{2+} ion. Due to the fact that the angular dependence of a ^5D term is exactly the same as that of a single d electron, the response to an external crystal field will be the same, and thus the qualitative arguements presented in the previous section based on a single d electron are completely valid. Similar to a d electron, this ^5D term is split by the crystal field into two terms ($^5T_{2g}$ and ^5E_g) separated by 10Dq as shown in Figure 7.

The term $^5T_{2g}$ corresponds to the d-electron arrangement $t_{2g}^4\, e_g^2$, while the ^5E_g term corresponds to $t_{2g}^3\, e_g^3$.

Optical spectra of the present compounds[21] show that the cubic field splittings 10Dq are in the range 9300-10,000 cm^{-1}. Thus there will

FIGURE 7

Splitting of the ^5D Term of Fe^{2+} by the Crystal Field

FIGURE 7

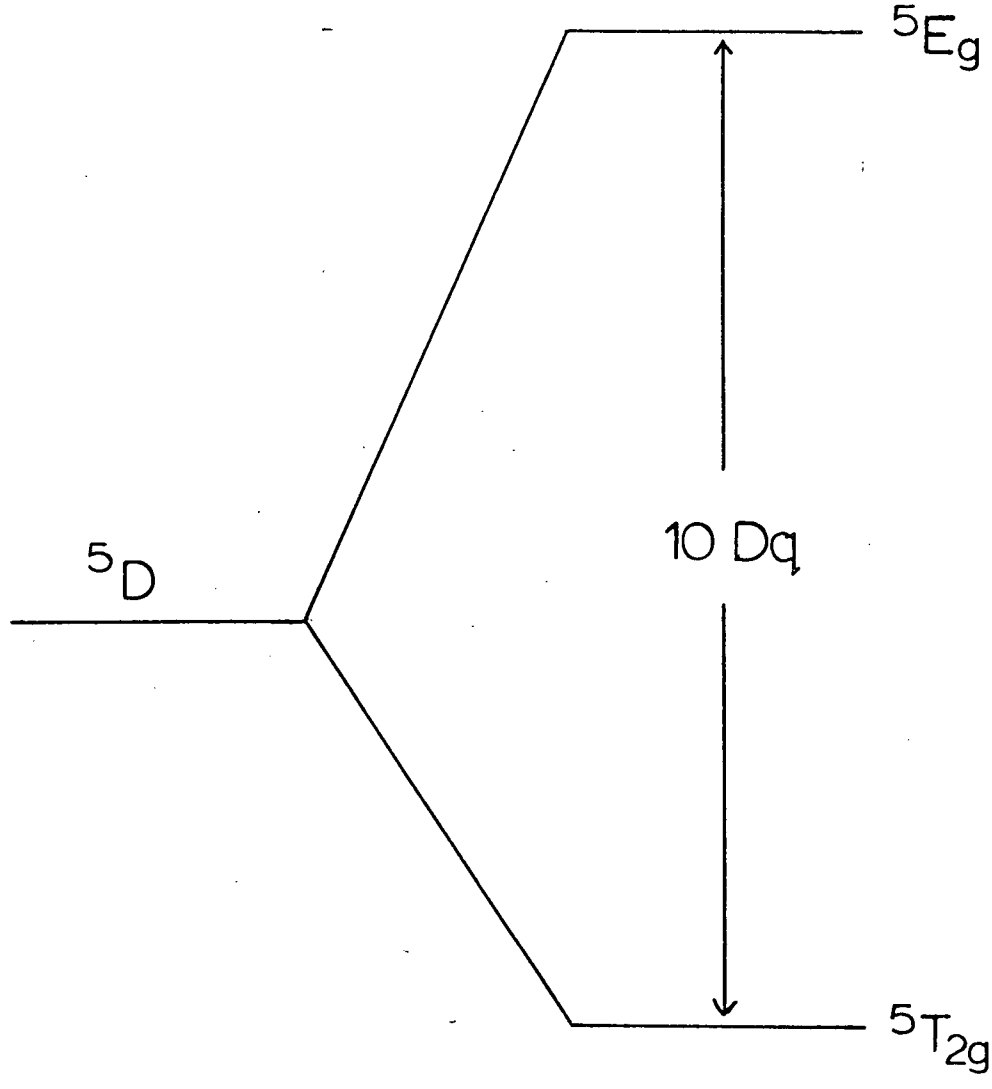

be no appreciable admixture of $^5T_{2g}$ and ^5E_g terms under our experimental conditions. Since only the ground state and the thermally accessible excited states ($\sim$200 cm^{-1} higher) are of interest in the calculation of Mössbauer and magnetic parameters, it is quite sufficient to involve only the $^5T_{2g}$ term. Thus, in order to lessen the computation times required, the ^5E_g term has been neglected (hence the absence of the cubic field term V_o in $\mathcal{H}$). This allows us to truncate the 25 x 25 matrix to a 15 x 15 matrix which contains only the $^5T_{2g}$ set of orbitals.

For the trigonally distorted complexes, the basis set of 15 $^5T_{2g}$ wavefunctions used is

$$|2,0\rangle|M_s\rangle \ , \tag{43}$$

$$\left(\sqrt{\frac{2}{3}}|2,\pm2\rangle \mp \sqrt{\frac{1}{3}}|2,\pm1\rangle\right)|M_s\rangle \tag{44}$$

where in the $|L,M_L\rangle\,|M_s\rangle$ notation, M_L is the z component of the total orbital angular momentum L, and M_s = 0, ±1, ±2 is the z component of spin angular momentum. For tetragonal distortions the corresponding basis set is

$$\frac{1}{\sqrt{2}}\left(|2,2\rangle - |2,-2\rangle\right)|M_s\rangle \ , \tag{45}$$

$$\frac{1}{\sqrt{2}}\left(|2,1\rangle \pm |2,-1\rangle\right)|M_s\rangle \ . \tag{46}$$

With these two basis sets, the 15 x 15 Hamiltonian matrices can be set up as shown in Appendix II.

The quantities Ds/λ, Dr/λ and $D\sigma/\lambda$ were treated as independent parameters which were read into the computer. The matrix was then diagonalized to obtain the eigenvalues ε_i/λ and corresponding eigenvectors $|i\rangle$ such that

$$|i\rangle = \sum_{M_s}^{5}\Big[A_{M_s}|2,0\rangle|M_s\rangle+b_{M_s}\Big(\sqrt{\tfrac{2}{3}}\,|2,-2\rangle+\sqrt{\tfrac{1}{3}}\,|2,1\rangle\Big)|M_s\rangle + C_{M_s}\Big(\sqrt{\tfrac{2}{3}}\,|2,2\rangle-\sqrt{\tfrac{1}{3}}\,|2,-1\rangle\Big)|M_s\rangle\Big] \tag{47}$$

in the trigonal case, and

$$|i\rangle = \sum_{M_s}^{5}\Big\{A_{M_s}\Big[\frac{1}{\sqrt{2}}(|2,2\rangle-|2,-2\rangle)|M_s\rangle\Big] + b_{M_s}\Big[\frac{1}{\sqrt{2}}(|2,1\rangle+|2,-1\rangle)|M_s\rangle\Big] + C_{M_s}\Big[\frac{1}{\sqrt{2}}(|2,1\rangle-|2,-1\rangle)|M_s\rangle\Big]\Big\} \tag{48}$$

in the tetragonal case, where A_{M_s} etc. are constants. These were subsequently used to calculate the quadrupole splittings and magnetic moments.

The contributions to the nine components V_{ab} $(a,b = x,y,z)$ of

the efg tensor were calculated by means of the formula[18]

$$V_{ab} = -\frac{2}{2I}\langle r^{-3}\rangle \left[\frac{3}{2} (\hat{L}_a\hat{L}_b + \hat{L}_b\hat{L}_a) - \delta_{ab}L(L+1) \right] \tag{49}$$

where $\hat{L}_a$, $\hat{L}_b$ are angular momentum operators. For each eigenstate $|i\rangle$ the ensemble averages

$$Z^{-1} \sum_{i=1}^{15} \langle i|V_{ab}/e|i\rangle \exp(-\varepsilon_i/kT) \tag{50}$$

were formed, where $Z = \sum_i \exp(-\varepsilon_i/kT)$ is the partition function, and the efg matrix was diagonalized. In the principal axis system the quadrupole splitting can be written as [see eqn.(30)]

$$\Delta E_Q = \tfrac{1}{2}eQ(1+\tfrac{\eta^2}{3})^{\frac{1}{2}} [(1-R)eq_{VALENCE} + (1-\gamma_\infty)eq_{LATTICE}] \tag{51}$$

As discussed in Chapter I, the major contribution to the efg at iron in high-spin Fe^{2+} complexes comes from the asymmetric distribution of 3d electrons. Thus to a first approximation the small lattice contribution can be neglected[18]. Secondly, since all six ligands are identical the electron distribution in the d^2sp^3 hybrid bonding orbitals should not depart significantly from spherical symmetry. Thus, we have approximated ΔE_Q as

$$\Delta E_Q = \tfrac{1}{2}e^2qQ(1-R)(1+\tfrac{\eta^2}{3})^{\frac{1}{2}} \tag{52}$$

where it is understood that q now contains contributions from the t_{2g} orbitals only. Rearranging,

$$\Delta E_Q = \tfrac{1}{2}e^2Q(1-R)[q^2+\tfrac{1}{3}(\eta q)^2]^{\frac{1}{2}}$$

$$= \tfrac{1}{2}e^2Q(1-R)(\tfrac{4}{7}\langle r^{-3}\rangle)(F_q^2+\tfrac{1}{3}F_{\eta q}^2)^{\frac{1}{2}} \qquad (53)$$

where F_q and $F_{\eta q}$ are given in terms of the principal components of the efg by[18]

$$F_q = (\tfrac{4}{7}\langle r^{-3}\rangle Z)^{-1} \sum_i \langle i|V_{zz}/e|i\rangle \exp(-\varepsilon_i/kT) \qquad (54)$$

$$F_{\eta q} = (\tfrac{4}{7}\langle r^{-3}\rangle Z)^{-1} \sum_i \langle i|(V_{xx}-V_{yy})/e|i\rangle \exp(-\varepsilon_i/kT) \qquad (55)$$

The quantity $\frac{2}{7}e^2Q(1-R)\langle r^{-3}\rangle$ has been estimated[18,37] to have a numerical value of about 4.1 mm s^{-1}, whence

$$\Delta E_Q = 4.1(F_q^2+\tfrac{1}{3}F_{\eta q}^2)^{\frac{1}{2}} \text{ mm } s^{-1} \qquad (56)$$

For various choices of the splitting parameters Ds, Dr, Dσ and λ, eqn.(56) can be used to generate curves of ΔE_Q as a function of temperature, which can then be compared with experimental data. The parameter values obtained will of course depend on the numerical factor in eqn. (56); the value of 4.1 mm s^{-1} is the one which has usually been employed by other workers.[18,36,37]

In order to deduce crystal field parameters from the Mössbauer data via eqn. (56), one can proceed as follows. For three of the compounds the spectra obtained in applied magnetic fields indicated that $\eta \approx 0$, so that the efgs in these cases have effectively axial symmetry. For these, Dr was set to zero. (The exception was the TMSO complex which is discussed below.) Also, the restriction $70 \leq \lambda \leq 103$ cm^{-1} was imposed. Theoretical curves were plotted in the form ΔE_Q vs kT/λ. Comparison of such curves, calculated for several different ranges of parameter values, with the experimental data then provided reasonable first estimates of Ds, $D\sigma$ and λ. Since changes in these three parameters affect the computed curves in rather different ways (see below and ref.36), it is relatively straightforward to decide the direction in which these first estimates should be varied, and at this point, least squares techniques were adopted to refine the parameter values. λ was allowed to vary in steps of ± 5 cm^{-1}, 3Ds in steps of ± 10 cm^{-1} and $D\sigma$ in steps of ± 2 cm^{-1}. Within these step limitations "best fit" sets of Ds, $D\sigma$, λ values (as judged by standard deviations,) were obtained, and these appear in Table V. Figure 8 compares the experimental quadrupole splitting data with theoretical curves computed from these parameter values.

For $Fe(TMSO)_6(ClO_4)_2$ the magnetic perturbation spectrum indicated that η was quite large, about 0.7, showing clearly the presence of a rhombic distortion, so that in this case $Dr \neq 0$. This might seem to complicate matters somewhat, since as Gibb[36] pointed out, changes in Dr have rather similar effects on the calculated curves as do changes in Ds. Indeed, Gibb[36] has questioned whether one can make meaningful estimates of Dr from ΔE_Q data. What he failed to consider, however, is that one now has an additional experimental quantity to hand, namely the value of η,

TABLE V

Crystal Field Parameters Derived from Quadrupole Splitting Data

Compound	3Ds(cm^{-1})	12Dr(cm^{-1})	λ(cm^{-1})	Dσ(cm^{-1})	κ[b]
$Fe(DMSO)_6(ClO_4)_2$	-500		103	28	0.89
$Fe(DPSO)_6(ClO_4)_2$	-475		90	23	0.90
$Fe(PyNO)_6(ClO_4)_2$	-455		80	24	0.94
$Fe(TMSO)_6(ClO_4)_2$	-440	-250	80	28	0.88

[b] Orbital reduction factor derived by fitting magnetic moment data, using Ds, λ and Dσ values obtained from Mössbauer data.

FIGURE 8

Comparison of Observed and Calculated Quadrupole Splittings as a Function of Temperature for the $FeL_6(ClO_4)_2$ Complexes

× Observed

Ⓞ Calculated

FIGURE 8

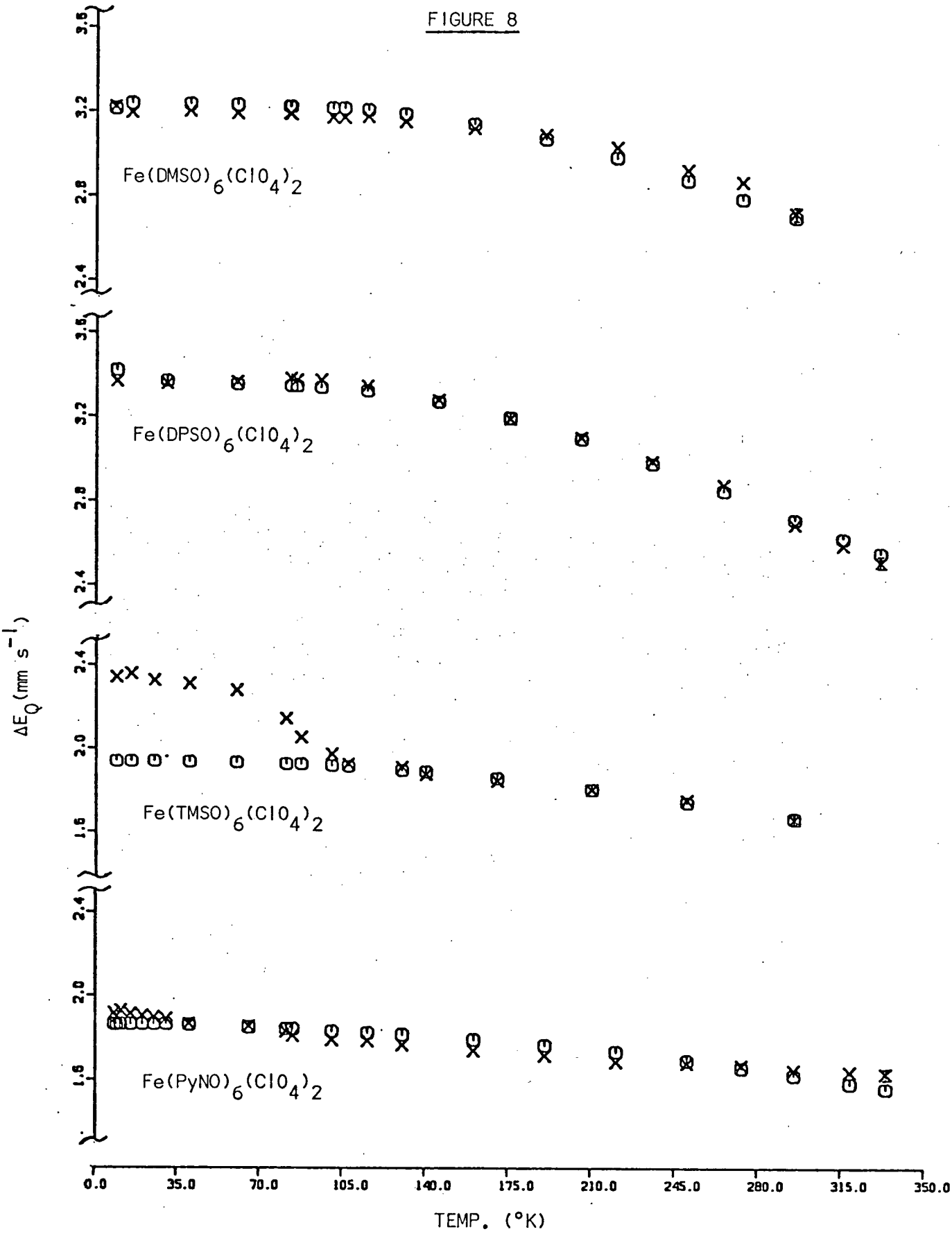
Fe(DMSO)6(ClO4)2
Fe(DPSO)6(ClO4)2
Fe(TMSO)6(ClO4)2
Fe(PyNO)6(ClO4)2
ΔEQ (mm s-1)
TEMP. (°K)
0.0
35.0
70.0
105.0
140.0
175.0
210.0
245.0
280.0
315.0
350.0

so that one need only consider pairs of Ds and Dr values consistent with both $\Delta E_Q(T)$ and η. The crystal field parameters listed in Table V for the TMSO derivative were therefore obtained with the additional constraint $0.6 \leq \eta_{calc.} \leq 0.8$. It should be noted that only the high temperature portion of the ΔE_Q vs T curve was fitted, since as mentioned above there appears to be anomalous behaviour of ΔE_Q for this compound at low temperature.

The effective magnetic moment μ_{eff} can be calculated from the eigenvectors and eigenvalues obtained above, using second-order perturbation theory[30,38]. The susceptibility χ_k in a particular direction (k = x,y,z) is given by

$$\chi_k = N Z^{-1} \sum_i \left([W_{i,k}^{(1)}]^2/kT - 2W_{i,k}^{(2)} \right) \exp(-\varepsilon_i/kT) \qquad (57)$$

where

$$W_{i,k}^{(1)} = \langle i|\hat{\mu}_k|i\rangle \qquad (58)$$

$$W_{i,k}^{(2)} = \sum_{j \neq i} |\langle i|\hat{\mu}_k|j\rangle|^2/(\varepsilon_i - \varepsilon_j) \qquad (59)$$

$$\hat{\mu}_k = -\beta(\kappa\hat{L}_k + 2\hat{S}_k) \qquad (60)$$

N is Avogadro's number, β the Bohr magneton and κ the orbital reduction factor[39]. (In highly covalent compounds κ may be as small as 0.7, but in ionic complexes is usually close to unity.) The corresponding magnetic moment in the k direction is

$$\mu_k = (3kT\chi_k/N\beta^2)^{\frac{1}{2}} \qquad (61)$$

in units of Bohr magnetons, and the effective moment is then obtained as

$$\mu_{eff} = \frac{1}{3}(\mu_x^2 + \mu_y^2 + \mu_z^2)^{\frac{1}{2}} \qquad (62)$$

Owing to the small temperature dependence of μ_{eff} for all four complexes and to the fact that the measurements do not extend below 80°K, it was clearly impractical to try to estimate all the quantities Ds, Dσ, λ and κ from these data. Thus the values of Ds, Dσ and λ obtained from fitting the Mössbauer results were employed to fit the μ_{eff} vs T data by adjusting κ. In each case the value of κ so found is about 0.9, which seems very reasonable for complexes of this type[39]. It can be seen from Figure 9 that the fit of the data is certainly adequate, so that the μ_{eff} values are fully consistent with the parameters listed in Table V.

Since the crystal field treatment that has been employed here is only approximate, the derived parameters should be viewed accordingly. However, several comments on the results are appropriate here. Firstly, one sees that the magnitudes of the axial fields are very similar for all four solvates despite the fact that the ΔE_Q values show marked differences. This is, of course, a consequence of the different orbital ground states, but clearly illustrates that it is quite inappropriate to argue about the magnitude of the crystal field splitting in a compound on the basis of a single measurement of $|\Delta E_Q|$.

Secondly, with the exception of the DMSO complex, the λ values are about 80-90% of the free ion value (λ_o = 103 cm^{-1}), suggesting a slight delocalization of the ferrous 3d electrons onto the ligands[39]. A satisfactory fit of the data for $Fe(DMSO)_6(ClO_4)_2$ could not be obtained

FIGURE 9

Comparison of Observed and Calculated Effective Magnetic Moments as a Function of Temperature for the $FeL_6(ClO_4)_2$ Complexes

× Observed

Ⓞ Calculated

FIGURE 9

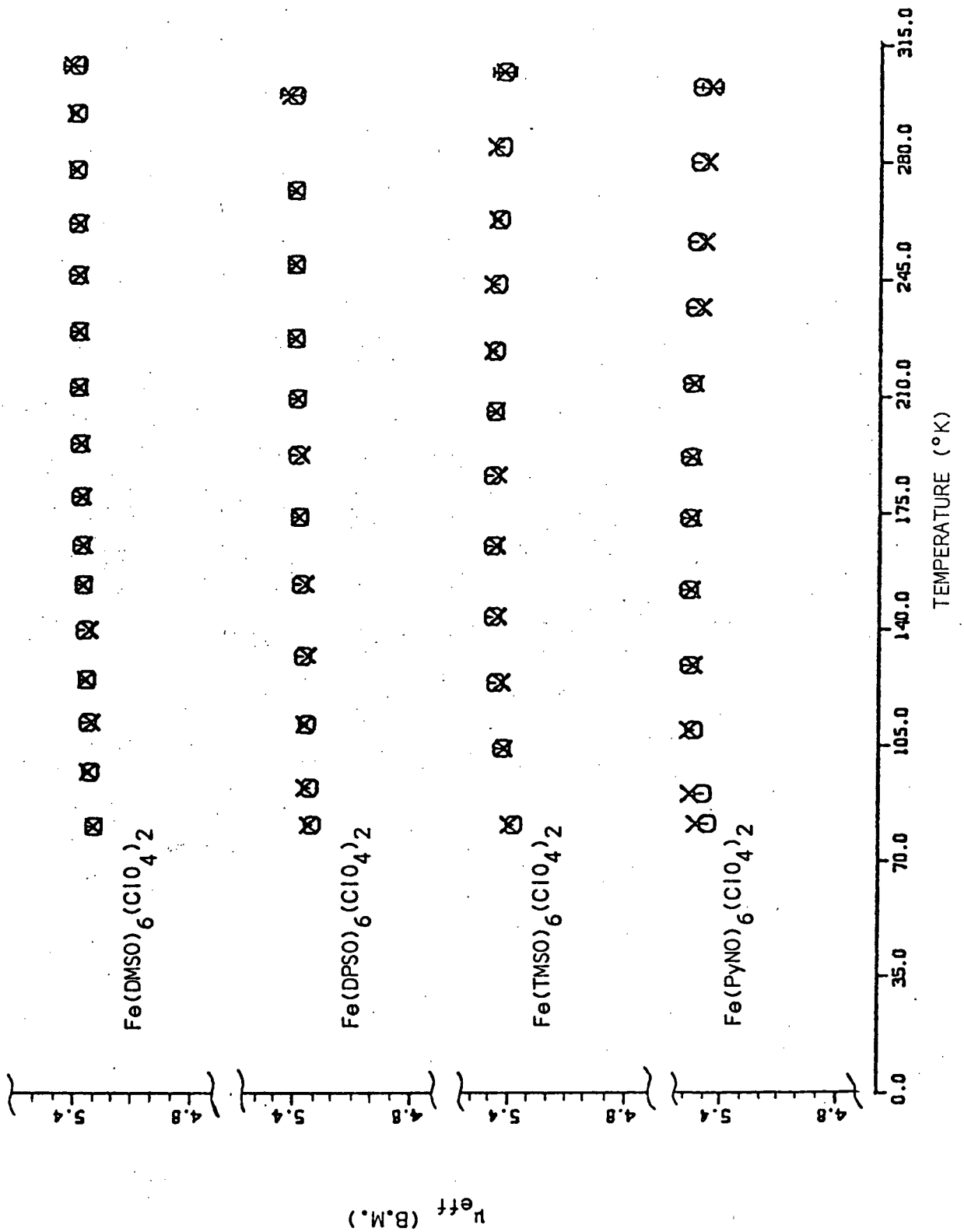
Fe(DMSO)6(ClO4)2
Fe(DPSO)6(ClO4)2
Fe(TMSO)6(ClO4)2
Fe(PyNO)6(ClO4)2
4.8
5.4
0.0
35.0
70.0
105.0
140.0
175.0
210.0
245.0
280.0
315.0
TEMPERATURE (°K)
μeff (B.M.)

using a λ value less than 100 cm^{-1}, which implies very little if any metal → ligand back π donation in this case. This may be due to an absence of low-lying π-acceptor orbitals in DMSO.

The spin-spin coupling term $D\sigma(S_z^2 - 2)$ was introduced here to account for the low temperature behaviour of ΔE_Q. An examination of Gibb's results[36] in which this term was omitted, shows that for the parameter ranges 100 $cm^{-1} \leq Ds \leq 300\ cm^{-1}$ and 60 $cm^{-1} \leq \lambda \leq 100\ cm^{-1}$, which are appropriate here, the ΔE_Q vs T curves exhibit maxima, and a decline in ΔE_Q at low temperature is predicted. This behaviour is not observed for any of our four complexes. Rather, it is found that below 80°K ΔE_Q is effectively constant for DMSO and DPSO derivatives and continues to increase for the TMSO and PyNO complexes. This temperature dependence cannot be duplicated in the theoretical curves unless the $D\sigma$ term is included.

The fact that the magnetic perturbation spectrum of $Fe(PyNO)_6(ClO_4)_2$ gives no indication of a non-zero η (see Figure 10) raises an interesting question. Since Kramer's theorem does not apply to even-electron systems, a non-degenerate orbital ground state is demanded by the Jahn-Teller principle[40]. Furthermore, since neither spin-orbit nor spin-spin coupling lifts the orbital degeneracy, it is therefore deduced that unless the ground state is either $|xy\rangle$ or $|z^2\rangle$ there should be a Jahn-Teller-induced rhombic distortion to produce a singlet ground state. This should lead to a non-axially symmetric efg and a non-zero η. Since η values of 0.2 or less have almost no observable effect on the triplet-doublet Mössbauer spectrum[3], it seems more likely that Dr is non-zero but just too small to be detected, than that a violation of the Jahn-Teller principle has been observed. Another possibility is that although η is apparently zero at

FIGURE 10

Mössbauer Spectra in Longitudinal Applied Magnetic Fields: (a) $Fe(DPSO)_6(ClO_4)_2$ at 220° K and H_{ext} = 50 kG; (b) $Fe(PyNO)_6(ClO_4)_2$ at 230° K and H_{ext} = 35 kG. In Both cases $e^2qQ>0$ and $\eta \simeq 0$.

FIGURE 10

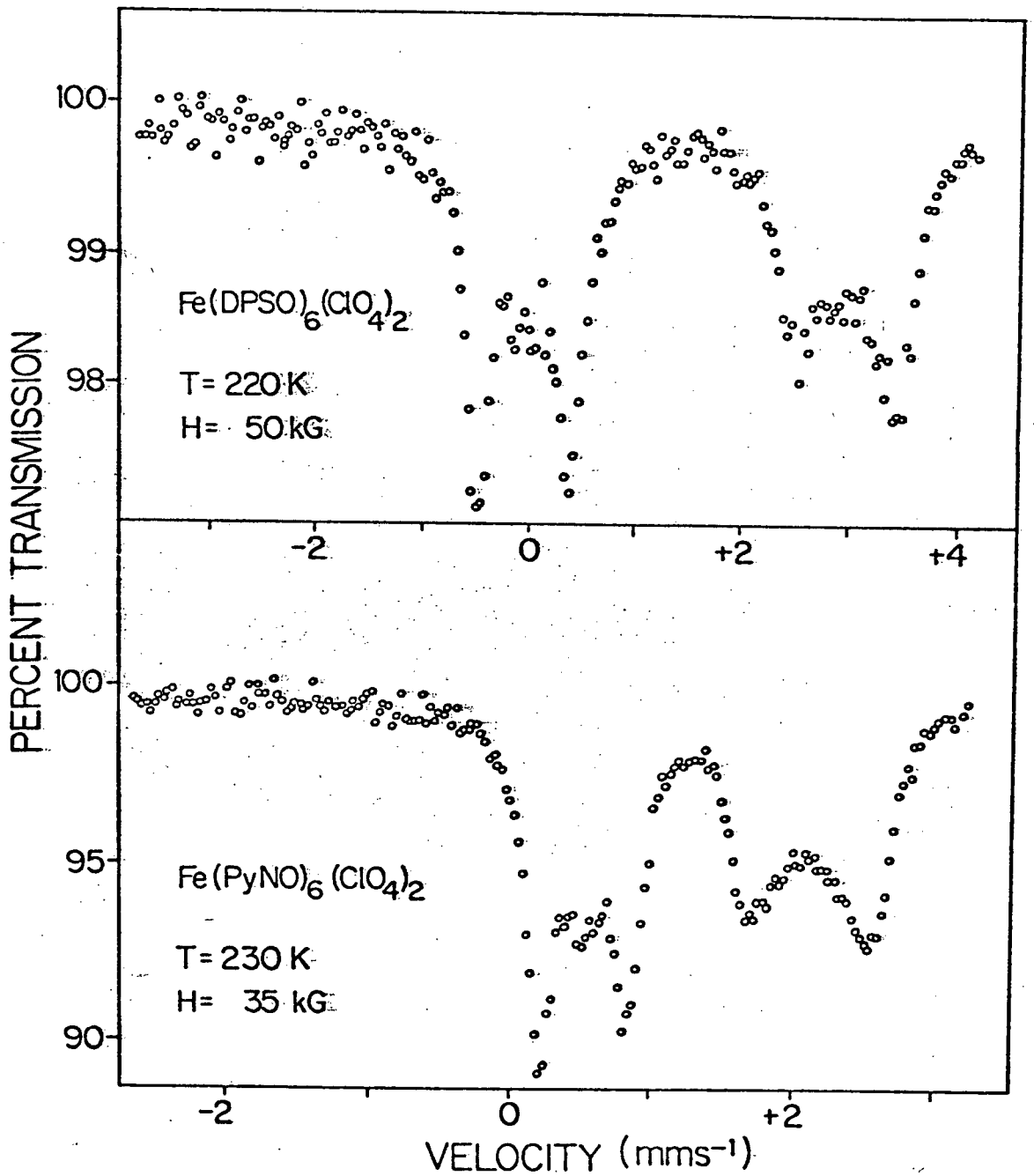
100
99
98
Fe(DPSO)6(ClO4)2
T= 220 K
H= 50 kG
-2
0
+2
+4
100
95
90
Fe(PyNO)6(ClO4)2
T= 230 K
H= 35 kG
-2
0
+2
PERCENT TRANSMISSION
VELOCITY (mms-1)

230°K where the magnetic perturbation spectrum was obtained, it may be temperature dependent and non-zero at 4.2°K. (Temperature dependent η values have been observed before.[41,42]) However, results presented below show that η cannot be as large as 0.1 even at 4.2°K, which allows us to set an upper limit of about 15 cm^{-1} for the Jahn-Teller splitting of the orbital doublet ground state in $Fe(PyNO)_6(ClO_4)_2$.

Slow Spin-Lattice Relaxation and Paramagnetic Hyperfine Splitting

In the absence of cooperative effects, spin-lattice relaxation of Fe^{2+} is usually extremely rapid. Ingalls[18] has estimated the relaxation time for Fe^{2+} in an approximately octahedral environment as about 10^{-9} - 10^{-11} sec, significantly shorter than the nuclear Larmor precession time ($\sim 10^{-7}$ sec.) Thus, if a ferrous complex is still paramagnetic down to very low temperatures, its Mössbauer spectrum is expected to remain a sharp doublet, and in the absence of an applied field, no magnetic hyperfine structure will be observed[11].

Typical of such fast-relaxing paramagnets are the $Fe(DMSO)_6(ClO_4)_2$ and $Fe(DPSO)_6(ClO_4)_2$ complexes. As shown in Figure 11 the spectra of both compounds are sharp quadrupole doublets down to about 8°K (they are still sharp at 4.2°K), and there is no evidence of paramagnetic hyperfine splitting. Similar results were reported[20] for $Fe(H_2O)_6(ClO_4)_2$ at 5°K. However, very different behaviour is observed for $Fe(PyNO)_6(ClO_4)_2$, where below 30°K the lines broaden asymmetrically (see Figure 12).

There are several possible mechanisms for asymmetric line broadening in Mössbauer spectra, all but one of which can be rejected in

FIGURE II

Zero-Field Mössbauer Spectra of $Fe(DMSO)_6(ClO_4)_2$ and $Fe(DPSO)_6(ClO_4)_2$, Showing the Absence of Line Broadening at Low Temperatures.

FIGURE 11

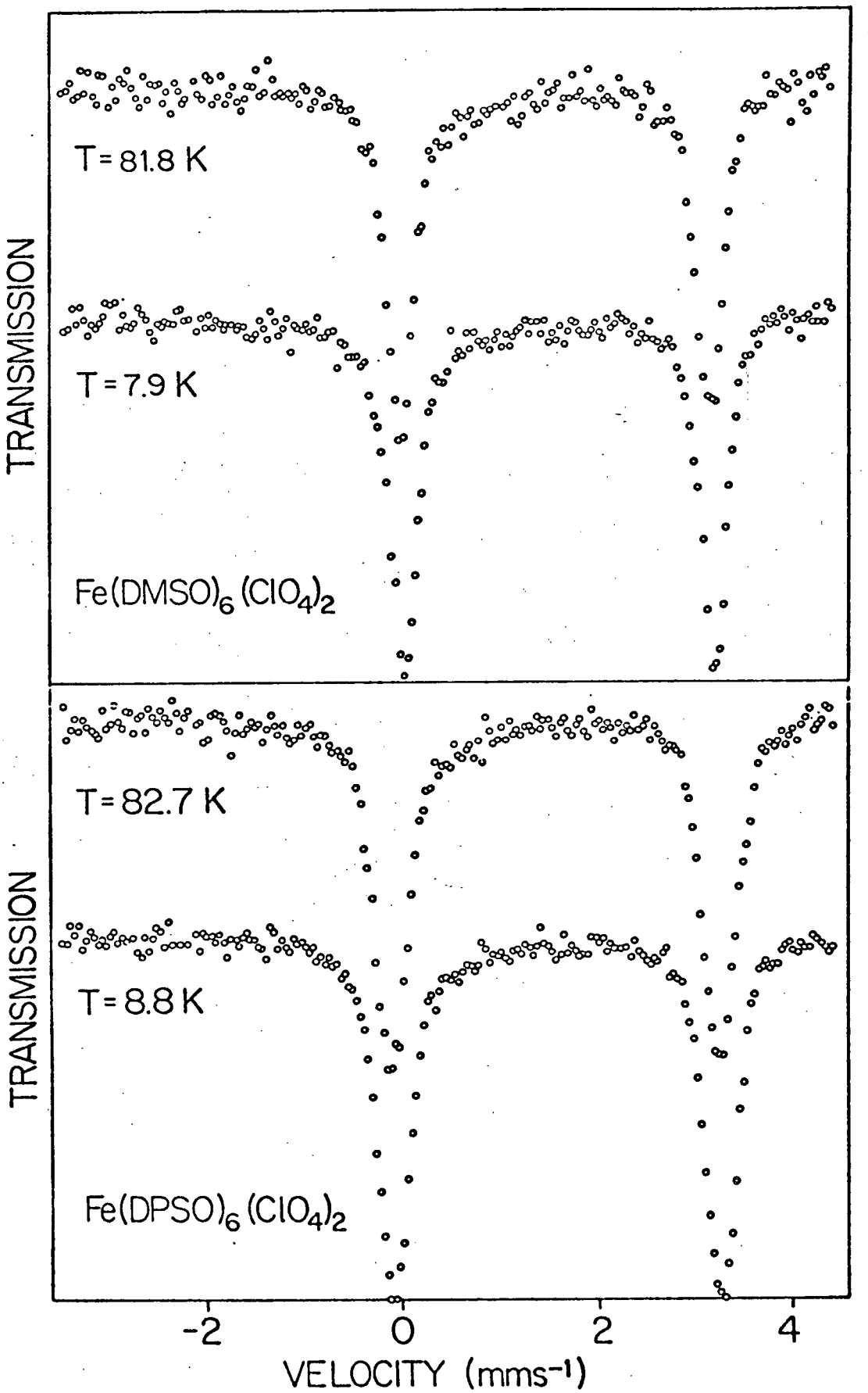
TRANSMISSION
T = 81.8 K
T = 7.9 K
Fe(DMSO)6 (ClO4)2
TRANSMISSION
T = 82.7 K
T = 8.8 K
Fe(DPSO)6 (ClO4)2
-2
0
2
4
VELOCITY (mms-1)

FIGURE 12

Mössbauer Spectra of $Fe(PyNO)_6(ClO_4)_2$ Between 30.1 and 8.2° K, Showing the Asymmetric Line Broadening Observed at Low Temperatures.

FIGURE 12

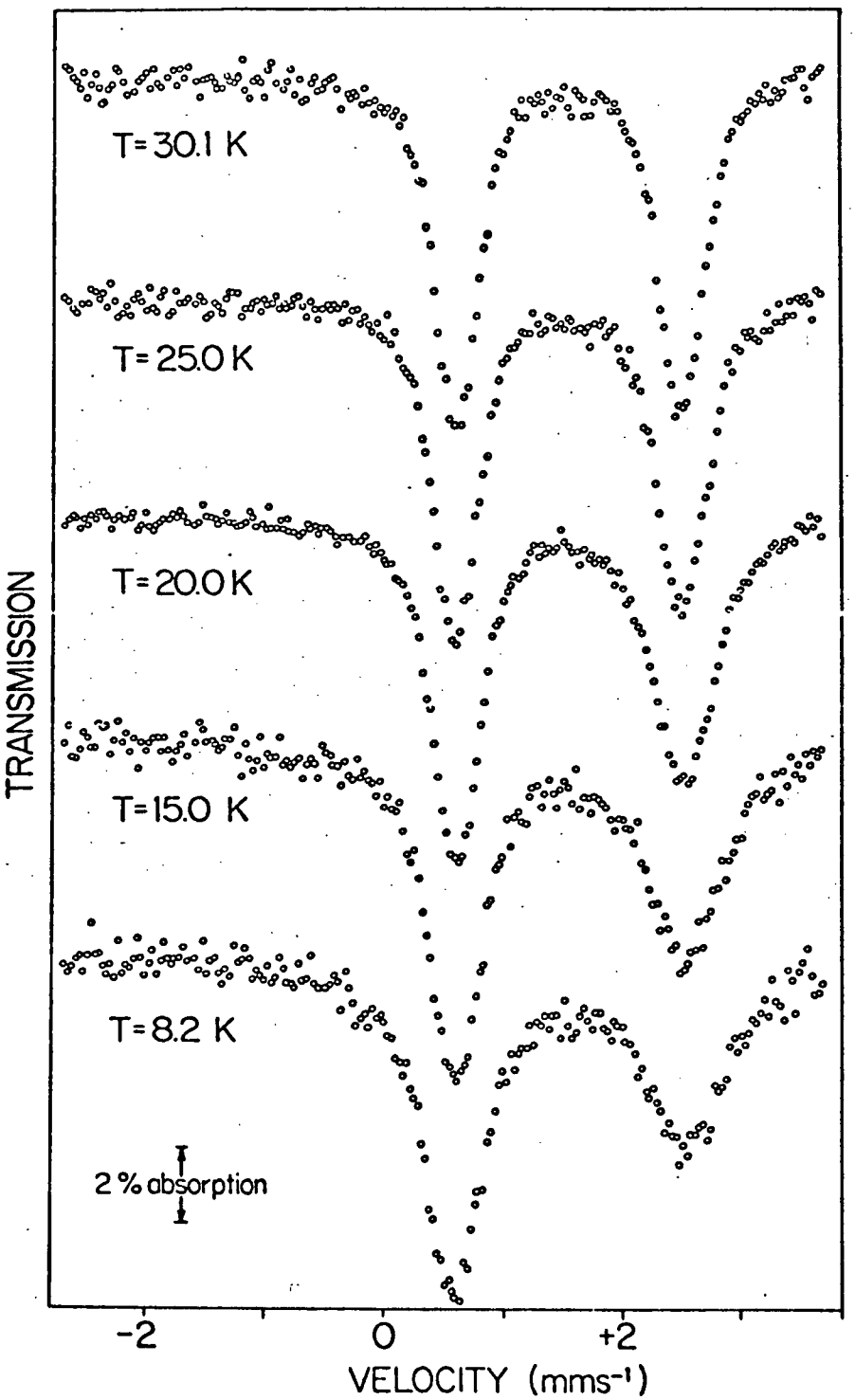
T=30.1 K
T=25.0 K
T=20.0 K
T=15.0 K
T=8.2 K
2 % absorption
TRANSMISSION
-2
0
+2
VELOCITY (mms⁻¹)

the present case.

(1) Preferential orientation of the crystallites[43]: This possibility can be eliminated at once, since the resulting asymmetry should appear at higher temperatures as well. Moreover, the samples were thoroughly ground before obtaining the spectra, and different samples of the compound showed identical behaviour.

(2) Gol'danskii-Karyagin asymmetry[44,45]: This effect arises from an anisotropy of the recoil-free fraction, and has a temperature dependence opposite to that observed here. That is, the spectrum is symmetric or nearly so at low temperature, but becomes asymmetric as the temperature increases. Moreover, in this case although the intensity ratio varies with temperature, the widths of the two lines are not affected.

(3) Antiferromagnetic exchange coupling[46-48]: With certain Fe^{3+} magnetic dimers the exchange interaction is sufficiently strong so that only the diamagnetic ground state is populated at 4.2°K, but weak enough that higher states can be populated on raising the temperature. In such cases the Mössbauer spectrum is symmetric at 4.2°K and becomes asymmetric with increasing temperature as fluctuations of the electron spins become possible. Not only is the temperature dependence of this asymmetry contrary to our observations, but such exchange coupling would be highly unlikely with six bulky ligands surrounding the Fe^{2+} ion.

(4) Slow spin-spin relaxation between Kramers doublets[49-51]: This effect is qualitatively similar to the magnetic dimer case, and again the asymmetry should increase as the temperature is raised from 4.2°K. Moreover, Fe^{2+} is not a Kramers ion, so this explanation can be discarded.

(5) Two inequivalent sites for the Fe^{2+} ions: The possibility of having two sites with slightly different isomer shifts and quadrupole splittings below 30°K cannot be excluded rigorously at this point. Such a situation might arise either from an isomeric conversion or incomplete phase transition. However, to obtain the smooth variation in spectral shape seen in Figure 12 would require that the site populations, δ and $|\Delta E_Q|$ all change continously with temperature. Magnetic perturbation spectra obtained at 4.2°K (see below) allow us to reject this possibility, since they correspond to a system in which there is only one Fe^{2+} site.
(6) Slow spin-lattice relaxation[12,50]: The spin-lattice relaxation time is temperature dependent, and increases with decreasing temperature. If the fluctuations of the electronic spins are not fast compared to the nuclear precession frequency, asymmetric line broadening will occur, with the asymmetry increasing as the temperature is lowered.

Thus, the only explanation consistent with the spectra shown in Figure 12 is an increase in the spin-lattice relaxation time at low temperature, leading to an onset of paramagnetic hyperfine splitting. This appears to be the first example of this effect in an approximately octahedral ferrous complex. The only other cases of slow-relaxing Fe^{2+} reported thus far are in the mineral gillespite ($BaFeSi_4O_{10}$)[52,53] and the tetrakis(1,8-naphthyridine) complex $Fe(C_8H_6N_2)_4(ClO_4)_2$.[15] In the former, the ferrous ions are in a square planer environment of oxygens, whilst in the latter they are octacoordinate, both arrangements being quite unusual for Fe^{2+}.

From Griffith's results[54,55] for even-electron systems, one expects that in the PyNO complex the line of the quadrupole doublet

arising from the $|\pm\frac{1}{2}\rangle_g \rightarrow |\pm\frac{3}{2}\rangle_e$ nuclear spin transitions will broaden before the $|\pm\frac{1}{2}\rangle_g \rightarrow |\pm\frac{1}{2}\rangle_e$ line as the relaxation rate decreases. This is because the lowest spin-orbit-split state is a doublet which has an effective hyperfine field parallel to the trigonal z axis[55,56]. As can be seen from Figure 2 for $\Theta = 0$, if the fluctuations are sufficiently slow so that this effective field is not time-averaged to zero, the $|\pm\frac{3}{2}\rangle_e$ state will be split by 3α whereas the $|\pm\frac{1}{2}\rangle_e$ state is split only by an amount α ($\alpha = g_I \beta_n H_{eff}$). The magnetic perturbation spectrum shown in Figure 10 confirms that the broad high-velocity line corresponds to the $|\pm\frac{1}{2}\rangle_g \rightarrow |\pm\frac{3}{2}\rangle_e$ transitions.

When the compounds $Fe(DMSO)_6(ClO_4)_2$, $Fe(DPSO)_6(ClO_4)_2$ and $Fe(PyNO)_6(ClO_4)_2$ are placed in applied magnetic fields at 4.2°K, the Mössbauer spectra obtained are completely different from the magnetic perturbation spectra at high temperatures. (No attempt was made to study the TMSO complex in applied fields at low temperature because of the added complications of a large η value and the possibility of more than one site for the Fe^{2+} ion in this case.)

Some of the results are shown in Figures 13-15. These spectra are very complex, consisting sometimes of seven or more lines, and it is obviously not possible to fit them to a 'normal' triplet-doublet pattern. Furthermore, the spectra are strongly dependent on the magnetic field strength, and for a given field show marked differences from compound to compound. Due to the complexity and sensitivity of these spectra, theoretical interpretation could potentially provide a wealth of information concerning minute details of the electronic states in these paramagnetic systems. For the same reason, the interpretation of these spectra is not likely to be easy, and it is also likely that each

FIGURE 13

Mössbauer Spectra of $Fe(DMSO)_6(ClO_4)_2$ at 4.2° K in Applied Magnetic Fields. From top to bottom the Fields are 3.4, 10, 30 and 50 kG, respectively.

FIGURE 13

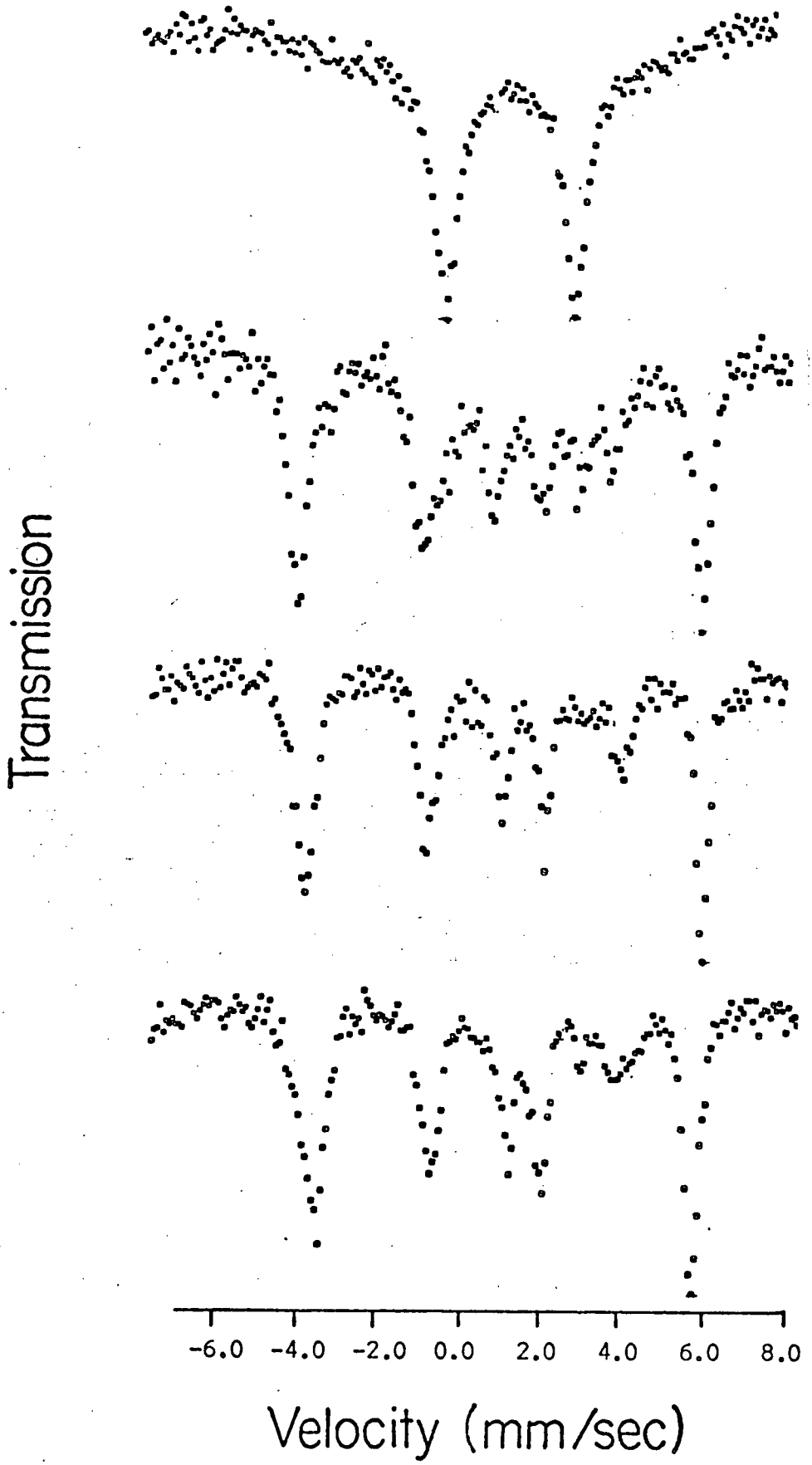

FIGURE 14

Mössbauer Spectra of $Fe(DPSO)_6(ClO_4)_2$ at 4.2° K in Applied Magnetic Fields. From top to bottom the fields are 5.6, 10, 35 and 50 kG, respectively.

FIGURE 14

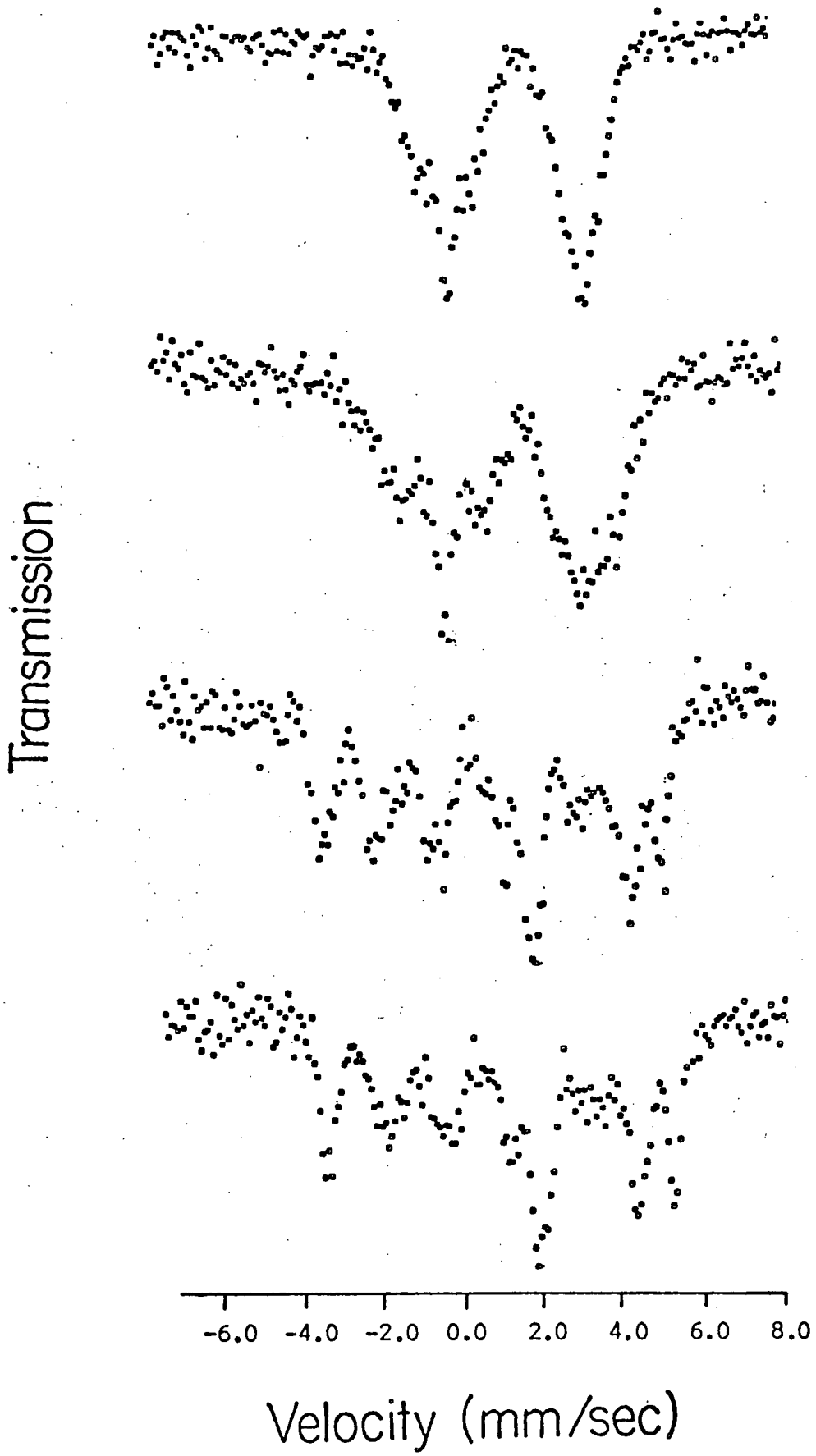

FIGURE 15

Mössbauer Spectra of $Fe(PyNO)_6(ClO_4)_2$ at 4.2° K in Applied Magnetic Fields. From top to bottom the fields are 1.1, 2.3, 5.0 and 30 kG, respectively.

FIGURE 15

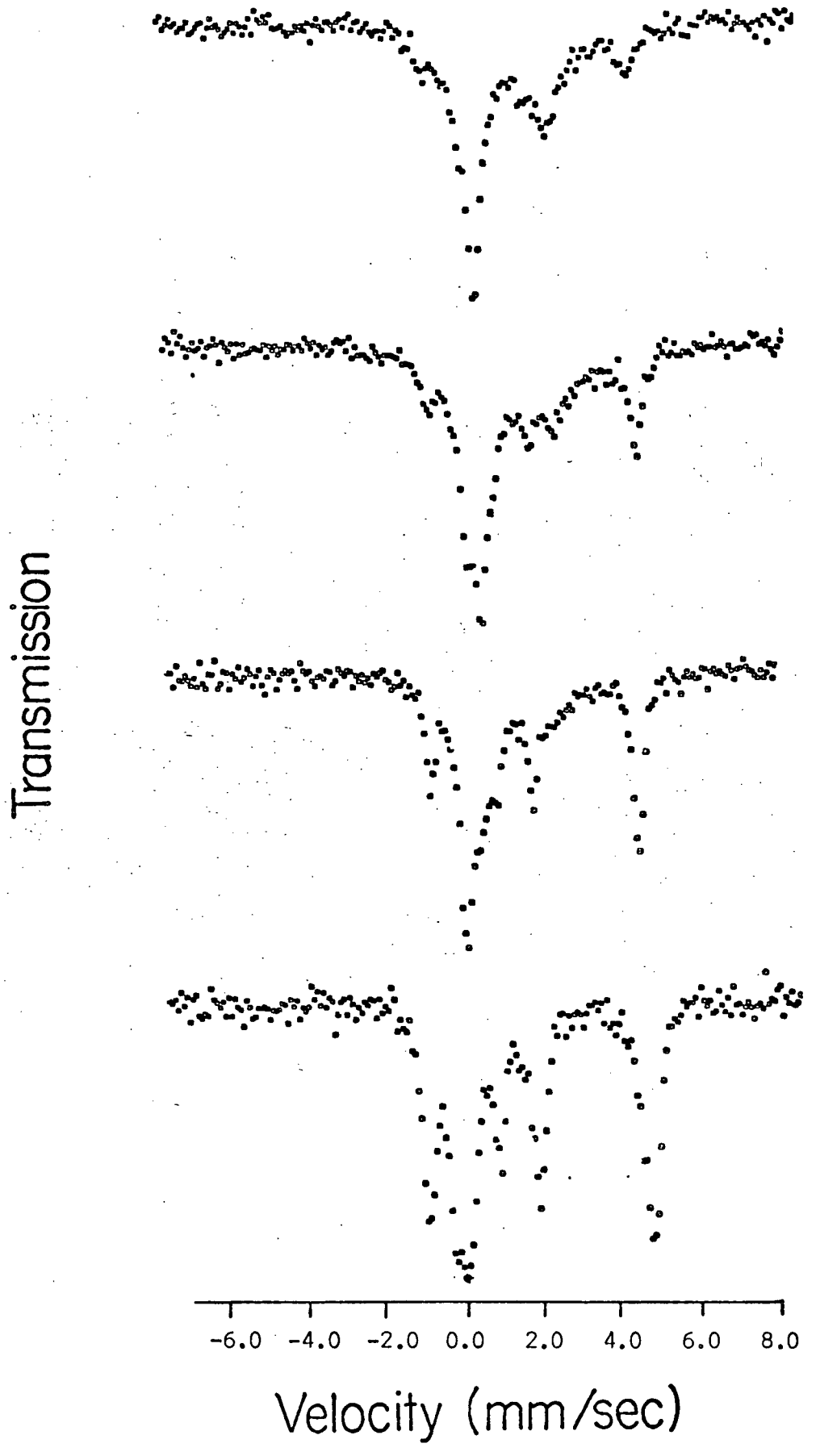

different case will have to be treated individually.

Energy level schemes obtained from the crystal field calculations above are shown in Figure 16 for the DMSO and PyNO complexes. (The scheme for L = DPSO is quite similar to the DMSO case.) One of the most interesting features of this diagram is that for $Fe(DMSO)_6^{2+}$ the ground spin-orbit multiplet is spread over only 14 cm^{-1} with the two lowest states split by only 2 cm^{-1}, while for $Fe(PyNO)_6^{2+}$ the ground doublet lies 110 cm^{-1} below the next higher spin-orbit-split state. Thus in the former case there will be significant population of both the two lowest levels at 4.2°K, whereas in the latter only the ground state will be occupied.

The fact that in the PyNO complex the lowest spin-orbit doublet is well separated from any other state suggested that it might be possible to treat this system approximately as a Kramers doublet, using the spin Hamiltonian formalism[57]. The Hamiltonian used in this approximation is

$$\mathcal{H} = \beta \underline{H} \cdot \underline{\underline{g}} \cdot \hat{\underline{S}} + \left(\frac{eQV_{zz}}{4}\right)\left[\hat{I}_z^2 - \frac{5}{4} + \frac{\eta}{3}\left(\hat{I}_x^2 - \hat{I}_y^2\right)\right]$$

$$+ \hat{\underline{I}} \cdot \underline{\underline{A}} \cdot \hat{\underline{S}} - g_n \beta_n \hat{\underline{I}} \cdot \underline{H} \qquad (63)$$

where the first term is the electronic Zeeman interaction, the second the nuclear quadrupole interaction, the third the magnetic interaction between the electron spin and the nucleus, and the fourth the direct nuclear Zeeman interaction with the external field. The $\underline{\underline{g}}$, $\underline{\underline{A}}$ and efg tensors are all assumed to have the same principal axes. We have attempted to fit the 10 kG applied field spectrum of $Fe(PyNO)_6(ClO_4)_2$ in both the slow and fast relaxation limits, and the procedure is

FIGURE 16

Energy Level Diagrams for $Fe(DMSO)_6(ClO_4)_2$ and $Fe(PyNO)_6(ClO_4)_2$ Derived from the Crystal Field Model, Showing the Effects of the Axial Field and Spin-Orbit Coupling.

$Fe(PyNO)_6(ClO_4)_2$

Excited State $|z^2\rangle$

Ground State $\sqrt{\frac{2}{3}}\,|x^2-y^2\rangle - \sqrt{\frac{1}{3}}\,|xz\rangle$

$\sqrt{\frac{2}{3}}\,|xy\rangle + \sqrt{\frac{1}{3}}\,|yz\rangle$

$Fe(DMSO)_6(ClO_4)_2$

Excited State $|xz\rangle$

$|yz\rangle$

Ground State $|xy\rangle$

FIGURE 16

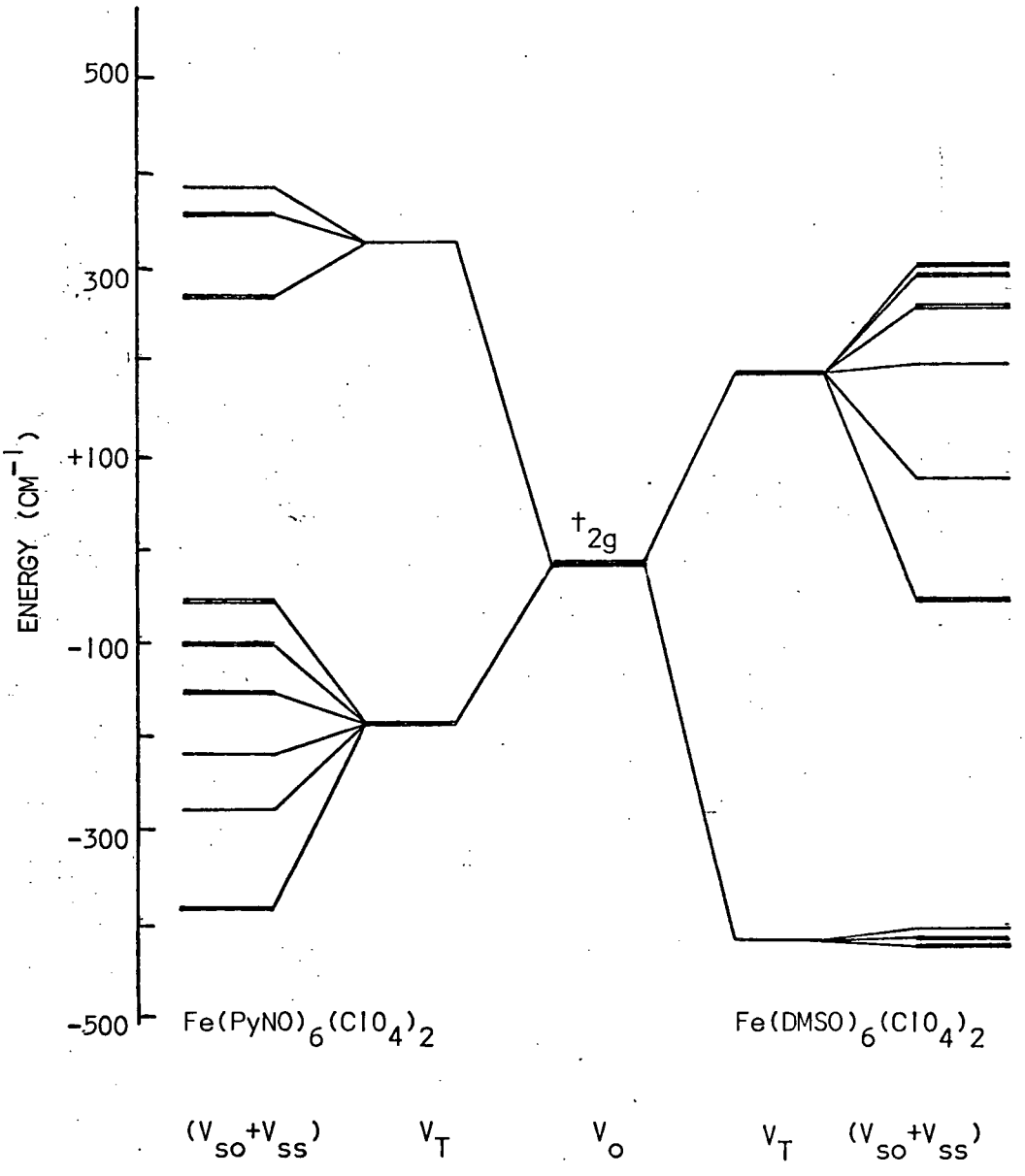
500
300
+100
-100
-300
-500
ENERGY (CM^{-1})
t_{2g}
Fe(PyNO)$_6$(ClO$_4$)$_2$
Fe(DMSO)$_6$(ClO$_4$)$_2$
$(V_{so}+V_{ss})$
V_T
V_o
V_T
$(V_{so}+V_{ss})$

briefly outlined.

Since the electronic Zeeman term in eqn.(63) is larger than the remaining terms, the first step is to use the Hamiltonian

$$\mathcal{H} = \beta \, \underline{H} \cdot \underline{\underline{g}} \cdot \hat{\underline{S}} \tag{64}$$

to find the "effective spins" $\langle \underline{S}_- \rangle$ and $\langle \underline{S}_+ \rangle$ for both members of the Kramers doublet, when the external field $\underline{H}$ makes angles θ_H, ϕ_H to the z axis of the efg. In the slow relaxation limit, the internal field due to the lower member of the doublet is given by

$$\underline{H}_{int} = - \underline{\underline{A}} \cdot \langle \underline{S}_- \rangle / g_n \beta_n \tag{65}$$

so that the last two terms in eqn.(63) become

$$\hat{\underline{I}} \cdot \underline{\underline{A}} \cdot \hat{\underline{S}} - g_n \beta_n \, \hat{\underline{I}} \cdot \underline{H} = -g_n \beta_n \, \hat{\underline{I}} \cdot (\underline{H}_{int} + \underline{H})$$

$$= - g_n \beta_n \, \hat{\underline{I}} \cdot \underline{H}_{eff} \tag{66}$$

An identical procedure is used to obtain $\underline{H}_{eff}$ for the upper member of the doublet. Spectra are then computed for each state by Lang's programme[17] as described in Chapter II, but using the $\underline{H}_{eff}$ values instead of the applied field. The thermal average of these two spectra (i.e., weighted by the appropriate Boltzmann factors) then gives the composite spectrum in the slow relaxation limit, for a given direction of $\underline{H}$ relative to the z axis of the efg. The powder averaged spectrum is obtained by integrating over all possible orientations (θ_H, ϕ_H) of $\underline{H}$

as discussed in Appendix I.

In the fast relaxation limit, once the "effective spins" have been obtained one computes the thermally averaged spin of the Kramers doublet, given by

$$\underline{\bar{S}} = \frac{\langle \underline{S}_- \rangle \exp(-g\beta H/2kT) + \langle \underline{S}_+ \rangle \exp(+g\beta H/2kT)}{\exp(-g\beta H/2kT) + \exp(+g\beta H/2kT)} \qquad (67)$$

$\underline{H}_{int}$ is now calculated as in eqn.(65), but using $\underline{\bar{S}}$ instead of $\langle \underline{S}_\pm \rangle$, and the resulting $\underline{H}_{eff}$ is employed in Lang's programme[17] to compute the spectrum for a particular direction of $\underline{H}$ and then the powder averaged spectrum.

Due to the fact that $\eta \simeq 0$ for this complex it was assumed in the parameterization that $g_x = g_y = g_\perp$ and $A_x = A_y = A_\perp$. The components of the $\underline{g}$ and $\underline{\underline{A}}$ tensors, $g_\perp$, $g_{||}$ ($= g_z$) and $A_\perp$, $A_{||}$ ($=A_z$) were then varied in order to fit the measured 10 kG magnetic perturbation spectrum. A satisfactory fit was achieved in the slow relaxation limit with the parameters:

$$g_\perp = 1.0,\ g_{||} = 7.0,\ A_\perp = 1.4 \text{ mm s}^{-1} \text{ and } A_{||} = -1.9 \text{ mm s}^{-1}.$$

The fitted spectrum is shown in Figure 17. The agreement between the theoretical and experimental spectra is quite good considering the approximate nature of the model used in the calculations.

In the process of comparing experimental and theoretical spectra, several interesting observations were made. Firstly, it was found that the shape of the computed spectrum is very sensitive to the

FIGURE 17

The 10 kG Magnetic Perturbation Spectrum of $Fe(PyNO)_6(ClO_4)_2$ at 4.2° K. The Solid Line is the Theoretical Spectrum Calculated in the Spin Hamiltonian Approximation.

FIGURE 17

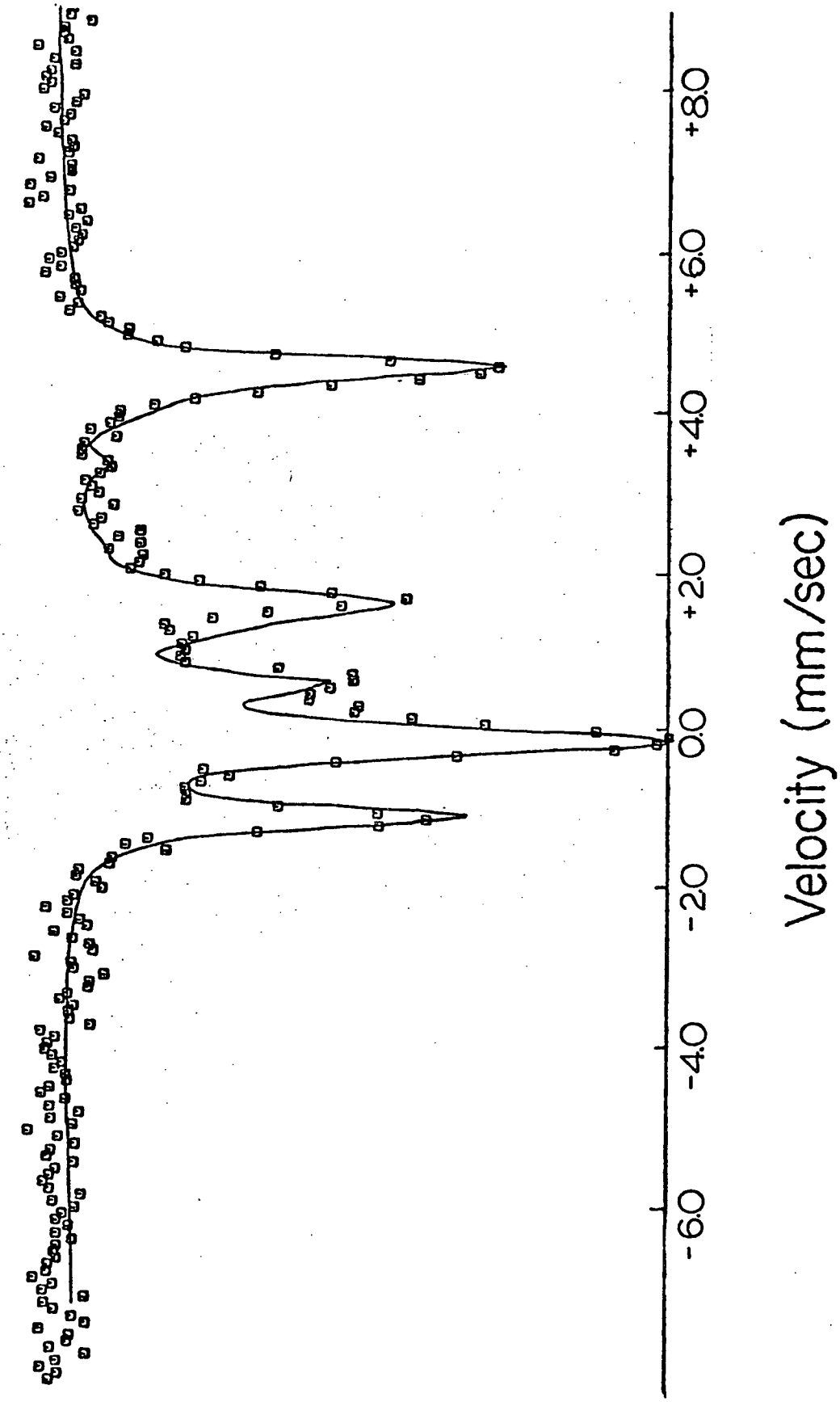

values chosen for $A_{\perp}$ and $A_{\parallel}$, particularly the latter, although not very sensitive to a change of sign of $A_{\parallel}$. (This parameter is tentatively assigned to be negative since a slightly better fit was obtained in this case.) On the other hand the spectra were fairly insensitive to the g values assumed, as long as they were highly anisotropic. Secondly, the very important fact emerged that spectra calculated on the assumption of fast spin relaxation between the two members of the doublet (i.e., using a time-averaged H_{eff}) do not resemble the experimental spectrum for any combination of the parameter values. Slow electronic relaxation is therefore confirmed for this system. Thirdly, an attempt was made to fit the spectrum with a non-zero asymmetry parameter by setting $\eta = 0.1$ in eqn.(63). Even this small η value (which corresponds to a rhombic distortion of 15 cm^{-1}) caused significant changes in the computed spectrum, and agreement with the measured spectrum was worse than with $\eta = 0$. This sensitivity of the spectra to small values of η is quite different from the usual diamagnetic case[3]. Fourthly, it was not possible to produce spectra that resemble the experimental results for either the DMSO or DPSO complexes using this type of ground state, in either the slow or fast relaxation limits. Because of the small splittings of the ground spin-orbit multiplets in these complexes, a more elaborate treatment will be needed to explain the observed spectra.

From the g and A values obtained it is seen that the z axis of the efg tensor is the easy axis of magnetization, with $|A_{\parallel}| > |A_{\perp}|$. The highly anisotropic g values also reflect the fact that the internal field is strong along the efg z axis. An anisotropic $\underline{\underline{g}}$ tensor is expected for high-spin Fe^{2+} systems because the ground state doublet is

not of pure spin character. The extensive mixing of orbital character into the doublet imposes spatial dependences on the g and A values as observed.

CHAPTER IV

Compounds Showing High-Spin - Low-Spin Crossover

Introduction

It has long been predicted theoretically, that depending on the strength of the crystal field some transition metal ions can exist in either of two ground states, commonly known as the "high-spin" and "low-spin" states. The Tanabe-Sugano diagram[58] (Figure 18) shows term splittings for a d^6 electron system, such as a ferrous iron, in an octahedral crystal field. When the crystal field is weak, i.e. 10Dq/B is small (where B is the interelectronic repulsion parameter), it is seen that the ground state is $^5T_2$ which corresponds to the arrangement $t_{2g}^4 e_g^2$, with four unpaired electrons per ferrous ion. For the strong field case, it is seen that the ground state is $^1A_1$ with no unpaired electrons, i.e., $t_{2g}^6 e_g^0$.

For intermediate crystal fields where the energies of these two states are similar, it should be possible for both forms to coexist, and one might expect a crossover from one spin state to another at a particular 10Dq/B value. Since B = 1058 cm^{-1} for Fe^{2+}, the value of 10Dq appropriate to a crossover situation in this case is approximately 20,000 cm^{-1}.

This crossover phenomenon is by no means restricted to a d^6 configuration. In fact, for octahedral symmetry it is theoretically possible for d^4, d^5 and d^7 systems to exhibit crossover behaviour as well. In practice, however, only $Fe^{3+}(d^5)$, $Fe^{2+}(d^6)$ and $Co^{2+}(d^7)$

FIGURE 18

The Tanabe-Sugano Diagram for a d^6 Electron System

(Taken from Ref. 39)

FIGURE 18

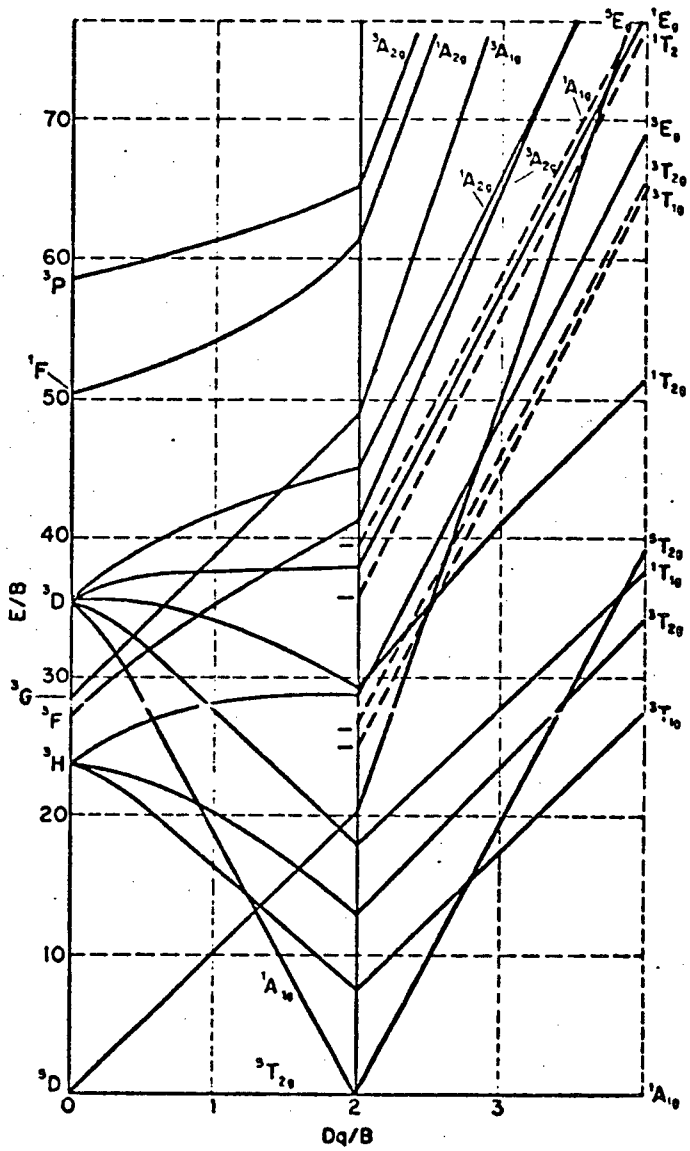
E/B
Dq/B
70
60
50
40
30
20
10
0
1
2
3
^3P
^1F
^3D
^3G
^3F
^3H
^5D
$^3A_{2g}$
$^1A_{2g}$
$^3A_{1g}$
$^1A_{1g}$
$^3A_{2g}$
$^1A_{2g}$
^3E_g
^1E_g
$^1T_2$
^3E_g
$^3T_{2g}$
$^3T_{1g}$
$^1T_{2g}$
$^3T_{2g}$
$^1T_{1g}$
$^3T_{2g}$
$^3T_{1g}$
$^1A_{1g}$
$^1A_{1g}$
$^3T_{2g}$

octahedral complexes have been found to show ground state crossover, although the phenomenon has been observed for $Ni^{2+}(d^8)$ in a square planar environment[59].

A number of iron(II) compounds are known which exhibit spin crossover, and in every case iron is bonded to six nitrogen atoms. Since the details differ significantly from one system to another, we shall review briefly the earlier work.

The first ferrous compounds for which a $^5T_2 - {}^1A_1$ crossover was observed were $Fe(phen)_2(NCS)_2$ and $Fe(phen)_2(NCSe)_2$ [60,61] (phen = 1,10-phenanthroline; see Figure 19 for the structures of this and other ligands discussed here). Many other $Fe(phen)_2X_2$ complexes are known, but all are either fully high-spin or fully low-spin depending on the ligand field strength of X. $Fe(phen)_2(NCS)_2$ has a room-temperature magnetic moment of 5.2 B.M., as expected for high-spin Fe^{2+}, while at liquid nitrogen temperature the moment is about 0.65 B.M. A Mössbauer study was carried out over the temperature range 80-300°K by Dézsi, et al.[62] In the transition region, which occurs at about 175°K, there are four lines in the Mössbauer spectra, the outer pair being characteristic of the S = 2 state and the inner pair corresponding to the S = 0 configuration. The transition is quite abrupt, and occurs over a temperature range of less than 20°K. Thus, it is not possible to interpret the crossover simply in terms of changes in thermal population of close-lying $^5T_2$ and $^1A_1$ manifolds. The observation of lines due to both S = 0 and S = 2 states in the transition region indicates that the electronic relaxation between the two spin states is slow compared to the Larmor precession frequency of the ^{57}Fe nucleus. This feature is common to

FIGURE 19

Structures of the Ligands Discussed in Chapter IV

FIGURE 19

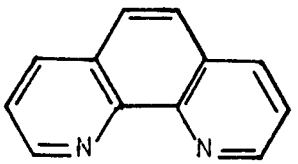

1,10-PHENANTHROLINE
(phen)

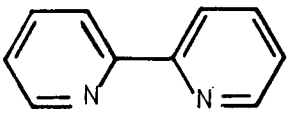

2,2'-BIPYRIDYL
(bipy)

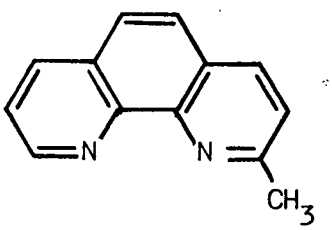

2-METHYL-1,10-PHENANTHROLINE
(mephen)

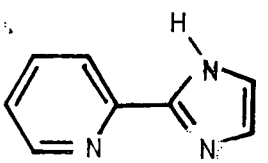

2-(2'-PYRIDYL)IMIDAZOLE
(pyim)

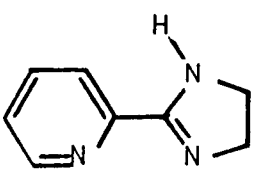

2-(2'-PYRIDYL)IMIDAZOLINE
(pyiH)

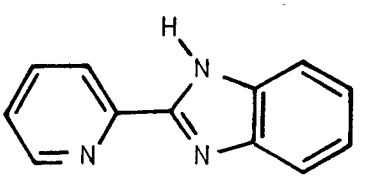

2-(2'-PYRIDYL)BENZIMIDAZOLE
(pyben)

all cases of $^5T_2$ - $^1A_1$ transitions observed to date. Fisher and Drickamer[63] studied the response to high pressure of several iron(II) phenanthroline complexes and found a complicated dependence of high-low spin equilibrium on pressure.

König and co-workers[64,65] have carried out an X-ray structure analysis of $Fe(bipy)_2(NCS)_2$ (bipy = 2,2'-bipyridyl, Figure 19), which shows behaviour similar to $Fe(phen)_2(NCS)_2$, and found that the low-spin species in fact has a shorter Fe-N (mean) bond distance than does the high-spin species.

Spin crossover has also been observed in a ferrous complex with the chelating ligand hydro-tris(1-pyrazolyl)borate[66,67]. By changing organic substituents on the ligand it was possible to prepare compounds which were either pure high-spin, pure low-spin, or which showed spin equilibrium. For the latter complex it was found that a single crystal was completely pulverized by slow thermal cycling through the transition region, and it was suggested that the two spin forms have different crystal structures[67].

The four salts $Fe(mephen)_3X_2$ (mephen = 2-methyl-1,10-phenanthroline, Fig. 19; X = ClO_4^-, BF_4^-, I^-, BPh_4^-) have been studied in detail[68,69]. In each case there is an incomplete change in ground state, with lines due to high-spin iron(II) still present in the Mössbauer spectra at 4.2°K. These results were interpreted as indicating that not all of the molecules are involved in the $^5T_2$ - $^1A_1$ equilibrium, and that there is a permanently paramagnetic fraction of molecules. It has also been shown in these and other cases[68-70] that the energy separation between the $^5T_2$ and $^1A_1$ terms is not constant, but has a pronounced

temperature dependence.

Certain ferrous complexes of both 2-(2'-pyridyl)imidazole (pyim, Figure 19) and 2-(2'-pyridyl)imidazoline (pyiH, Figure 19) also show behaviour indicative of the $^5T_2$ - $^1A_1$ crossover, but there are important differences in detail. For example, $Fe(pyiH)_3(ClO_4)_2$ exists as two magnetic isomers. One is diamagnetic at room temperature and below, whereas the other shows an abrupt change in magnetic moment at about 120°K (μ_{eff} = 5.25 B.M. at 295°K and 2.7 B.M. at 83°K)[71]. The Mössbauer spectrum of the latter isomer at 80°K shows lines due to both high- and low-spin iron(II), with only the high-spin species present at 294°K. On the other hand, $Fe(pyim)_3(ClO_4)_2 \cdot H_2O$ and several other $Fe(pyim)_3^{2+}$ salts[73] show very gradual changes in magnetic moment with temperature. The μ_{eff} values do not exceed about 4.0 B.M. at room temperature and are in the range 0.6 - 2.9 B.M. at about 90°K. Mössbauer spectra of all the pyim complexes studied thus far indicate a greater population of the S = 0 state at 295°K.

In summary, none of the $^5T_2$ - $^1A_1$ crossovers in iron(II) complexes observed to date can be explained by a simple thermal equilibrium between two states. The electronic relaxation time is long ($\gtrsim 10^{-7}$ s) and the transition often seems to involve a change in dimensions or configuration of the complex. The transition may occur over a temperature range of only a few degrees, or may be spread over more than 100 degrees. König and Kremer[70] have classified compounds of the former type where one can define a specific transition temperature as "Group I" compounds, and those of the latter type where the moment changes gradually with temperature as "Group II" compounds.

The ligands pyim and pyiH are of particular interest because the $\geq$NH group on the imidazole ring shows changes in acidity when the ligands are chelated to various metals[74]. Moreover, the marked differences in behaviour of the $Fe(pyim)_3^{2+}$ and $Fe(pyiH)_3^{2+}$ complexes shows that the crossover phenomenon is extremely sensitive to minor changes in the ligand structure. It was thought that ferrous complexes of the closely related compound 2-(2'-pyridyl)benzimidazole (pyben, Figure 19) might also show high-spin - low-spin crossover. If so, they might provide more information on the effect of the imino hydrogen on the transition characteristics. We have therefore prepared and studied a number of salts of formula $Fe(pyben)_3A_2 \cdot xH_2O$ ($A = ClO_4^-$, NO_3^-, NCS^-, Br^-, I^-, BF_4^-, BPh_4^-, $[Cr(NH_3)_2(NCS)_4]^-$; x = 0,1,2, but not all combinations). These complexes do indeed show $^5T_2$ - $^1A_1$ spin equilibria, and the details are strongly affected by the nature of the anion A and the number of waters of crystallization.

Materials

The chemicals used were obtained commercially and used without further purification. The sources of these compounds were as follows:

Ferrous chloride, anhydrous: Alfa Inorganics;

Ferrous perchlorate hexahydrate: Matheson, Coleman and Bell;

Ferrous bromide (99%) and ammonium tetrafluoroborate: ROC/RIC;

Ferrous ammonium sulphate, potassium iodide, potassium thiocyanate, sodium tetraphenylborate and ammonium tetrathiocyanatodiamminechromate(III) (Reinecke salt): Fisher Scientific;

Ammonium nitrate: BDH

2-(2'-pyridyl)benzimidazole: Aldrich Chemicals.

Preparation of the Complexes

Some of the complexes synthesized were found to be slightly moisture sensitive, while the ferrous starting materials were very sensitive to oxygen. Thus the initial mixing of reagents in the preparation of these compounds was carried out under a dry nitrogen atmosphere. Analytical data are listed in Table VI.

Tris[2-(2'-pyridyl)benzimidazole]iron(II) perchlorate monohydrate, $Fe(pyben)_3(ClO_4)_2 \cdot H_2O$

4 g of ferrous perchlorate hexahydrate in 30 ml of 100% ethanol was added to 6.5 g of ligand in 200 ml of 100% ethanol at room temperature. The complex precipitated after a few minutes and was filtered and washed with 100% ethanol. The orange coloured product was dried *in vacuo*.

Tris[2-(2'-pyridyl)benzimidazole]iron(II) perchlorate dihydrate, $Fe(pyben)_3(ClO_4)_2 \cdot 2H_2O$

This was obtained by leaving the above monohydrate in air for one-half hour. The brown crystals were then collected and analysed.

Tris[2-(2'-pyridyl)benzimidazole]iron(II)bromide, $Fe(pyben)_3Br_2$

A typical preparation was as follows: 0.8 g of anhydrous ferrous bromide in 30 ml of 100% ethanol was added to 2.4 g of ligand in 100 mlof 100% ethanol at room temperature. The deep red solution was filtered, concentrated under reduced pressure to half volume and left to stand overnight. The orange crystals were collected, washed with 100% ethanol, and dried *in vacuo*.

Tris[2-(2'-pyridyl)benzimidazole]iron(II) iodide, $Fe(pyben)_3I_2$

0.2 g of anhydrous ferrous chloride in 30 ml methanol was added to 1.1 g of ligand in 80 ml methanol. The deep red solution was filtered through a fine sintered glass filter into 50 ml of an aqueous solution containing 5 g of potassium iodide. The volume was reduced to about 80 ml, and the solution was cooled in an ice bath for 4 h. The red-orange crystals were collected by filtration and washed several times with cold water. The product was dried *in vacuo*.

Tris[2-(2'-pyridyl)benzimidazole]iron(II) nitrate monohydrate, $Fe(pyben)_3(NO_3)_2 \cdot H_2O$

0.5 g of $Fe(pyben)_3(ClO_4)_2 \cdot H_2O$ in 200 ml of methanol was added to a large excess of ammonium nitrate in a minimum volume ($\sim$ 30 ml) of water. The solution was concentrated under reduced pressure to a volume of about 60 ml and left to stand overnight. The red-orange crystals were collected and washed with water. The product was recrystallized from cold methanol and dried *in vacuo*.

Tris[2-(2'-pyridyl)benzimidazole]iron(II) thiocyanate monohydrate, $Fe(pyben)_3(NCS)_2 \cdot H_2O$

1.2 g of 2-(2'-pyridyl)benzimidazole was dissolved in 70 ml of 95% ethanol and 55 ml of water added. 0.7 g of ferrous ammonium sulphate was dissolved in 70 ml of water to which was added 50 ml of 95% ethanol. The ice cold ferrous ammonium sulphate solution was added with stirring to the ligand solution in an ice bath, and 1.6 g of potassium thiocyanate dissolved in 30 ml of ice cold water was immediately added to the above mixture. The resulting red solution was left in the ice bath overnight. The large orange crystals were filtered, washed with water several times, and dried *in vacuo*.

Dithiocyanatobis[2-(2'-pyridyl)benzimidazole]iron(II), $Fe(pyben)_2(NCS)_2$

0.5 g of ferrous chloride in 50 ml of methanol was added to 2.3 g of ligand in 100 ml of methanol. The deep red solution formed was added to 5 g (large excess) of potassium thiocyanate dissolved in a minimum volume of water. The solution was boiled under reflux for 15 min. The red precipitate which formed was collected, recrystallized from methanol, and dried *in vacuo*.

Tris[2-(2'-pyridyl)benzimidazole]iron(II) tetrafluoroborate monohydrate, $Fe(pyben)_3(BF_4)_2 \cdot H_2O$

1.3 g of $Fe(pyben)_3Br_2$ in 230 ml of methanol was added to 4 g of ammonium tetrafluoroborate in 150 ml of water, and the red solution

was concentrated to 180 ml volume. The puple crystals which formed were collected on a filter and washed with water several times to remove excess ammonium tetrafluoroborate. The crude compound was recrystallized by dissolving it in 150 ml of methanol and concentrating the solution to about 30 ml volume; precipitation was then affected by the addition of 5 ml of water. The purple crystals were collected and washed with water. The monohydrate was obtained as an orange product after the purple crystals were dried *in vacuo*.

Tris[2-(2'-pyridyl)benzimidazole]iron(II) tetrafluoroborate dihydrate, $Fe(pyben)_3(BF_4)_2 \cdot 2H_2O$

The procedure was identical to that used for the monohydrate derivative above, except that the purple crystals were dried in air to give a stable brown compound.

Tris[2-(2'-pyridyl)benzimidazole]iron(II) tetraphenylborate monohydrate, $Fe(pyben)_3(BPh_4)_2 \cdot H_2O$

1.0 g of $Fe(pyben)_3Br_2$ dissolved in 400 ml 95% ethanol was added to 2.0 g of sodium tetraphenylborate in 150 ml of 95% ethanol. The solution was concentrated to about 175 ml and left to stand overnight at 0°. The red precipitate which formed was filtered and dried *in vacuo*.

Tris[2-(2'-pyridyl)benzimidazole]iron(II) tetrathiocyanatodiamminechromate-(III), $Fe(pyben)_3[Cr(NH_3)_2(NCS)_4]$

1.1 g of $Fe(pyben)_3Br_2$ in 175 ml of methanol was added to 1.0 g of Reinecke salt in 160 ml of methanol. 20 ml of water was added and the volume of the solution reduced to about 100 ml. The precipitate which formed was collected by filtration, washed with a 1:1 methanol/water mixture and dried in vacuo.

TABLE VI

Analytical Data for the Ferrous Complexes of 2-(2'-Pyridyl)benzimidazole

Compounds		C%	H%	N%	Fe%	Colour [a]
$Fe(pyben)_3(ClO_4)_2 \cdot H_2O$						
	Found	50.42	3.25	14.75	6.50	Orange (RT)
	(Calc.	50.34	3.37	14.67	6.50)	Purple (LN)
$Fe(pyben)_3(ClO_4)_2 \cdot 2H_2O$						
	Found	49.00	3.49	14.38	6.35	Brown (RT)
	(Calc.	49.30	3.54	-	6.39)	Purple (LN)
$Fe(pyben)_3Br_2$						
	Found	53.42	3.40	15.81	6.93	Orange (RT)
	(Calc.	53.90	3.37	15.70	6.97)	Purple (LN)
$Fe(pyben)_3I_2$						
	Found	47.97	3.00	14.00	6.23	Orange (RT)
	(Calc.	48.27	3.02	14.10	6.24)	Purple (LN)
$Fe(pyben)_3(NO_3)_2 \cdot H_2O$						
	Found	54.60	3.66	19.70	7.14	Orange (RT)
	(Calc.	55.20	3.70	19.70	7.15)	Purple (LN)
$Fe(pyben)_3(NCS)_2 \cdot H_2O$						
	Found	58.55	3.86	19.88	7.20	Orange (RT)
	(Calc.	58.83	3.74	19.87	7.20)	Brown (LN)
$Fe(pyben)_2(NCS)_2$						
	Found	55.59	3.38	19.74	9.88	Red (RT)
	(Calc.	55.50	3.20	19.90	9.93)	Red (LN)
$Fe(pyben)_3(BF_4)_2 \cdot H_2O$						
	Found	52.14	3.37	15.42		Orange (RT)
	(Calc.	51.90	3.40	15.15	6.70)	Purple (LN)

TABLE VI - Continued/-

$Fe(pyben)_3(BF_4)_2 \cdot 2H_2O$					
	Found	50.31	3.30	14.61	Purple (RT)
	(Calc.	50.80	3.64	14.80 6.50)	Purple (LN)
$Fe(pyben)_3(BPh_4)_2 \cdot H_2O$					
	Found	77.86	4.95	9.68	Purple (RT)
	(Calc.	77.80	5.30	9.71 4.30)	Purple (LN)
$Fe(pyben)_3[Cr(NH_3)_2(NCS)_4]_2$					
	Found	41.41	3.02	22.68	Purple (RT)
	(Calc.	41.40	3.05	23.00 4.37)	Purple (LN)

[a] RT = room temperature, LN = liquid nitrogen temperature

General Observations

The ligand 2-(2'-pyridyl)benzimidazole forms two types of compounds with ferrous salts, depending on the strength of the anion as a coordinating ligand and the conditions of the reaction.

The first type is $Fe(pyben)_3A_2 \cdot xH_2O$. These compounds are not oxygen sensitive as first suspected. This might be due to the bulkiness of the ligands surrounding the iron(II) centre, making it inaccessible to oxidative attack. The ferrous nature of these compounds was confirmed by ferro- and ferri-cyanide tests. The monohydrates are moisture sensitive, while those which could be isolated as anhydrous complexes or dihydrates are not affected by atmospheric moisture. Although the dihydrates are readily converted to the monohydrates at room temperature on the vacuum line, attempts to drive off the last water of crystallization in the monohydrates were unsuccessful. A typical experiment involved heating a sample to 150° in vacuo for four to six hours, and measuring the weight loss. In no case was there an appreciable loss of weight. The presence of water after heating was also confirmed by the appearance of a 3300 cm^{-1} peak in the I.R. spectra.

In the case of the thiocyanate anion a second type of compound, $Fe(pyben)_2(NCS)_2$, is also formed, in which the anion is coordinated directly to the central metal ion. The formation of the tris(pyben) complex, $Fe(pyben)_3(NCS)_2 \cdot H_2O$, can be affected by keeping the reaction temperature at 0° and using excess ligand in a mixed water/methanol solvent. The bis adduct is by far the more stable complex in this case. It can be prepared either by boiling the tris complex in methanol or directly at room temperature using a ligand:metal mole ratio of 2:1 in methanol.

Even at room temperature, $Fe(pyben)_3(NCS)_2$ decomposes quickly in methanol losing one mole of the ligand to form $Fe(pyben)_2(NCS)_2$. This was observed by means of I.R. and electronic spectra, conductance measurements and microanalysis of the final product.

The behaviour of the thiocyanate derivatives is quite unique in the series since the other salts appear to be very stable in solution. For example, the bromide salt can be left in methanol for several weeks at room temperature and the original tris(pyben) complex can be retrieved, as confirmed by microanalysis, conductance, and electronic spectra.

Several attempts were made to prepare the chloride salt, since a compound of the formula $Fe(pyben)_3Cl_2 \cdot 6H_2O$ was reported by Chiswell et al.[75]. However, all attempts to obtain this hexahydrate were unsuccessful. An impure salt thought to be $Fe(pyben)_3Cl_2$ contaminated with free ligand was obtained instead (no band due to H_2O was found in the I.R. spectrum). The difficulty here is that the chloride salt is very soluble in methanol and moderately soluble in water as well, so that the precipitation process used for the other salts is ineffective in this case. When the water/methanol ratio is raised sufficiently to bring down the salt, free ligand coprecipitates. Attempts to make the chloride from acetone/water or ethanol/water were equally unsuccessful.

Efforts to prepare salts of the type $Fe(pyben)_3B$, where B is a dinegative ion, yielded very intractable products for B = CO_3^{2-}, SO_4^{2-} and $S_2O_3^{2-}$, and were not pursued further.

Conductance Measurements

The molar conductances of the complexes are given in Table VII. All the complexes except $Fe(pyben)_2(NCS)_2$ have similar values of conductances and these all lie within the range expected for 10^{-3} M solutions of 2:1 electrolytes in methanol (160 - 220 Ω^{-1} mol^{-1} cm^{+2}).[76] The values are near the lower end of the range however, presumably because of the large mass of the cation $Fe(pyben)_3^{2+}$. Additional lattice water seems to enhance the conductance in those cases where more than one hydrate could be isolated. The complex $Fe(pyben)_2(NCS)_2$ shows a much lower conductance than the rest, indicating an essential difference in structure for this compound. However the value 78 lies barely in the range expected for 1:1 electrolytes (80 - 115 Ω^{-1} mol^{-1} cm^{+2} for 10^{-3} M solutions in methanol)[76]. This could be due to the solvolysis of the covalent complex in methanol into species such as $[Fe(pyben)_2(CH_3OH)(NCS)]^+$ and $[Fe(pyben)_2(CH_3OH)_2]^{2+}$.[77]

Infrared Data

Infrared spectra between 4000 and 250 cm^{-1} were obtained for all the compounds. These spectra are very complex due to the large number of ligand bands present. Thus, instead of tabulating all the data, we shall only discuss those bands which provide structural and bonding information about the compounds. The I.R. spectra of pyben and some pyben-metal complexes have been studied previously by Lane *et al.*[78]. The spectra of our iron complexes are very similar to those reported for other transition metal complexes with this ligand, thus indicating that interaction between the central ion and the ligand is similar.

TABLE VII

Molar Conductances of the Pyben Complexes in Methanol at 25°

Complexes	$\Lambda_M(\Omega^{-1}mol^{-1}cm^2)$	Concentration(10^{-3}M)
$Fe(pyben)_3(ClO_4)_2 \cdot H_2O$	176.0	1.158
$Fe(pyben)_3(ClO_4)_2 \cdot 2H_2O$	188.0	0.861
$Fe(pyben)_3Br_2$	160.0	0.817
$Fe(pyben)_3(NO_3)_2 \cdot H_2O$	164.5	0.938
$Fe(pyben)_3(NCS)_2 \cdot H_2O$	decomposed	
$Fe(pyben)_3I_2$	169.0	1.130
$Fe(pyben)_3(BF_4)_2 \cdot H_2O$	177.0	1.118
$Fe(pyben)_3(BF_4)_2 \cdot 2H_2O$	192.0	0.985
$Fe(pyben)_3[Cr(NH_3)_2(NCS)_4]_2$	Not soluble	
$Fe(pyben)_3(BPh_4)_2 \cdot H_2O$	Not soluble	
$Fe(pyben)_2(NCS)_2$	78.8	0.96

The pyridine ring band[79] at 996 cm^{-1} is shifted by $\sim$ 10 cm^{-1} to 1007 cm^{-1}. Also, other pyridine bands at 1279 cm^{-1}, 1154 cm^{-1}, 1046 cm^{-1},[79] are all shifted upwards similarly. These upward shifts indicate unequivocally the involvement of the pyridine nitrogen in bonding. The two bands which could be assigned to the benzene ring, namely those at 1119, 1012 cm^{-1}, do not show any apparent upward shift. Examination of the spectra of pyben and its metal complexes[78] reveals that there is a strong band at 1314 cm^{-1} in the free ligand which splits into two sharp bands on chelation. These occur at 1324 and 1302 cm^{-1} in the case of the iron complexes. This band does not belong to either ortho-substituted benzene or pyridine, and can tentatively be assigned to the imidazole fragment. The splitting of this band on chelation can thus be regarded as an indication of the involvement of the imidazole nitrogen in bonding.

$Fe(pyben)_3(ClO_4)_2 \cdot xH_2O$ (x = 1,2) give identical infrared spectra in the range 3200-250 cm^{-1}, and both show a band due to water of hydration at 3180 cm^{-1}. The dihydrate shows an additional band at 3500 cm^{-1} which can be eliminated by evacuating the sample at room temperature. In both compounds the ν_3 perchlorate band[80] centred at $\sim$ 1083 cm^{-1} is split by 60 cm^{-1}. (This can be compared to $HClO_4$, where the ν_3 splitting is 280 cm^{-1}).[81] The moderate splitting seen here is probably due to a small distortion of the ClO_4^- anion by lattice effects. The $\nu_4 ClO_4^-$ band is unsplit at 624 cm^{-1}, while ν_1 and ν_2 are assigned to very weak bands at 968 and 458 cm^{-1}, respectively.

In the case of $Fe(pyben)_3(NO_3)_2 \cdot H_2O$, the nitrate ν_3 band at 1350 cm^{-1} is split by 59 cm^{-1}. This is small compared to coordinated NO_3^- groups, which typically show ν_3 splittings of $\sim$ 200 cm^{-1},[80] and can

be attributed to a lattice distortion. The ν_1 and ν_2 anion modes appear as very weak bands at 1038 and 825 cm^{-1}, respectively, while ν_4 is very likely masked by a broad ligand absorption at 744 cm^{-1}.

The lattice water in the compound $Fe(pyben)_3(NCS)_2 \cdot H_2O$ absorbs at 3350 cm^{-1} and this H_2O molecule cannot be removed by pumping. The CN stretch (ν_1) of the NCS^- anion occurs at a slightly lower frequency (2030 cm^{-1}) than in potassium thiocyanate (2050 cm^{-1}), but the line remains unsplit. The ν_2 band appears as a weak absorption at exactly the same position as in KNCS (471 cm^{-1}) while ν_3 is not observed, probably masked by a strong ligand band at 744 cm^{-1}.

There is no appreciable difference between the spectrum of $Fe(pyben)_2(NCS)_2$ and that of $Fe(pyben)_3(NCS)_2 \cdot H_2O$ as far as ligand bands are concerned. However, $Fe(pyben)_2(CNS)_2$ does not have a lattice water band in the region above 3000 cm^{-1}, and the thiocyanate CN stretch appears as a strong doublet at 2080 and 2022 cm^{-1}. The reported splitting of this band is about 10 cm^{-1} for the analogous phen and bipy complexes[64,82]. Assuming a <u>cis</u>-configuration is adopted, the larger splitting here (58 cm^{-1}) may be due to the fact that the pyben ligand is asymmetric while phen and bipy are symmetric ligands. The N-C-S bending mode (ν_2) is found at 474 cm^{-1} as a weak band. Further evidence that the thiocyanate group is coordinated to iron in $Fe(pyben)_2(NCS)_2$ is the appearance of a strong 788 cm^{-1} band which can be assigned[80] to the C-S stretch (ν_3) of the NCS ligand. The position of this band is indicative of N-bonded thiocyanate ligands[80].

For the pair $Fe(pyben)_3(BF_4)_2 \cdot H_2O$ and $Fe(pyben)_3(BF_4)_2 \cdot 2H_2O$, the spectra are identical except that there is one broad band at

3278 cm^{-1} for the monohydrate while the dihydrate has an extra band with a double maximum at 3528 and 3598 cm^{-1}. The latter can be eliminated by pumping the dihydrate at room temperature. The BF_4^- bands appear at the expected positions[83]: ν_3 at 1053 cm^{-1} is strong and broad, ν_4 is found at 518 cm^{-1} with a splitting of less than 5 cm^{-1} (due presumably to crystal distortion effects), and ν_1 appears as a strong band at 759 cm^{-1}.

The spectral bands due to the $Cr(NH_3)_2(NCS)_4^-$ ion in $Fe(pyben)_3[Cr(NH_3)_2(NCS)_4]_2$ are similar to those of other reineckates[84], indicating a similar anion environment. The CN stretch appears at 2063 cm^{-1}, and the NCS bending mode occurs at 494 cm^{-1}. The $Cr-NH_3$ stretch appears at 466 cm^{-1} as a weak shoulder. The NH_3 deformation absorptions are at the same positions as in ammonium reineckate[84]: the symmetric deformation at 1257 cm^{-1}, and the rocking mode at 708 cm^{-1}. A strong band at 350 cm^{-1} can be assigned to the Cr- NCS stretch while the C-S stretch appears at 848 cm^{-1}.

The lattice water absorption of the compound $Fe(pyben)_3(BPh_4)_2 \cdot H_2O$ produces a broad band at 3304 cm^{-1}. The infrared spectrum due to the anion fragment BPh_4^- is very complicated and a complete analysis of it could not be found in the literature. Comparison of the bands due to the BPh_4^- ion in the complex with the spectrum of Na BPh_4 in the range 2000-250 cm^{-1} revealed that both the positions and intensities of the bands are similar in the two compounds. This suggests a similarity of anion environment. The strongest bands are due to phenyl C-H out-of-plane deformations[85], and appear at 741 cm^{-1} and 714 cm^{-1} with intensities similar to the corresponding bands in Na BPh_4.

The major features of the I.R. spectra of these complexes can be summarized as follows: Firstly, it appears that both the pyridine and imidazole nitrogens are involved in bonding to the ferrous ion, suggesting that pyben is acting as a bidentate chelating ligand. Secondly, for most of the polyatomic anions there is evidence for some symmetry lowering. This could be caused by distortions arising from crystal packing forces, although the asymmetric nature of the pyben ligand is another possible cause.

Thirdly, for the perchlorate and tetrafluoroborate complexes there are clear differences between the monohydrates and dihydrates above 3000 cm^{-1}. Finally, the data provide good evidence that in $Fe(pyben)_2(NCS)_2$ the NCS groups are coordinated to iron via the nitrogen atoms.

Magnetic Data

The results of magnetic susceptibility measurements on the complexes between 80°K-300°K are listed in Table VIII. The molar susceptibilities and magnetic moments are plotted as functions of temperature in Figures 20 and 21, respectively. As seen from Fig. 21, the temperature dependence of μ_{eff} varies greatly from compound to compound. The complexes can be separated roughly into four groups, depending on the anion. The nitrate and the two thiocyanate complexes have μ_{eff} values between about 4.8 and 5.4 B.M. throughout the temperature range. The bromide, iodide, and tetrafluoroborate monohydrate derivatives show moments of $\sim$ 5.4 B.M. at room temperature, decreasing to about 3.5 - 4.2 B.M. at liquid nitrogen temperature. The moments for the perchlorate monohydrate and dihydrate, tetrafluoroborate dihydrate and

TABLE VIII

Molar Susceptibilities and Effective Magnetic Moments of the pyben Complexes as a Function of Temperature

T (°K)	X_1 (c.g.s.)	μ_{eff} (B.M.)	X_2 (c.g.s.)	μ_{eff} (B.M.)
FE(PYBEN)3(CLO4)2.H2O				
79.8	0.006268	2.00	0.006234	1.99
90.7	0.005795	2.05	0.005756	2.04
106.2	0.005549	2.17	0.005492	2.16
124.0	0.005812	2.40	0.005782	2.40
139.7	0.006373	2.67	0.006331	2.66
157.0	0.007441	3.06	0.007398	3.05
181.4	0.010856	3.97	0.010831	3.96
202.9	0.015673	5.04	0.015647	5.04
221.0	0.015865	5.30	0.015865	5.30
245.4	0.014867	5.40	0.014850	5.40
264.5	0.013956	5.43	0.013990	5.44
284.4	0.013028	5.44	0.013037	5.45
306.4	0.012030	5.43	0.012038	5.43
FE(PYBEN)3(CLO4)2.2H2O				
80.5	0.002581	1.29	0.002512	1.27
95.0	0.002334	1.33	0.002265	1.31
113.4	0.002391	1.47	0.002361	1.46
134.0	0.002562	1.66	0.002557	1.65
153.4	0.003018	1.92	0.003001	1.92
170.0	0.003535	2.19	0.003512	2.19
190.5	0.004443	2.60	0.004438	2.60
208.3	0.005626	3.06	0.005618	3.06
229.5	0.007377	3.68	0.007398	3.69
251.4	0.009855	4.45	0.009829	4.45
267.9	0.011204	4.90	0.011211	4.90
290.3	0.011760	5.23	0.011716	5.22
310.5	0.011527	5.35	0.011525	5.35
FE(PYBEN)3(NO3)2.H2O				
79.0	0.037373	4.86	0.037249	4.85
98.6	0.031276	4.97	0.031269	4.97
125.1	0.025658	5.07	0.025536	5.06
152.5	0.021904	5.17	0.021714	5.15
179.7	0.019278	5.26	0.019255	5.26
204.7	0.017087	5.29	0.017142	5.30
231.4	0.015315	5.32	0.015286	5.32
264.5	0.013517	5.35	0.013540	5.35
278.8	0.012828	5.35	0.012863	5.35
296.0	0.012089	5.35	0.012086	5.35
FE(PYBEN)3(NCS)2.H2O				
81.1	0.037909	4.96	0.037612	4.94
99.1	0.032794	5.10	0.032812	5.10
120.0	0.028067	5.19	0.028018	5.19
141.0	0.024632	5.27	0.024648	5.27
162.0	0.021739	5.31	0.021805	5.31
180.2	0.019709	5.33	0.019744	5.33
200.0	0.018048	5.37	0.018075	5.38
219.9	0.016585	5.40	0.016555	5.40
241.1	0.015156	5.41	0.015204	5.41
259.2	0.014107	5.41	0.014196	5.43
283.7	0.012999	5.43	0.013025	5.44
310.2	0.011943	5.44	0.011924	5.44
FE(PYBEN)3BR2				
80.4	0.020657	3.65	0.020584	3.64
94.0	0.019689	3.85	0.019639	3.84
104.5	0.019336	4.02	0.019318	4.02
116.4	0.018955	4.20	0.018996	4.20
128.3	0.018720	4.38	0.018710	4.38
138.8	0.018573	4.54	0.018580	4.54
149.3	0.018529	4.70	0.018398	4.69
163.1	0.018339	4.89	0.018233	4.88
174.6	0.018016	5.02	0.018033	5.02
185.0	0.017664	5.11	0.017651	5.11
194.4	0.017282	5.18	0.017365	5.20
205.6	0.016592	5.22	0.016610	5.23
219.7	0.015932	5.29	0.015916	5.29
241.1	0.014905	5.36	0.014909	5.36
263.0	0.013936	5.41	0.013998	5.43
287.1	0.012880	5.44	0.012940	5.45
FE(PYBEN)3I2				
81.1	0.019791	3.58	0.019531	3.56
96.0	0.019451	3.86	0.019474	3.87
112.8	0.019569	4.20	0.019623	4.21
131.2	0.019821	4.56	0.019620	4.54
150.5	0.019392	4.83	0.019427	4.84
169.9	0.018903	5.07	0.018829	5.06
188.1	0.018075	5.21	0.017917	5.19
206.8	0.016935	5.29	0.016888	5.28
225.8	0.016018	5.38	0.015863	5.35
247.6	0.014745	5.40	0.014747	5.40
264.0	0.013913	5.42	0.013881	5.41
287.1	0.012865	5.44	0.012923	5.45
309.5	0.012022	5.45	0.011973	5.44
FE(PYBEN)3(BF4)2.H2O				
82.0	0.026723	4.19	0.026578	4.18
102.2	0.023501	4.38	0.023173	4.35
120.6	0.021078	4.51	0.021034	4.50
137.6	0.019834	4.67	0.019808	4.67
156.2	0.018567	4.82	0.018576	4.82
171.5	0.017922	4.96	0.017738	4.93
187.6	0.017189	5.08	0.017011	5.05
204.8	0.016382	5.18	0.016247	5.16
220.1	0.015667	5.25	0.015507	5.23
240.0	0.014633	5.30	0.014686	5.31
256.1	0.013989	5.35	0.013979	5.35
281.4	0.013033	5.42	0.012959	5.40
305.5	0.012233	5.47	0.012088	5.44
FE(PYBEN)3(BF4)2.2H2O				
81.1	0.002918	1.38	0.002808	1.35
101.1	0.002451	1.41	0.002445	1.41
119.0	0.002298	1.48	0.002287	1.48
139.4	0.002279	1.59	0.002321	1.61
159.9	0.002339	1.73	0.002369	1.74
178.8	0.002552	1.91	0.002609	1.93
198.8	0.003075	2.21	0.003065	2.21
218.5	0.003822	2.58	0.003882	2.60
238.0	0.005009	3.09	0.005092	3.11
256.3	0.006694	3.70	0.006756	3.72
279.0	0.008815	4.44	0.008884	4.45
304.0	0.010111	4.96	0.010145	4.97
FE(PYBEN)3(BPH4)2.H2O				
81.6	0.017512	3.38	0.017374	3.37
96.0	0.016230	3.53	0.015811	3.48
111.4	0.014659	3.61	0.014424	3.59
131.7	0.013588	3.78	0.013331	3.75
152.8	0.012652	3.93	0.012680	3.94
173.5	0.012156	4.11	0.012170	4.11
193.6	0.011647	4.25	0.011752	4.27
216.2	0.011256	4.41	0.011432	4.45
234.0	0.011065	4.55	0.011223	4.58
254.7	0.010874	4.71	0.010937	4.72
281.4	0.010499	4.86	0.010592	4.88
303.5	0.010272	4.99	0.010331	5.01
FE(PYBEN)2(NCS)2				
78.6	0.041233	5.09	0.041201	5.09
92.9	0.036161	5.18	0.036253	5.19
113.0	0.030599	5.26	0.030708	5.27
136.9	0.025758	5.31	0.025861	5.32
166.8	0.021524	5.36	0.021633	5.37
191.0	0.019002	5.39	0.019026	5.39
216.8	0.016762	5.39	0.016822	5.40
236.3	0.015504	5.41	0.015501	5.41
253.1	0.014395	5.40	0.014435	5.40
275.6	0.013189	5.39	0.013231	5.40
306.0	0.011897	5.40	0.011925	5.40
FE(PYBEN)3(CR(NH3)2(NCS)4)2				
81.2	0.004319	1.68	0.004228	1.66
103.3	0.003749	1.76	0.003600	1.73
122.4	0.003313	1.80	0.003357	1.81
144.6	0.002864	1.82	0.002988	1.86
165.0	0.002701	1.89	0.002825	1.93
184.2	0.002574	1.95	0.002616	1.96
203.8	0.002689	2.09	0.002709	2.10
220.7	0.002909	2.27	0.002912	2.27
240.4	0.003123	2.45	0.003307	2.52
260.3	0.003840	2.83	0.004067	2.91
282.7	0.005158	3.41	0.005225	3.44
308.9	0.006511	4.01	0.006520	4.01

X_1 measured in field strength of ~ 4.0 kG

X_2 " " " " " ~ 8.0 kG

FIGURE 20

Temperature Dependence of the Molar Susceptibilities of the Pyben Complexes

⊙	$Fe(pyben)_3(ClO_4)_2 \cdot H_2O$
Δ	$Fe(pyben)_3(ClO_4)_2 \cdot 2H_2O$
+	$Fe(pyben)_3(NO_3)_2 \cdot H_2O$
×	$Fe(pyben)_3(NCS)_2 \cdot H_2O$
◇	$Fe(pyben)_3Br_2$
↑	$Fe(pyben)_3I_2$
⧖	$Fe(pyben)_3(BF_4)_2 \cdot H_2O$
Z	$Fe(pyben)_3(BF_4)_2 \cdot 2H_2O$
Y	$Fe(pyben)_3(BPh_4)_2 \cdot H_2O$
✕	$Fe(pyben)_2(NCS)_2$
✱	$Fe(pyben)_3[Cr(NH_3)_2(NCS)_4]_2$

FIGURE 20

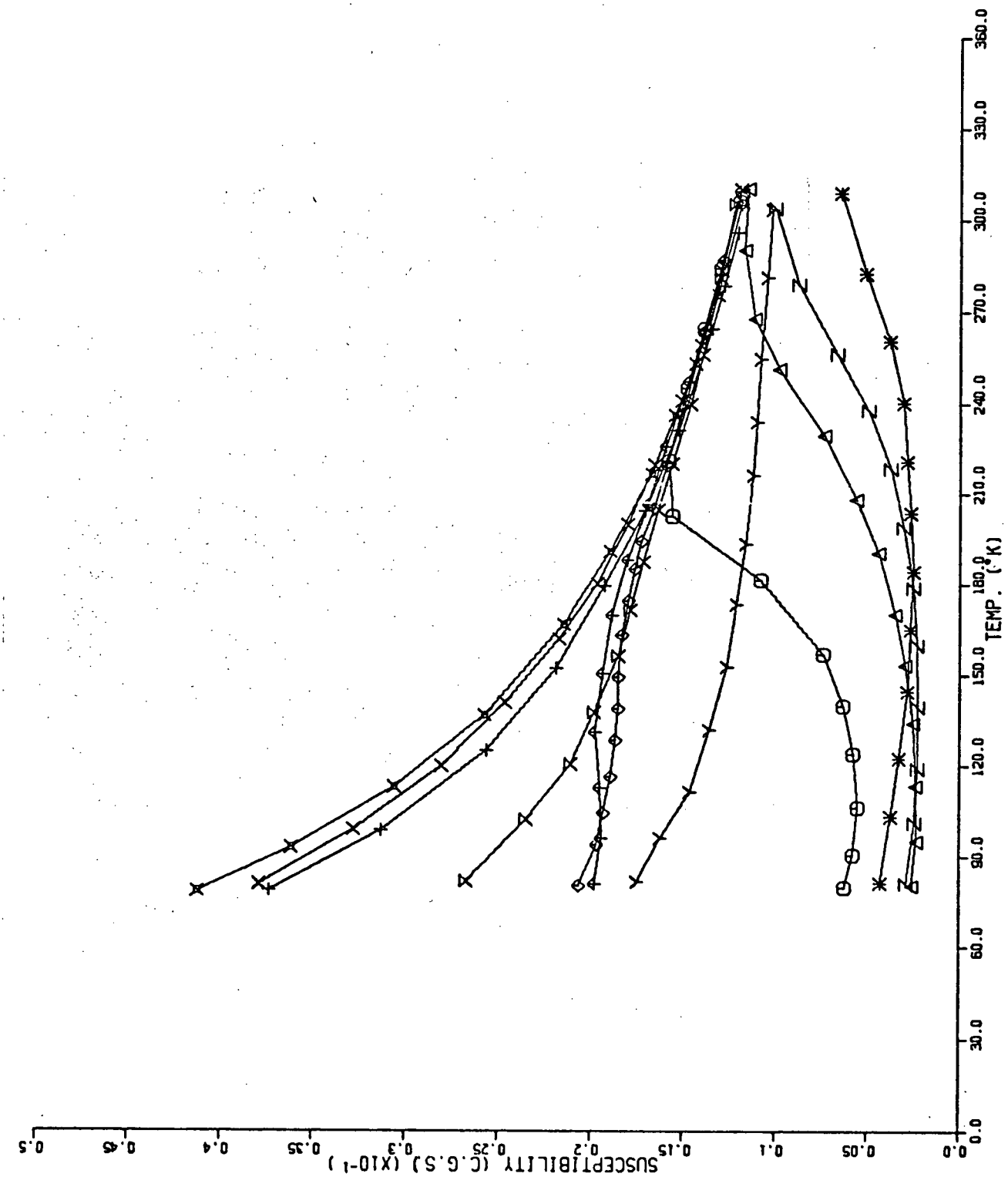
SUSCEPTIBILITY (C.G.S.) (X10-1)
0.0
0.05
0.1
0.15
0.2
0.25
0.3
0.35
0.4
0.45
0.5
TEMP. (°K)
0.0
30.0
60.0
90.0
120.0
150.0
180.0
210.0
240.0
270.0
300.0
330.0
360.0

FIGURE 21

Temperature Dependence of the Effective Magnetic Moments of the Pyben Complexes

⊙	$Fe(pyben)_3(ClO_4)_2 \cdot H_2O$
Δ	$Fe(pyben)_3(ClO_4)_2 \cdot 2H_2O$
+	$Fe(pyben)_3(NO_3)_2 \cdot H_2O$
×	$Fe(pyben)_3(NCS)_2 \cdot H_2O$
◈	$Fe(pyben)_3Br_2$
✦	$Fe(pyben)_3I_2$
✕	$Fe(pyben)_3(BF_4)_2 \cdot H_2O$
Z	$Fe(pyben)_3(BF_4)_2 \cdot 2H_2O$
Y	$Fe(pyben)_3(BPh_4)_2 \cdot H_2O$
✕	$Fe(pyben)_2(NCS)_2$
✱	$Fe(pyben)_3[Cr(NH_3)_2(NCS)_4]_2$

FIGURE 21

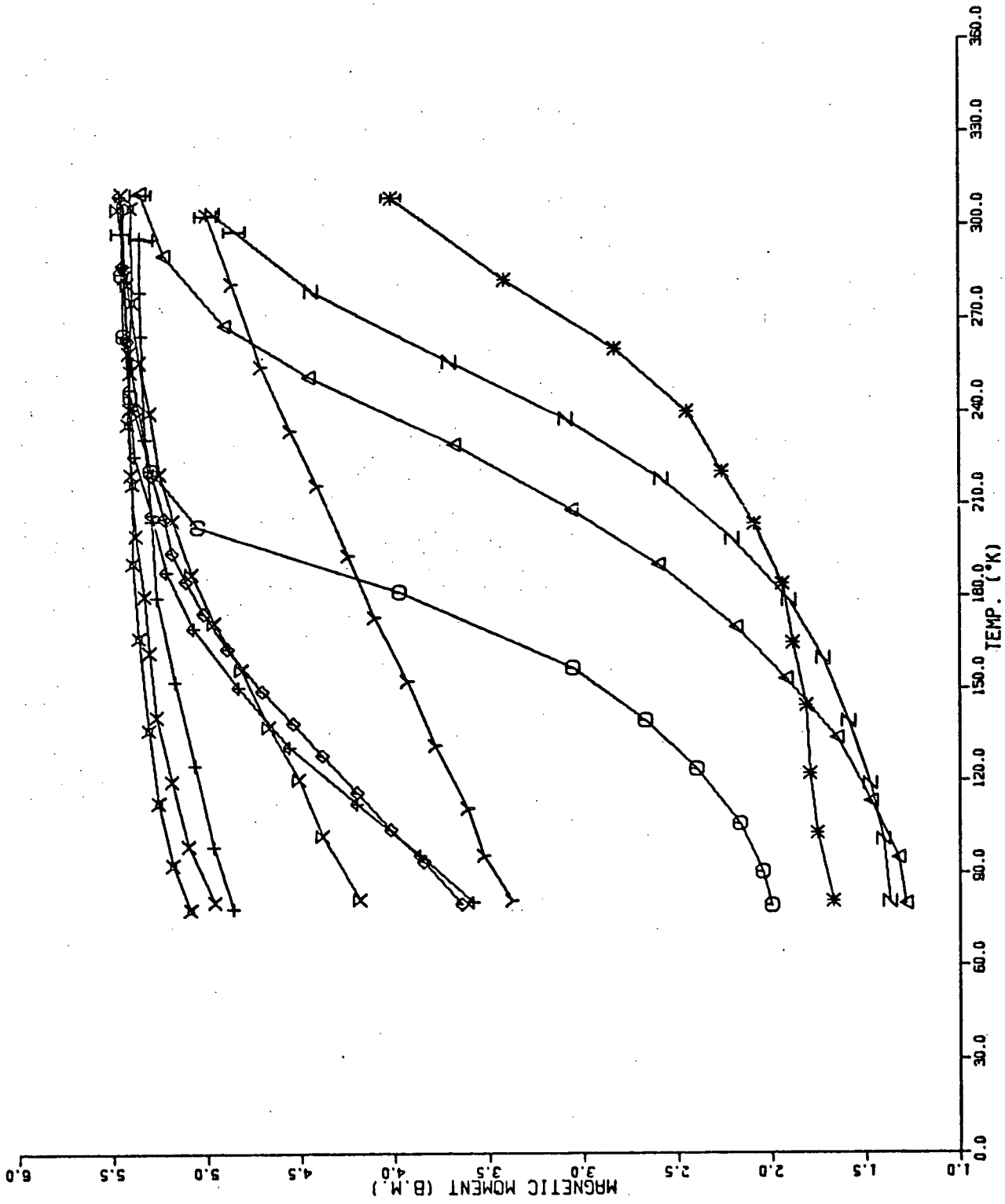
MAGNETIC MOMENT (B.M.)
1.0
1.5
2.0
2.5
3.0
3.5
4.0
4.5
5.0
5.5
6.0
TEMP. (°K)
0.0
30.0
60.0
90.0
120.0
150.0
180.0
210.0
240.0
270.0
300.0
330.0
360.0

reineckate salts have the most pronounced temperature dependence, being ≤ 2.0 B.M. at about 80°K, and in the range 4.0 - 5.4 B.M. at room temperature. For the tetraphenylborate complex the moment decreases almost linearly from 5.0 to 3.4 B.M. between 300 and 80°K.

In the previous Chapter it was seen that for typical high-spin ferrous complexes μ_{eff} is roughly 5.4 B.M. and varies by only about 0.2 B.M. between 80 and 300°K. It was also found that changing the six ligands of the inner coordination sphere of iron from, say DMSO to PyNO, caused only slight changes in either the magnitude or temperature dependence of μ_{eff}. The situation is clearly very different here, where changes outside the inner coordination sphere (i.e., a change of anion and/or number of waters of crystallization) can cause dramatic changes in the magnitude and temperature dependence of μ_{eff}. However, there does not appear to be any obvious correlation between μ_{eff} and the nature of the anion, as will be discussed in more detail below.

The magnetic data by themselves do not establish the existence of high-spin - low-spin equilibria, although antiferromagnetic iron-iron interactions (which could also cause such anomalous magnetic behaviour) seem very unlikely in these systems. However, Mössbauer data presented below definitely show the presence of ferrous ions in both $^5T_2$ and $^1A_1$ states, and that the relative populations of the two states depend on temperature, nature of the anion and degree of hydration. Thus, we will discuss the magnetic moment data in terms of the effects of these three variables on the composition of the high-spin - low-spin "mixture".

The temperature dependence of μ_{eff} for $Fe(pyben)_3(NO_3)_2 \cdot H_2O$ is not unusually large for a pure high-spin ferrous complex, although the Mössbauer spectra show there are some molecules in the $^1A_1$ ground state below about 180°K. Similarly, for the two thiocyanate complexes $Fe(pyben)_3(NCS)_2 \cdot H_2O$ and $Fe(pyben)_2(NCS)_2$, the moments have small temperature dependence and are nearly identical throughout the accessible temperature range, yet the former exhibits $^5T_2$ - $^1A_1$ crossover below ~ 170°K while the latter shows no $^1A_1$ component down to 115°K. It is clear from these examples that the magnetic data do not guarantee the purity of the spin system. Since the use of μ_{eff} values to extract such parameters as crystal field splittings spin-orbit couplings and orbital reduction factors is not valid if the compound exists as a mixture of spin states, it is essential in such cases to have other evidence (such as Mössbauer spectra) to ensure that the spin system is pure before analysing μ_{eff} values theoretically.

For the Br^- and I^- complexes the moments at 80°K are ~ 3.6 B.M., indicating that there is still a substantial fraction of high-spin species present even at this temperature. The fact that these two salts give almost identical μ_{eff} vs T curves suggests that the size of the anion alone is probably not the major factor controlling the ratio of high-spin to low-spin species (ionic radii are 1.96 Å for Br^- and 2.19 Å for I^-)[86]. On the other hand it appears that very large anions such as BPh_4^- and $[Cr(NH_3)_2(NCS)_4]^-$ lead to smaller room-temperature moments and thus favour the formation of complexes with $^1A_1$ ground states. If we assume that these ions are quasi-spherical (BPh_4^- is tetrahedral and the reineckate anion <u>trans</u>-octahedral[84]) the effective radii are

estimated to be about 4.4 and 4.9 Å, respectively.

Some of the most interesting results are those for the ClO_4^- and BF_4^- salts, where both mono- and dihydrates were obtained. $Fe(pyben)_3(ClO_4)_2 \cdot H_2O$ has a moment of 5.44 B.M. at 300°K, which drops to 2.00 B.M. at 80°K. On introduction of a second water molecule into the lattice, the room-temperature moment decreases slightly to 5.35 B.M., while at 80°K μ_{eff} is only 1.29 B.M. It thus appears that the extra H_2O molecule increases the fraction of low-spin molecules at all temperatures.

An even more dramatic example of this effect is seen with the BF_4^- derivatives, where the second lattice water molecule lowers the room-temperature moment by $\sim$ 0.5 B.M. and that at 80°K from 4.19 to 1.38 B.M. These results are especially striking in view of the ease with which the dihydrates can be converted to the monohydrates on a vacuum line, after which the original μ_{eff} vs T curves for the monohydrates are exactly restored. Except for one previous case, these are the first examples of complexes showing $^5T_2 - {}^1A_1$ crossover where two different hydrates of a given salt have been obtained, and the effect of the hydration state on the magnetic properties is much more pronounced than we had expected. More will be said about this below.

During the course of this work, Sasaki and Shigematsu[87] reported magnetic susceptibility data for $Fe(pyben)_3(ClO_4)_2 \cdot H_2O$. Although these authors suggest the occurrence of $^5T_2 - {}^1A_1$ spin equilibrium in the complex, their magnetic moment data are very different from ours. In particular, they report μ_{eff} values of 5.25 and 3.33 B.M. at 298 and 77.2°K respectively, compared to our values of 5.43 B.M.

(306.4°K) and 2.00 B.M. (79.8°K). We suggest that the discrepancy is most probably due to the existence of more than one magnetic isomer of $Fe(pyben)_3(ClO_4)_2 \cdot H_2O$ (similar to the situation in $Fe(PyiH)_3(ClO_4)_2$ mentioned above[71]) and that we and Sasaki and Shigematsu[87] have obtained and studied different isomers. Their preparation procedure involved mixing ethanolic solutions of pyben and $FeCl_2 \cdot 4H_2O$, followed by addition of perchloric acid and then water. Three separate preparations of this complex by our route described above gave consistent and reproducible magnetic and Mössbauer data, but we have observed that addition of small amounts of acid to a reaction mixture can change the room-temperature moments of these salts by 20% or more.

Electronic Spectra

Molar extinction coefficients (ε_{max}), and wavelengths of maximum absorption (λ_{max}) at 25° in methanol solution are listed in Table IX for most of the complexes. Both the peak positions and intensities are very similar for all the compounds except $Fe(pyben)_2(NCS)_2$ which has both a lower ε_{max} and λ_{max}, indicating the essential difference between this system and the rest of the complexes.

The assignment of the 490 nm abosrption to the d-d transition $^5T_{2g} \rightarrow {}^5E_g$ gives a 10Dq value of about 20,000 cm^{-1}, as expected for intermediate ligand fields near the high-spin - low-spin crossover point. However, the intensity of the band is abnormally high for a d-d transition. This could be due to the fact that there is a strong ligand band near 330 nm with enhancement of the d-d band being a result of "intensity stealing"[88]. An alternative explanation is that this is a

TABLE IX

Electronic Spectra of the Pyben Complexes in Methanol at 25°

COMPLEXES	$\varepsilon_{max} \times 10^{-2}$	λ nm
$Fe(pyben)_3(ClO_4)_2 \cdot H_2O$	10.3	490
$Fe(pyben)_3(ClO_4)_2 \cdot 2H_2O$	9.55	490
$Fe(pyben)_3(NO_3)_2 \cdot H_2O$	11.0	490
$Fe(pyben)_3(NCS)_2 \cdot H_2O$		decomposed
$Fe(pyben)_3Br_2$	10.2	490
$Fe(pyben)_3I_2$	9.80	490
$Fe(pyben)_3(BF_4)_2 \cdot H_2O$	10.2	490
$Fe(pyben)_3(BF_4)_2 \cdot 2H_2O$	9.80	490
$Fe(pyben)_3(BPh_4)_2 \cdot H_2O$	not sufficiently soluble	
$Fe(pyben)_3[Cr(NH_3)_4(NCS)_2]_2$	not sufficiently soluble	
$Fe(pyben)_2(NCS)_2$	5.72	474

charge transfer band of the $t_{2g} \rightarrow \pi^*$ type, but if this is the case, the intensity is an order of magnitude smaller than normally observed for such transitions[88].

An interesting feature of the solution spectral data in Table IX is that the 490 nm bands in $Fe(pyben)_3(ClO_4)_2 \cdot xH_2O$ and $Fe(pyben)_3(BF_4)_2 \cdot xH_2O$ have very similar extinction coefficients for x = 1 or 2, despite the fact that the mono- and dihydrates show very different magnetic behaviour in the solid state. As indicated in Table VII, most of the solid complexes in this series undergo very dramatic colour changes when cooled to about 80°K. However, these colour changes are not observed when methanol solutions of the complexes are cooled. These observations strongly suggest that the high-spin - low-spin crossover is exclusively a solid state effect, and it was therefore of interest to study the temperature dependence of the electronic spectra of some of these complexes as solids. No such measurements appear to have been reported previously for other compounds showing spin equilibrium.

The three complexes $Fe(pyben)_3(ClO_4)_2 \cdot H_2O$, $Fe(pyben)_3(NO_3)_2 \cdot H_2O$ and $Fe(pyben)_3Br_2$ were chosen to study in the form of KBr pellets. All three are bright orange in colour at room temperature, changing to dark purple when cooled in liquid nitrogen, and each exhibits a different temperature dependence of μ_{eff} (see Fig. 21). The solid state spectral data for these three derivatives are given in Table X.

At room temperature, in addition to the strong ligand band at 330 nm, each spectrum contains a weak feature at about 490 nm, which shifts to slightly longer wavelength and increases in intensity as the

TABLE X

Solid State Visible Bands of the $Fe(pyben)_3A_2 \cdot xH_2O$ Complexes as a Function of Temperature

T(°K)	λ_{max} Peak 1	λ_{max} Peak 2	Intensity Peak 1	Intensity Peak 2
FE(PYBEN)3(CLO4)2.H2O				
88.0		544.		22.4
107.0		544.		21.0
128.0		544.		18.8
172.0		538.		14.0
185.0		538.		12.4
208.0		534.		10.1
223.0		530.		8.2
235.0		530.		6.4
246.0	510.		3.2	
257.0	510.		3.2	
263.0	510.		3.0	
273.0	510.		2.4	
293.0	505.		1.3	
303.0	495.		0.8	
313.0	490.		0.2	
323.0	490.		0.2	
FE(PYBEN)3(NO3)2.H2O				
79.0	500.	545.		4.8
103.0	500.	545.		4.8
134.0	500.	545.		4.9
167.0	505.	540.		4.8
171.0	505.	540.		4.9
194.0	500.	540.		4.8
213.0	500.	535.		4.2
224.0	500.		1.8	
241.0	500.		1.8	
254.0	490.		1.5	
268.0	495.		1.4	
298.0	490.		1.3	
320.0	485.		0.9	
327.0	485.		0.8	
FE(PYBEN)3BR2				
103.0	505.	544.		9.6
147.0	505.	543.		9.8
157.0	505.	540.		9.5
168.0	505.	538.		9.2
179.0	505.	535.		9.0
185.0	515.		8.8	
193.0	515.		8.6	
204.0	515.		8.4	
217.0	510.		8.0	
227.0	505.		7.2	
234.0	505.		7.0	
247.0	500.		6.8	
255.0	498.		1.8	
261.0	490.		1.6	
273.0	490.		1.7	
293.0	490.		1.3	

temperature is lowered. For the nitrate derivative the intensity of the latter band shows a sudden jump below ∿ 220°K, coincident with the appearance of another band of equal intensity at ∿ 540 nm. The intensities of both bands remain essentially constant on further cooling. In the bromide complex there is a sharp increase in intensity of the 490 nm band at ∿ 250°K, but there is no clear separation into two bands until the temperature is lowered to ∿ 180°K. For the perchlorate monohydrate, only the 540 nm band is seen clearly below ∿ 240°K, and its intensity continues to rise with decreasing temperature.

The 540 nm absorption at low temperature is obviously responsible for the colour changes observed in these complexes. Moreover, as we shall see below, the temperature at which this band appears is approximately the same as that at which the presence of a low-spin species can be detected in the Mössbauer spectra, and the intensities show a qualitative correlation with the fraction of $^1A_1$ molecules deduced from Mössbauer area ratios.

This 540 nm band is almost certainly due to a charge transfer transition involving the ligand π* orbitals. The intensity and position of the band are characteristic of a unique class of compounds containing "methine chromaphores"[89]. The appearance of this band indicates the formation of a five-membered aromatic ring system in which the iron t_{2g} electrons contribute substantially to the π-electron resonance system of the methine chromaphore:

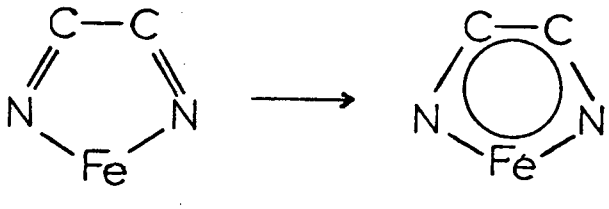

This chromaphore is known to arise only for a low-spin ground state in ferrous complexes[88], which confirms that the 540 nm band is associated with the $^1A_1$ species.

Mössbauer Data

The ^{57}Fe Mössbauer parameters for all the complexes are listed in Table XI. Most of the spectra obtained for this series of compounds consisted of four lines, which could readily be identified as two quadrupole doublets, and the relative intensities of these doublets changed with temperature. This behaviour is illustrated in Figures 22 and 23 where spectra obtained for $Fe(pyben)_3(ClO_4)_2 \cdot H_2O$ between 295 and 8°K are shown. At 250°K and above only one pair of lines is seen, with δ and $|\Delta E_Q|$ values in the ranges commonly observed for high-spin ferrous salts[1]. At 230°K two weak shoulders have appeared on the low-velocity line of the high-spin doublet. With further lowering of the temperature, the inner pair of lines gains intensity relative to the outer pair. The parameters (δ and $|\Delta E_Q|$) of the inner doublet are typical of those expected for low-spin ferrous derivatives[1]. Thus, the Mössbauer spectra unequivocally show the existence of temperature-dependent $^5T_2 - {}^1A_1$ spin equilibria in these complexes. It can also be seen from Figures 22 and 23 that the transition in $Fe(pyben)_3(ClO_4)_2 \cdot H_2O$ is spread over at least 100°, and thus conforms to König's "Type II" classification[70], and moreover, that there is an incomplete change in spin state since the high-spin component is still present at 8.7°K.

For all the complexes δ and $|\Delta E_Q|$ values for the high-spin species are very similar both in magnitude and temperature dependence,

TABLE XI

^{57}Fe Mössbauer Parameters for the pyben Complexes

T (°K)	S=0 δ (mm s^{-1})	S=0 ΔE_Q (mm s^{-1})	S=0 Γ_1 (mm s^{-1})	S=0 Γ_2 (mm s^{-1})	S=2 δ (mm s^{-1})	S=2 ΔE_Q (mm s^{-1})	S=2 Γ_1 (mm s^{-1})	S=2 Γ_2 (mm s^{-1})	AREA FRACTION ($^5T_2$/TOTAL)
FE(PYBEN)3(CLO4)2.H2O									
8.7	.75	.48	.23	.23	1.37	2.46	.39	.39	.23
84.0	.75	.48	.25	.25	1.36	2.52	.33	.33	.16
100.0	.75	.48	.25	.25	1.36	2.56	.33	.37	.20
130.0	.75	.47	.27	.27	1.34	2.56	.32	.37	.22
160.0	.74	.46	.27	.30	1.33	2.51	.40	.38	.31
180.0	.73	.46	.29	.25	1.31	2.53	.31	.36	.38
190.0	.73	.45	.29	.27	1.30	2.51	.32	.35	.45
200.0	.73	.44	.29	.28	1.30	2.49	.33	.36	.63
210.0	.70	.41	.24	.24	1.30	2.47	.32	.36	.77
220.0	.72	.38	.24	.24	1.30	2.44	.33	.35	.87
230.0	.66	.38	.24	.24	1.29	2.42	.32	.35	.90
250.0					1.29	2.30	.36	.33	1.00
295.0					1.25	2.17	.38	.33	1.00
FE(PYBEN)3(CLO4)2.2H2O									
8.5	.75	.46	.25	.25					.0
85.0	.74	.46	.25	.25					.0
120.0	.75	.47	.23	.23	1.36	2.56	.36	.36	.18
160.0	.74	.45	.25	.24	1.34	2.48	.36	.36	.27
180.0	.73	.46	.25	.29	1.33	2.56	.38	.38	.34
200.0	.73	.44	.25	.25	1.31	2.52	.38	.38	.48
220.0	.70	.48	.29	.29	1.29	2.51	.33	.33	.57
240.0	.78	.43	.29	.29	1.28	2.42	.34	.33	.69
293.0	.75	.42	.25	.25	1.25	2.21	.36	.33	.84
FE(PYBEN)3(NO3)2.H2O									
8.0	.78	.45	.28	.28	1.36	2.52	.36	.40	.80
40.0	.78	.44	.27	.25	1.36	2.62	.34	.36	.81
85.0	.74	.42	.29	.29	1.35	2.65	.34	.36	.82
100.0	.74	.37	.29	.29	1.36	2.63	.34	.35	.86
120.0	.72	.32	.29	.29	1.36	2.60	.34	.35	.90
150.0	.67	.29	.26	.26	1.34	2.56	.32	.34	.92
180.0					1.34	2.45	.36	.34	1.00
210.0					1.32	2.35	.31	.32	1.00
240.0					1.31	2.27	.33	.34	1.00
270.0					1.30	2.17	.33	.30	1.00
295.0					1.24	1.89	.33	.29	1.00
FE(PYBEN)3(NCS)2.H2O									
8.3	.76	.46	.27	.27	1.41	2.56	.32	.37	.89
40.0	.76	.46	.27	.27	1.41	2.65	.30	.35	.89
84.0	.77	.44	.27	.27	1.40	2.65	.29	.32	.89
105.0	.74	.49	.27	.27	1.39	2.62	.28	.30	.89
115.0	.76	.47	.27	.27	1.37	2.61	.28	.30	.89
140.0	.75	.46	.27	.27	1.38	2.54	.29	.29	.90
170.0					1.38	2.42	.33	.28	1.00
200.0					1.36	2.33	.33	.28	1.00
230.0					1.35	2.23	.34	.30	1.00
260.0					1.33	2.13	.33	.30	1.00
295.0					1.27	2.06	.33	.30	1.00
FE(PYBEN)3BR2									
8.4	.77	.45	.27	.25	1.38	2.56	.28	.31	.41
40.0	.76	.44	.26	.24	1.38	2.64	.27	.28	.41
84.0	.76	.44	.25	.24	1.38	2.68	.28	.28	.41
110.0	.74	.43	.25	.24	1.36	2.66	.28	.28	.50
140.0	.73	.41	.24	.24	1.35	2.63	.26	.29	.61
170.0	.73	.37	.25	.25	1.33	2.57	.30	.29	.72
200.0	.72	.38	.25	.25	1.32	2.49	.30	.29	.83
230.0	.68	.34	.24	.25	1.30	2.46	.30	.29	.87
260.0					1.30	2.37	.35	.28	1.00
293.0					1.25	2.23	.32	.28	1.00

TABLE XI

(Continued/-)

T (°K)	S=0 δ (mm s^{-1})	S=0 ΔE_Q (mm s^{-1})	S=0 Γ_1 (mm s^{-1})	S=0 Γ_2 (mm s^{-1})	S=2 δ (mm s^{-1})	S=2 ΔE_Q (mm s^{-1})	S=2 Γ_1 (mm s^{-1})	S=2 Γ_2 (mm s^{-1})	AREA FRACTION ($^5T_2$/TOTAL)
FE(PYBEN)3I2									
8.3	.75	.43	.25	.25	1.37	2.53	.28	.26	.40
80.0	.74	.41	.26	.26	1.37	2.65	.27	.27	.43
115.0	.75	.42	.26	.26	1.36	2.65	.27	.27	.59
130.0	.75	.39	.26	.26	1.36	2.64	.27	.27	.64
160.0	.72	.41	.26	.26	1.35	2.60	.28	.29	.74
190.0	.70	.37	.26	.26	1.34	2.53	.30	.28	.84
220.0	.76	.34	.26	.26	1.31	2.46	.28	.29	.88
295.0					1.27	2.20	.32	.32	1.00
FE(PYBEN)3(BF4)2.H2O									
8.5	.75	.44	.23	.24	1.36	2.56	.28	.32	.52
86.0	.75	.42	.23	.24	1.36	2.67	.30	.29	.53
100.0	.74	.40	.23	.24	1.36	2.65	.30	.29	.61
130.0	.74	.40	.24	.23	1.35	2.62	.31	.32	.67
160.0	.73	.40	.27	.25	1.34	2.59	.32	.34	.71
190.0	.70	.39	.26	.26	1.31	2.54	.32	.35	.77
220.0	.67	.37	.28	.31	1.30	2.44	.32	.35	.83
250.0	.58	.29	.24	.25	1.28	2.34	.34	.38	.89
295.0	.59	.26	.25	.25	1.24	2.17	.38	.38	.88
FE(PYBEN)3(BF4)2.2H2O									
115.0	.73	.50	.29	.25					.0
130.0	.73	.48	.29	.25					.0
160.0	.72	.47	.28	.25	1.29	2.34	.30	.30	.11
190.0	.71	.46	.28	.25	1.29	2.34	.31	.31	.11
220.0	.71	.46	.28	.25	1.31	2.36	.30	.30	.13
250.0	.68	.43	.30	.25	1.27	2.17	.30	.30	.21
273.0	.68	.38	.29	.28	1.24	2.10	.30	.30	.35
295.0	.77	.42	.29	.29	1.21	1.83	.30	.30	.61
FE(PYBEN)3(BPH4)2.H2O									
8.4	.75	.36	.29	.24	1.36	2.55	.39	.40	.33
87.0	.74	.34	.30	.27	1.35	2.67	.39	.39	.34
100.0	.72	.33	.30	.30	1.37	2.71	.39	.39	.38
120.0	.74	.34	.28	.25	1.36	2.66	.36	.35	.40
150.0	.71	.34	.28	.25	1.34	2.60	.36	.35	.45
180.0	.72	.34	.28	.25	1.33	2.54	.36	.35	.48
210.0	.67	.33	.28	.25	1.32	2.42	.36	.35	.54
240.0	.66	.34	.28	.25	1.29	2.36	.36	.35	.57
270.0	.64	.34	.28	.25	1.27	2.22	.36	.35	.59
295.0	.57	.32	.28	.25	1.22	2.12	.36	.35	.63
FE(PYBEN)2(NCS)2									
115.0					1.42	2.58	.30	.28	1.00
295.0					1.32	1.89	.30	.28	1.00
FE(PYBEN)3(CR(NH3)2(NCS)4)2									
115.0	.72	.37	.27	.27					.0
295.0	.67	.29	.28	.26					.0

FIGURE 22

Mössbauer Spectra of $Fe(pyben)_3(ClO_4)_2 \cdot H_2O$ between 200 and 295 °K

FIGURE 22

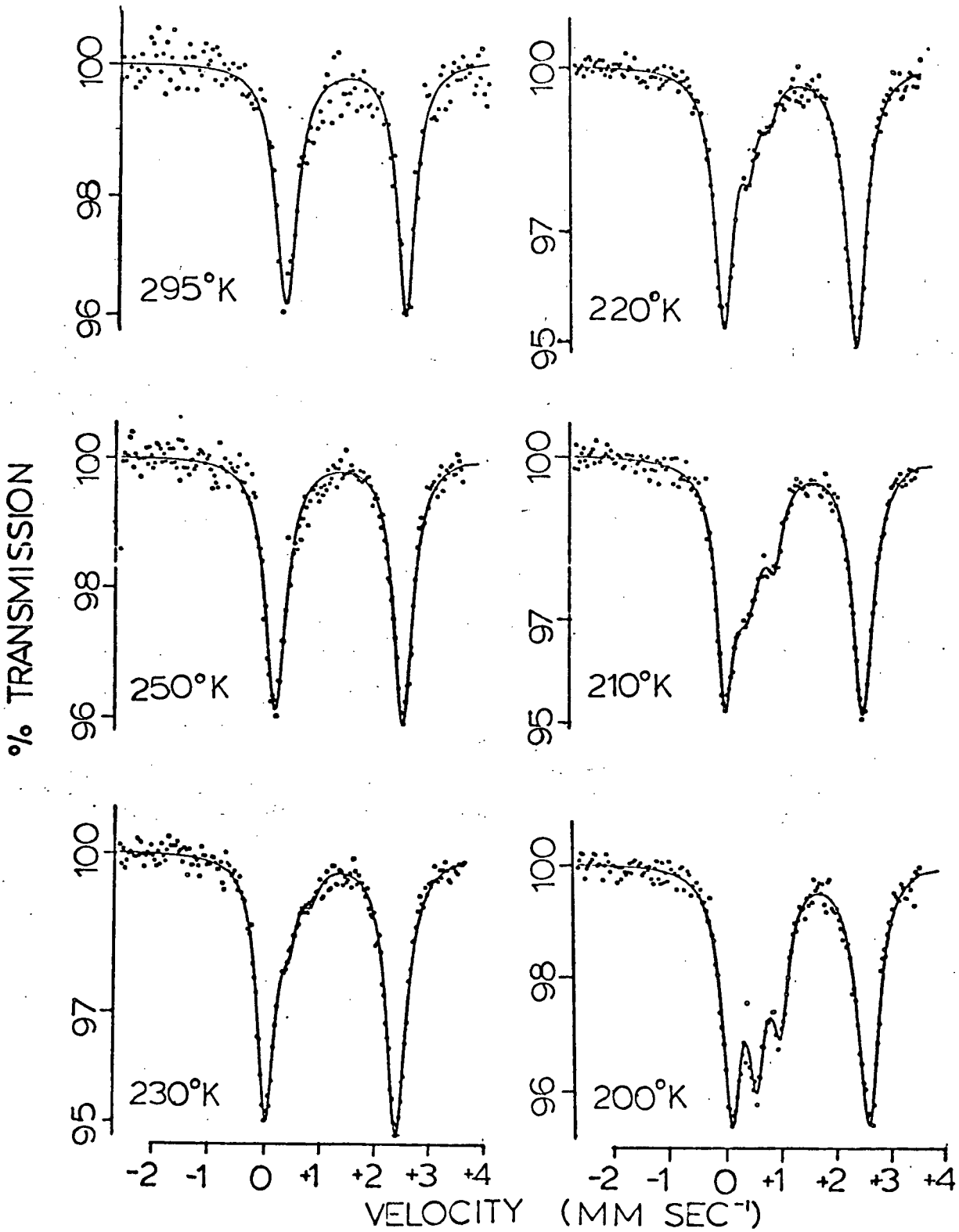
% TRANSMISSION
100
98
96
295°K
100
97
95
220°K
100
98
96
250°K
100
97
95
210°K
100
97
95
230°K
100
98
96
200°K
-2 -1 0 +1 +2 +3 +4
-2 -1 0 +1 +2 +3 +4
VELOCITY (MM SEC⁻¹)

FIGURE 23

Mössbauer Spectra of $Fe(pyben)_3(ClO_4)_2 \cdot H_2O$ between 8.7 and 190 °K

FIGURE 23

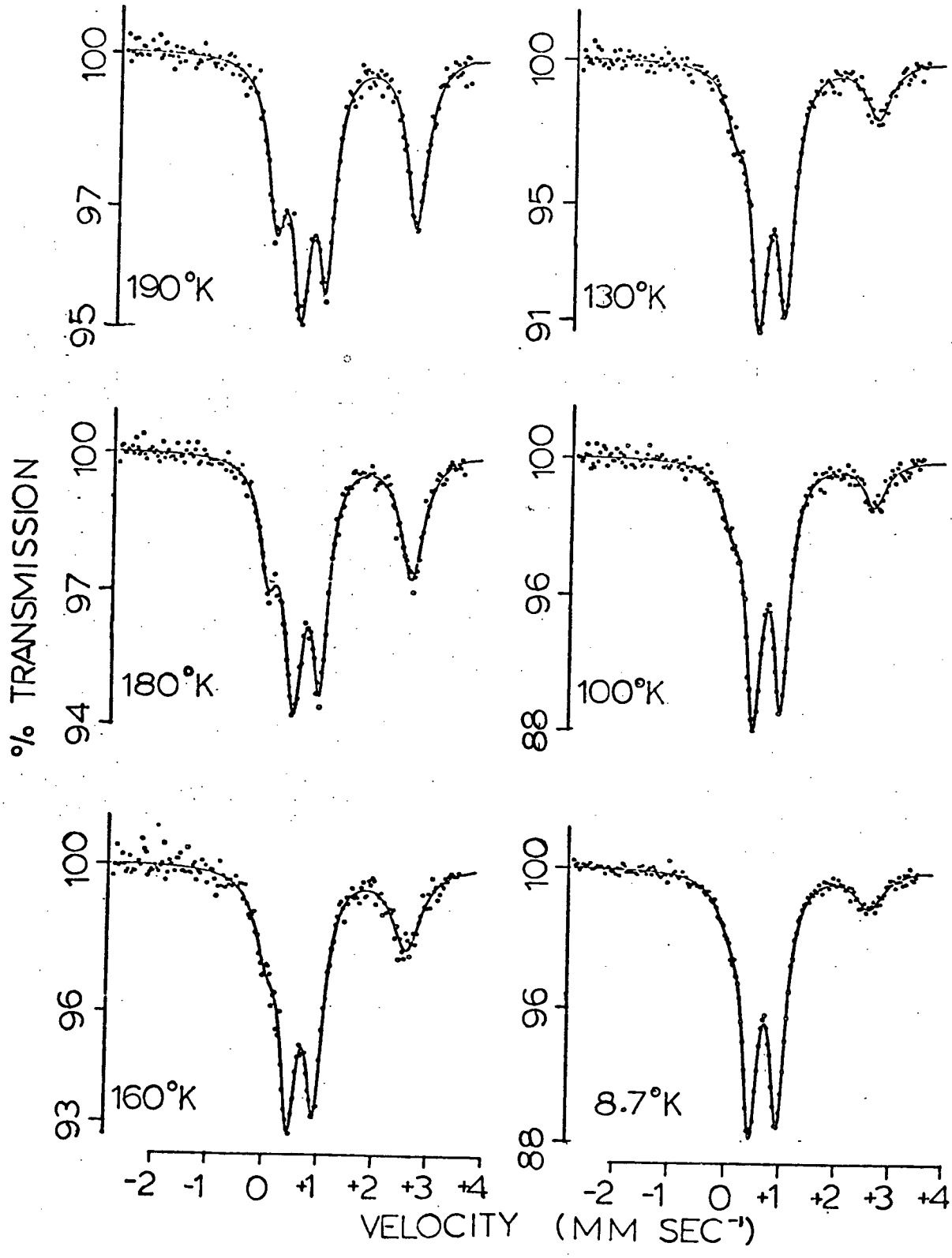
% TRANSMISSION
100
97
95
190°K
100
95
91
130°K
100
97
94
180°K
100
96
88
100°K
100
96
93
160°K
100
96
88
8.7°K
-2 -1 0 +1 +2 +3 +4
VELOCITY (MM SEC⁻¹)

and the nature of the anion appears to have little or no effect on these parameters. The same is true of the parameters for the low-spin species. However, the relative intensities of the two doublets are strongly dependent on the nature of the anion and the number of waters of crystallization.

In order to estimate the relative amounts of high-spin and low-spin species present at a given temperature, one can define an "area fraction" as

$$\text{A.F.} = \frac{\text{Area under the } {}^5T_2 \text{ pair of lines}}{\text{Total spectral area}}$$

These values are listed in the final column of Table XI. It is important to realize that in equating A.F. to the actual fraction of high-spin ions present one is tacitly making the assumption that the recoil-free fractions are identical for both high-spin and low-spin species in a given sample. This assumption may not be strictly valid, but it seems improbable that the recoil-free fractions for the two-spin states will differ appreciably. In practice, when A.F. is very close to zero or unity, statistical error introduced from fitting of the Mössbauer spectrum makes its estimation very difficult. However, within the range $0.1 \leq \text{A.F.} \leq 0.9$ the uncertainty in this parameter is judged to be < 0.05, based on different runs of the same compound.

The A.F. data in Table XI indicate that $Fe(pyben)_2(NCS)_2$ is essentially a pure high-spin complex in the temperature range studied, whereas $Fe(pyben)_3[Cr(NH_3)_2(NCS)_4]_2$ is purely low-spin. For all the

FIGURE 24

Temperature Dependence of the Mössbauer Area Fractions of the Pyben Complexes

⊙	$Fe(pyben)_3(ClO_4)_2 \cdot H_2O$
△	$Fe(pyben)_3(ClO_4)_2 \cdot 2H_2O$
+	$Fe(pyben)_3(NO_3)_2 \cdot H_2O$
×	$Fe(pyben)_3(NCS)_2 \cdot H_2O$
◇	$Fe(pyben)_3Br_2$
✦	$Fe(pyben)_3I_2$
⧖	$Fe(pyben)_3(BF_4)_2 \cdot H_2O$
Z	$Fe(pyben)_3(BF_4)_2 \cdot 2H_2O$
Y	$Fe(pyben)_3(BPh_4)_2 \cdot H_2O$

FIGURE 24

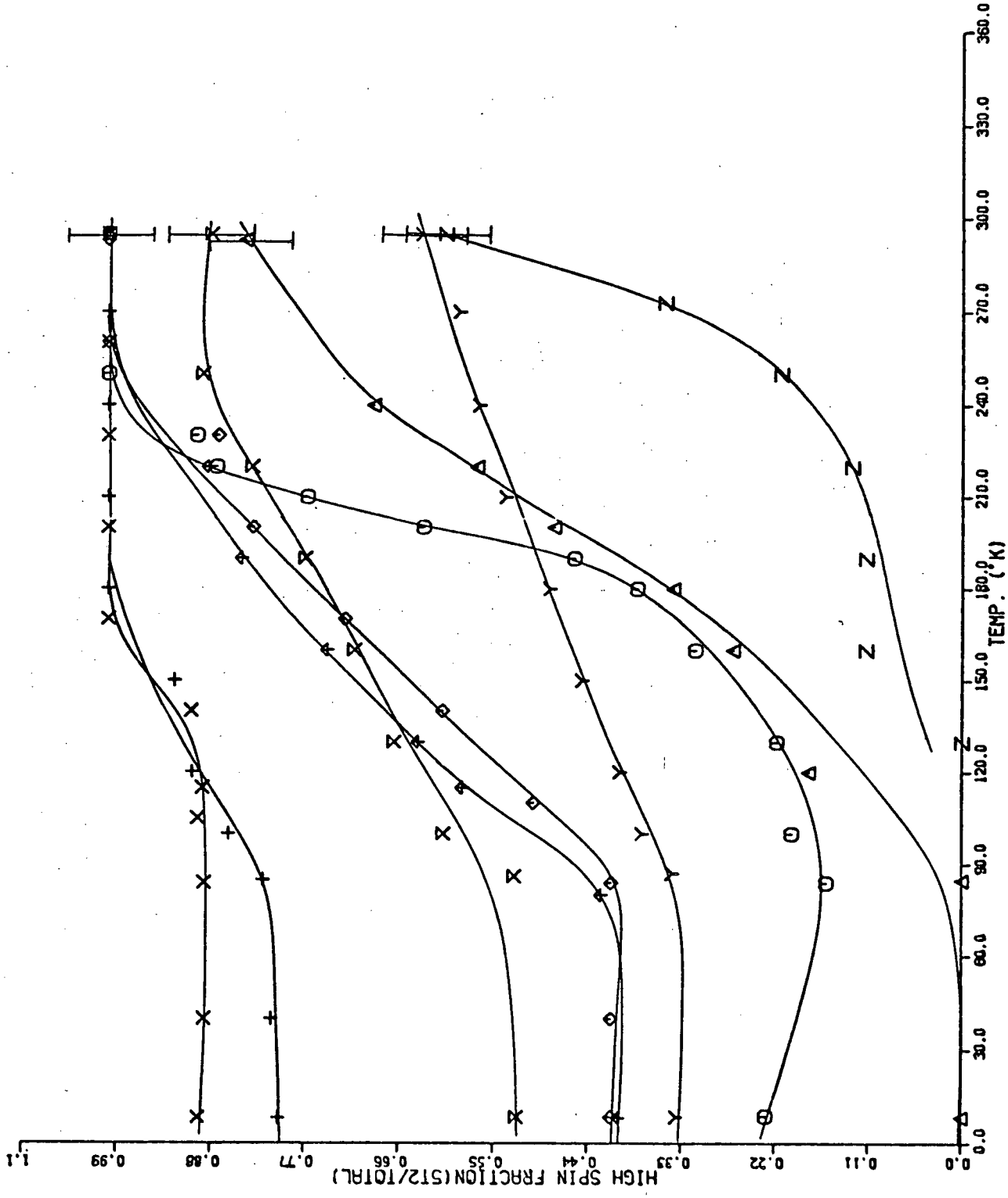
HIGH SPIN FRACTION(S12/TOTAL)
TEMP.(°K)
0.0
0.11
0.22
0.33
0.44
0.55
0.66
0.77
0.88
0.99
1.1
0.0
30.0
60.0
90.0
120.0
150.0
180.0
210.0
240.0
270.0
300.0
330.0
360.0

other complexes spin crossover is observed, but in no case is there a complete change in ground state between 8 and 300°K (see Fig. 24).

As mentioned above, the temperature at which the solid state visible band at 540 nm appears is roughly the same as that at which A.F. begins to depart from unity in the three complexes for which solid state visible spectra were obtained. It was also seen in Table X that the intensity of this band increased very slightly with decreasing T for the nitrate derivative, somewhat more for the bromide complex, and quite strongly for the perchlorate monohydrate. The A.F. values indicate that these intensity changes are at least qualitatively related to the fraction of low-spin species present (1 - A.F.).

Although there is a clear qualitative correlation between μ_{eff} and A.F., there is no quantitative correlation as a few examples will illustrate. In the simplest possible approach one might assign a zero moment to the $^1A_1$ state, a moment of about 5.4 B.M. to the $^5T_2$ state, and then compute an "average moment" at a given temperature from the area fraction. This invariably leads to calculated moments much smaller than the observed values, as shown in Table XII. Further indications that this approach is incorrect are seen in the low temperature data for the perchlorate and tetrafluoroborate dihydrates, and the reineckate salt. All three complexes appear to be fully in the $^1A_1$ state at liquid nitrogen temperature, yet have moments of $\sim$ 1.3 - 1.7 B.M. at 80°K. Even if we assume that we cannot detect an A.F. value smaller than 0.1., the maximum moments obtained for these salts would be only $\sim$ 0.5 B.M. on the basis of this procedure.

König and Kremer[90] have discussed this problem in some detail.

TABLE XII

Comparison of Observed Room Temperature Magnetic Moments with those Calculated by the Simple Model Described in the Text

Salt	μ(Calc. from A.F.) (B.M.)	μ(expt) (B.M.)
$Fe(pyben)_3(ClO_4)_2 \cdot 2H_2O$	4.5	5.35
$Fe(pyben)_3(BF_4)_2 \cdot 2H_2O$	3.29	4.96
$Fe(pyben)_3(BPh_4)_2 \cdot H_2O$	3.40	4.99
$Fe(pyben)_3[Cr(NH_3)_2(NCS)_4]_2$	< 0.54	4.01

They point out that it is inappropriate to assign a moment value of about 5.4 B.M. to the high-spin state due to the effects of spin-orbit coupling on ground and excited states near the spin crossover energy. There is also extensive mixing of eigenstates in this range of energies, which they suggest could lead to a non-zero moment for the low-spin state. Furthermore, the moments carried by both species vary as the energy difference $\Delta\varepsilon$ between the two states changes. König and Kremer[70,90] have postulated that in general $\Delta\varepsilon$ changes with temperature in complexes showing spin crossover, implying that both the high-spin and low-spin fractions have temperature-dependent moments.

There are two aspects of the data presented so far which are rather puzzling and require further comment. The first is that $Fe(pyben)_3(NCS)_2 \cdot H_2O$ shows spin crossover (although to only a limited extent) whereas $Fe(pyben)_2(NCS)_2$ remains fully high-spin down to 115°K. Of the anions used in this study NCS^- lies highest in the spectrochemical series, i.e., it is the strongest field ligand, and when bonded directly to iron as in $Fe(pyben)_2(NCS)_2$ might be expected to enhance the low-spin character of the ferrous ion by increasing 10Dq A tentative explanation of why this does not happen will be offered below.

The second strange feature is that for $Fe(pyben)_3(ClO_4)_2 \cdot xH_2O$ and $Fe(pyben)_3(BF_4)_2 \cdot xH_2O$, both $\mu_{eff}(T)$ and A.F.(T) change drastically when x goes from 1 to 2. It is clear from the ease with which the second lattice water molecule can be pumped off at room temperature that it is only loosely bound, whereas further dehydration of the complexes cannot be achieved <u>in vacuo</u> even at 150°. There seem to be only two possible mechanisms by which the $^5T_2/^1A_1$ ratios could be affected by this second

water molecule:

(1) Crystal packing effects. König and Watson[65] have shown that the Fe-N bonds in $Fe(bipy)_2(NCS)_2$ are slightly shorter in the low-spin than in the high-spin state. If the pyben complexes are similar in this respect it might be supposed that the additional water molecule produces a lattice compression effect which increases the low-spin fraction. However, Fisher and Drickamer[63] have studied the effect of pressure on a number of phen and bipy Fe(II) complexes, and it appears from this work that pressures of the order of 10 kbar or more are required to produce a net high-spin → low-spin conversion. It is almost inconceivable that this loosely held water molecule could cause an effect of this magnitude.

(2) Hydrogen bonding effects. As was mentioned above the imino hydrogen on the benzimidazole portion of the pyben molecule is slightly acidic. The acidity increases on chelation[74], and seems to bear a direct relation to the strength of the N-metal bond. This effect was attributed[74] to a resonance mechanism of the type:

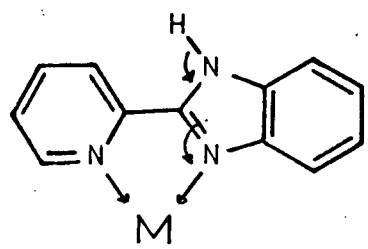

According to this scheme, the formation of a multiple N-metal bond will enhance the acidity of the imino hydrogen. To turn this argument around, a weakening of the N-H bond by hydrogen bonding to a water molecule should cause a strengthening of the N-metal σ bond. In order to prevent

too much charge accumulation on the metal, such an increase in N → metal σ-donation would probably be accompanied by an increase in back π-donation from the metal t_{2g} orbitals to assist formation of the methine chromophore[89] characteristic of the low-spin state. These effects would be synergically related, since strengthening of the N-metal σ bond and of the methine chromophore will both enhance the low-spin fraction.

The energy of such an N-H...O hydrogen bond would presumably lie between those of an N-H...N bond (1.3 kcal $mole^{-1}$ in NH_3)[91] and an N-H...F bond (5 kcal $mole^{-1}$ in NH_4F)[91]. These energies are typical of those encountered in physical adsorption systems such as the rare gases on graphite, where the adsorbed species can be readily pumped off[92], and would account for the ease with which the dihydrates are converted to the monohydrates.

Hydrogen bonding may also account for the behaviour of the thiocyanate complexes. If we assume that NCS^- and pyben are approximately equal in the spectrochemical series, and chemical evidence suggests this is likely to be true, then it is perhaps not too surprising to find that $Fe(pyben)_2(NCS)_2$ is a high-spin complex. In $Fe(pyben)_3(NCS)_2 \cdot H_2O$, on the other hand, since the NCS^- ions are not directly bonded to iron, it would be possible for them to form weak hydrogen bonds with the N-H groups on the ligands. Note that this is the only anion studied here which would even remotely be expected to hydrogen bond.

Discussion of the Cation Structure

In order to obtain more information on the electronic and geometrical structure of the $Fe(pyben)_3^{2+}$ cation in these complexes, it was decided to use magnetic perturbation Mössbauer spectroscopy to determine the η values and signs of V_{zz} in some of the compounds. As pointed out above, for both the low-spin and high-spin species, isomer shift and quadrupole splitting values show only a very slight dependence on the nature of the anion, suggesting that the basic structure of the cation in a given spin state is probably very similar in all the complexes. This suggestion is further supported by the fact that the I.R. spectra of the cations are identical throughout the series. For these reasons, and because of the difficulties encountered in obtaining magnetic perturbation spectra at high temperatures, only $Fe(pyben)_3(ClO_4)_2 \cdot H_2O$ was studied by this technique at 295°K, while such spectra were obtained for three complexes which are fully low-spin at 80°K: $Fe(pyben)_3(ClO_4)_2 \cdot 2H_2O$, $Fe(pyben)_3(BF_4)_2 \cdot 2H_2O$ and $Fe(pyben)_3[Cr(NH_3)_2(NCS)_4]$. The results of these measurements are presented in Table XIII, and the spectrum of BF_4^- salt is shown in Figure 25. For the high-spin perchlorate monohydrate derivative, we find $V_{zz} > 0$ and $\eta \simeq 0.5$. The three complexes with $^1A_1$ ground states all show η values very close to unity and the signs of the efg's cannot be determined unambiguously.

The two nitrogens of the pyben ligand which are bonded to iron are not equivalent. If we denote the pyridine nitrogen by N and the imidazole nitrogen by n, then the ligands can arrange themselves around the iron atom to give either a mer- or fac-octahedral structure:

TABLE XIII

Signs of V_{zz} and Magnitudes of η Deduced from Magnetic Perturbation Mössbauer Measurements

	SIGN OF V_{zz}	η	TEMP(°K)
$Fe(pyben)_3(ClO_4)_2 \cdot H_2O$ (high-spin)	+	~ 0.5	295
$Fe(pyben)_3(ClO_4)_2 \cdot 2H_2O$ (low-spin)	?	~ 0.9	80
$Fe(pyben)_3(BF_4)_2 \cdot 2H_2O$ (low-spin)	?	~ 0.9	80
$Fe(pyben)_3[Cr(NH_3)_2(NCS)_4]_2$ (low-spin)	?	~ 0.9	80

FIGURE 25

Mössbauer Spectrum of $Fe(pyben)_3(BF_4)_2 \cdot 2H_2O$ at 80° K in a Longitudinal Magnetic Field of 50 kG. Computed Spectra for $V_{zz}>0$ and $\eta = 0.7$ and 0.9 are Shown for Comparison.

FIGURE 25

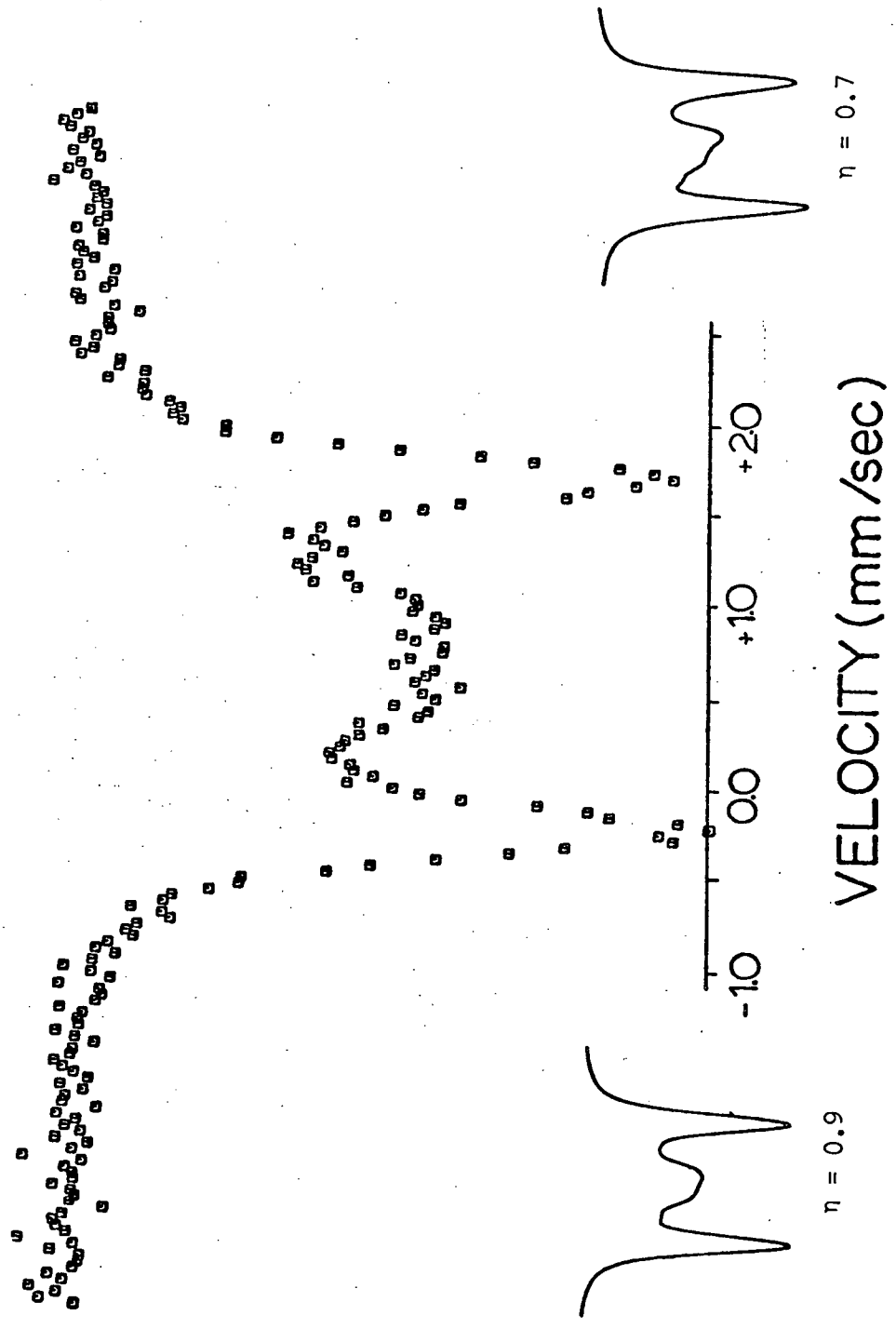

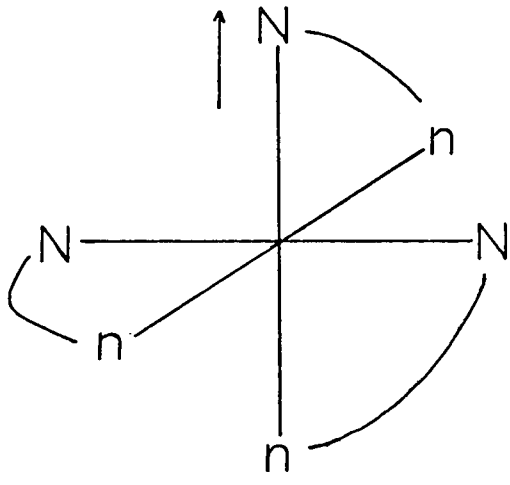

mer

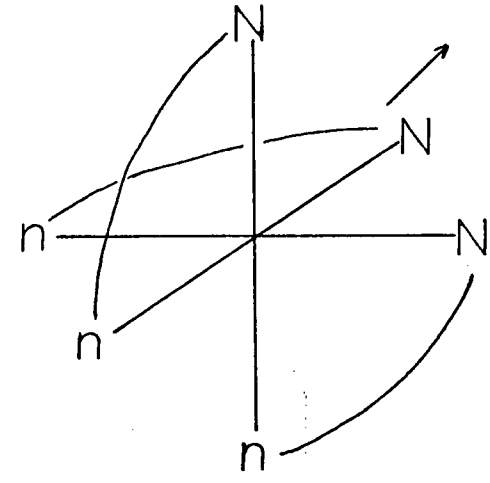

fac

In the mer-octahedral form, the symmetry about iron will be C_{2v} along the N-Fe-n direction, while in the fac- form, it is C_{3v} along the trigonal [1, 1, 1] axis of the octahedron. Due to the asymmetry of the ligand, steric requirements will favour the mer-octahedral form since in this case the threebenzimidazole groups can be further apart than in the fac-octahedral case.

The $^5T_2$ ground state can be treated in the same way as the complexes discussed in Chapter III. The mer-octahedral structure corresponds to a tetragonal distortion with the z axis along the N-Fe-n direction, and since the N-Fe-N and n-Fe-n axes are not equivalent there will be a substantial rhombic field as well. On the other hand, the fac-octahedral structure corresponds to a trigonal distortion and the rhombic term is expected to be small. The magnitude and temperature dependence of ΔE_Q for $Fe(pyben)_3(ClO_4)_2 \cdot H_2O$ (see Table XI) strongly

suggest that the ground state is an orbital singlet. In the tetragonal case the singlet is $|xy\rangle$, which will give $V_{zz}>0$ as observed, in contrast to the trigonal case where the $|z^2\rangle$ singlet will produce a negative V_{zz}. A fit of the ΔE_Q vs T data using the crystal field model outlined in Chapter III yields a tetragonal distortion of $-385\ cm^{-1}$ and a rhombic splitting of $-270\ cm^{-1}$. With these crystal field parameters the calculated η value is 0.45 in good agreement with the observed value. Thus, the Mössbauer data show conclusively that the cation in $Fe(pyben)_3(ClO_4)_2 \cdot H_2O$ adopts a mer-octahedral configuration, and there seems little reason to doubt that the other pyben complexes are similar.

From the crystal field treatment the spin-orbit coupling constant λ is estimated to be $\sim 100\ cm^{-1}$. This indicates that there is no extensive delocalization of the t_{2g} electrons onto the ligands, consistent with an "ionic" $^5T_2$ ferrous system.

The low-spin ground state is more difficult to treat in a reasonably exact way. Both the σ and π bonding systems will contribute to the efg,[93,94] and the effects of these two contributions cannot be separately calculated. However, low-spin ferrous complexes are expected to follow the point charge model[95] fairly closely. This model predicts[96,97] $V_{xx} = V_{yy} = V_{zz} = 0$ for a fac-octahedral structure, and hence zero quadrupole splitting (although distortions from regular geometry could make $|\Delta E_Q| \neq 0$). For the mer-octahedral case the predictions are $V_{xx} = 0$ and $V_{yy} = -V_{zz}$, to give $\eta = 1$ and an indeterminate sign of the efg. Thus, our results for the low-spin complexes are also fully consistent with mer-octahedral structures.

It is interesting to compare these results with those obtained for $Fe(mephen)_3(BF_4)_2$ and $Fe(mephen)_3(CLO_4)_2$.[68] In the $^5T_2$ state the temperature dependence of $|\Delta E_Q|$ for these compounds suggests that the ferrous ion has an orbital singlet ground state, although in magnitude the splittings are considerably smaller than those of the pyben derivatives. This implies a smaller crystal field distortion in the mephen complexes, which is very likely due to the fact that the two nitrogens in mephen (see Fig. 19) are essentially equivalent, in contrast to the situation in pyben. This difference between the two types of ligands is even more clearly seen in the $^1A_1$ states. In the mephen complexes V_{zz} is also positive, but η is close to zero showing a quite symmetric environment about the ferrous ion.

Our studies on the $Fe(pyben)_3^{2+}$ complexes have brought to light some new features of the $^5T_2$ - $^1A_1$ spin crossover phenomenon. From solution and solid state visible spectra we have been able to show that the crossover very probably occurs only in the solid state. This implies that the phenomenon depends not only on the field strengths of the ligands bonded to iron, but is ultimately controlled by crystalline forces in the lattice. That these forces are either very weak or relatively remote from the ferrous ion is demonstrated by the fact that large changes in area fraction from one compound to another are not accompanied by any significant changes in crystal field splitting parameters (as indicated by ΔE_Q values for the high-spin fractions). As seen in Chapter III these parameters are normally quite sensitive to small changes in the Fe^{2+} environment.

Accompanying the $^5T_2 - {}^1A_1$ crossover in these complexes is the appearance of a strong visible absorption band, producing a dramatic colour change. This band has been interpreted as arising from the formation of a "methine chromaphore" typical of covalent systems, and indicates that redistributions of both the ferrous 3d electrons and the ligand π electrons are involved in the crossover process.

The influence of the hydration state of the crystal on the spin equilibrium has been attributed to hydrogen bonding between the water molecule and the acidic hydrogen on the benzimidazole fragment of the ligand. Dosser, et al.[73] have also observed that the magnetic moments of $Fe(pyim)_3SO_4 \cdot xH_2O$ (x = 2,3) were somewhat different (the trihydrate giving lower μ_{eff} values), but offered no explanation for this behaviour. Hydrogen bonding seems likely in this case as well.

The asymmetry of the pyben ligand allows in principle the existence of two geometrical isomers of the $Fe(pyben)_3^{2+}$ cation. Magnetic perturbation Mössbauer spectra for both spin states indicate that it is the meridional isomer which occurs in these complexes.

CHAPTER V

FERROUS PORPHYRINS AND THEIR DERIVATIVES

Introduction

The porphyrins constitute one of the most important classes of compounds in biological systems. The basic structure consists of four pyrrole units linked together to form a large planar aromatic ring system (the porphin nucleus), with substituents at the eight β positions of the pyrrole rings. A number of naturally occurring pigments are metal chelate complexes of the porhyrins. Thus the haeme prosthetic group found in haemeproteins contains a ferrous ion bonded to the four pyrrole nitrogens, and in haemoglobin for example, is attached to the protein via an imidazole nitrogen which occupies the fifth coordination site of the metal. In deoxyhaemoglobin the ferrous ion is in a high-spin (S = 2) state, whereas oxygenation induces a switch to the low-spin (S = 0) state.

The ability of the haeme unit to undergo reversible oxygenation must be strongly influenced by the detailed electronic structure of the ferrous ion. Since in most circumstances electron spin resonance cannot be observed in ferrous complexes, Mössbauer measurements may offer the only method of studying such structural details of the iron atom. Thus, considerable effort has been expended in the study of haemeproteins by this technique, and an excellent review has been published by Lang[98].

It seemed of interest to investigate synthetic iron porphyrins, both from the preparative and structural points of view. For example, it should be possible in principle to prepare a series of ferrous porphyrins in which systematic changes are made in the porphyrin structure, and to study the effects of these changes on the electronic ground state of iron. At the same time the influence of various axial ligands could be investigated. The present chapter describes some attempts in these directions.

It is difficult to isolate either natural or synthetic ferrous porphyrins as solid complexes, and only two applications of Mössbauer spectroscopy to such systems had been reported when this work began. Epstein, et al.[99] studied some hexacoordinate adducts of the type $FeLX_2$, where L was either protoporphyrin IX (PP) or meso-tetraphenylporphin (TPP), and X = pyridine (py), piperidine (pip) and imidazole (im). Only $Fe(TPP)(pip)_2$ was isolated and characterized, the other complexes only being studied as frozen solutions. Kobayashi and co-workers[100] have studied Fe(TPP) and its bis-adducts with pyridine and tetrahydrofuran (THF) in the solid state, using Mössbauer and magnetic susceptibility measurements. Fe(TPP) (structure I) was the first example of a ferrous

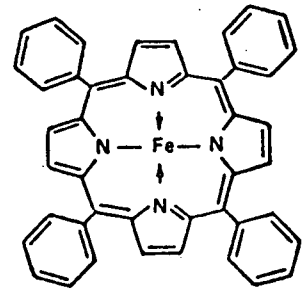

I

porphin to be isolated in the solid state without additional ligands in the axial coordination sites, and its preparation was reported independently by two groups.[101,102] This square planar complex has a high-spin ground state for the ferrous ion, whereas $Fe(TPP)(py)_2$ is diamagnetic[100-102]. For the THF adduct, Kobayashi, et al.[100] have assigned an intermediate-spin (S = 1) ground state to the ferrous ion on the basis of a magnetic moment value of 2.75 B.M. at room temperature, while Collman and Reed[102] have reported a value of 5.1 B.M., corresponding to an S = 2 ground state. $Fe(TPP)(THF)_2$ is relatively unstable with respect to loss of THF,[101] and this and other Fe(TPP) derivatives are quite readily oxidized to μ-O[Fe(TPP)]$_2$.[101,103] Epstein's[103] recent Mössbauer data for several similar oxo-bridged ferric porphin dimers are virtually identical to those reported[100] for "$Fe(TPP)(THF)_2$", so there is some doubt that this was the actual compound studied by Kobayashi, et al.[100] (elemental analyses quoted in ref. 101 were also poor). It should also be noted here that one of the important results of crystal field theory is that a ferrous ion can have only S = 0 or S = 2 spin states in a regular octahedral environment, and that there must be a substantial lowering of the symmetry to stabilize an S = 1 state.

Although these are the only Mössbauer studies to have been reported for synthetic ferrous porphyrins, the structurally related ferrous phthalocyanine [Fe(Pc)] system has been extensively investigated. In Fe(Pc) the pyrroles of the basic porphin nucleus are replaced by isoindole groups and the methine bridges by nitrogen atoms (see structure 2).

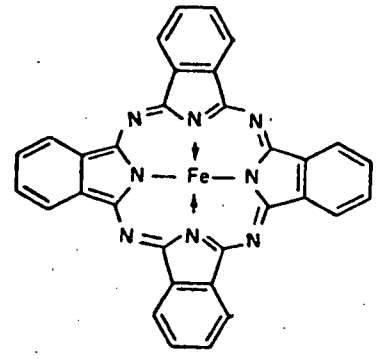

2

Johnson and co-workers[104-106] have shown that in the square planar Fe(Pc) complex the ferrous ion does in fact have an S = 1 ground state, although in hexacoordinate adducts with various amine bases it is fully low-spin[107,108]. Magnetic perturbation Mössbauer spectra of Fe(Pc) and $Fe(Pc)(py)_2$ show that $V_{zz}>0$ and $\eta \simeq 0$ in both cases[104,106]. This sign of V_{zz} is unexpected for the spin triplet ground state[109] of Fe(Pc), as discussed below, but for the diamagnetic $Fe(Pc)(py)_2$ the positive V_{zz} indicates that the bonding to iron is stronger in the Pc plane than in the axial direction[104].

In some ways neither Fe(TPP) nor Fe(Pc) represents a very good model system for haeme. The naturally occurring ferrous porphyrins have full β-substitution of the pyrrole rings, but no meso-substitution. On the other hand, Fe(TPP) has no β-substitution but complete meso-substitution. Although Fe(Pc) can in one sense be regarded as having full β-substitution, the fused benzene rings are hardly equivalent to the β-substituents of heme, and there is also the problem of the =N- rather than =CH- bridges.

Bonnett and co-workers[110,111] have reported the preparation of octamethyltetrabenzporphyrin (H_2OTBP) and its bispyridine Mg(II) chelate complex Mg(OTBP)$(py)_2$. The corresponding ferrous sytem Fe(OTBP) seemed an attractive one to investigate because of its structural similarity to the very stable Fe(Pc) system (see structure 3). We have also prepared

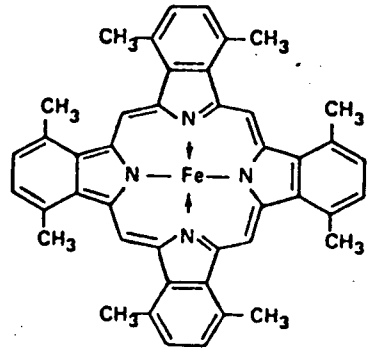

3

and studied octaethylporphyriniron(II), which is perhaps an even better model compound for haeme (see structure 4). It was hoped that Mössbauer

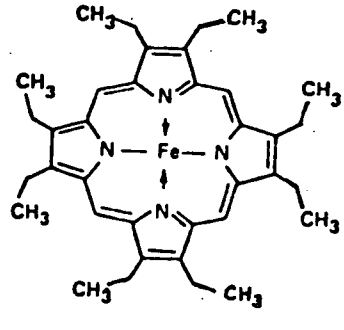

4

and other data on these porphyrin complexes would help clarify the influence of the different structural features on the electronic state of iron.

Preparation of the Complexes

All chemicals were of reagent grade and were obtained either from Fisher Scientific Company or Aldrich Chemical Company. The procedures described below were all carried out in a dry nitrogen atmosphere. The Soxhlet extractor used had a volume of 75 ml.

1,3,4,7-tetramethylisoindole was prepared from 2,5-hexanedione and ammonium sulphate as described by Fletcher[112]. The crude product was recrystallized from diethyl ether to yield the pure isoindole.

Crude octamethyltetrabenzporphyriniron(II).

3.6 g (21 mmol) of 1,3,4,7-tetramethylisoindole and 13 g (230 mmol) of reagent grade iron powder were sealed in a thick-walled glass tube of 180 ml volume, and allowed to react at 350° for 4 hr. The tube was opened and the solid residue was washed with petroleum ether (60 - 110°) and then benzene to afford the crude product I.

Bis(pyridine)octamethyltetrabenzporphyriniron(II)

30 g of I was extracted for 3 hr with 600 ml of a 10/1 pyridine/petroleum ether mixture. The green solution was filtered and the filtrate evaporated to 50 ml volume. The purple microcrystals which formed were collected by filtration and dried *in vacuo* at room temperature. When neat pyridine is used for the extraction, one obtains tetrakis(pyridine)octamethyltetrabenzporphyriniron(II).

Bis(tetrhydrofuran)octamethyltetrabenzporphyriniron(II)

800 ml of THF, which had been freshly distilled over calcium hydride, were used to extract 30 g of I for 0.75 hr. The green extract was filtered and evaported to 50 ml volume producing purple microcrystals of product. This was dried in a stream of dry nitrogen gas for 4 hr at room temperature.

Bis(3-picoline)octamethyltetrabenzporphyriniron(II)

3-Picoline was distilled over calcium hydride. 200 ml of the fraction collected at 144 ± 0.5° was used to extract I in a similar manner to the pyridine extraction above.

Tetrakis(4-picoline)octamethyltetrabenzporphyriniron(II)

4-Picoline was distilled over calcium hydride and the fraction boiling at 145 ± 0.5° collected. 200 ml of this distillate was used to extract I as above.

The corresponding isoquinoline adduct was prepared similarly using the isoquinoline fraction collected at 242°, to yield tetrakis(isoquinoline)octamethyltetrabenzporphyriniron(II)

Octamethyltetrabenzporphyriniron(II)

The bispyridine adduct was heated in vacuo at 180° for 1 hr to afford the blue square planar complex in pure form.

Poly[octamethyltetrabenzporphyriniron(II)]

2-Picoline, freshly distilled over calcium hydride, was used to extract I. The greenish brown extract was left to stand overnight and filtered to give a black product, thought to be $[Fe(OTBP)]_n$.

Bis(pyridine)octaethylporphyriniron(II)

Octaethylporphyrin (H_2OEP) was kindly supplied by Dr. David Dolphin of this Department, who also suggested the following synthetic route[113]. 1 g of H_2OEP was dissolved in 150 ml of refluxing DMF, followed by the addition of 2 g of $Fe(ClO_4)_2 \cdot 6H_2O$. The solution was boiled for 0.25 hr, cooled to room temperature, and added to 500 ml of saturated aqueous sodium chloride solution, the mixture being left to stand in air overnight. The colloidal precipitate which had formed was collected on an F grade sintered filter and washed with hot H_2O to remove excess NaCl. The residue was dissolved in 100 ml of $CHCl_3$ and the solution was treated with several 50 ml portions of 5M HCl in a separatory funnel. The chloroform layer was then washed with water, dried with anhydrous $CaCl_2$, and filtered. The volume of the filtrate was reduced to 100 ml on a hot plate, and then kept constant by addition of ethanolic HCL (100:1) while the solution was boiled. This procedure precipitates octaethylporphyriniron(III) chloride, Fe(OEP)Cl, which was washed with ethanol and dried in air. 1 g of Fe(OEP)Cl was dissolved in 170 ml of pyridine in a 500 ml flask equipped with condenser and dropping funnel. The solution was heated to 50° under a nitrogen atmosphere, and 3.3 ml of hydrazine hydrate was added through the dropping funnel. The solution immediately turned from brown to red. The temperature was maintained at 50° for 0.25 hr, and the solution was then cooled in an ice bath while nitrogen was bubbled through. 7 ml of deoxygenated acetic acid was added, and after a few minutes deoxygenated water was added to precipitate the product. The precipitate was washed with deoxygenated ice cold water and dried *in vacuo* to give the orange $Fe(OEP)(py)_2$.

Octaethylporphyriniron(II)

1 g of $Fe(OEP)(py)_2$ was heated *in vacuo* at 150° for 2.5 hr to yield the pure ferrous porphyrin.

Analytical data for the complexes are given in Table XIV.

Weight Loss Experiments

Since it was found that these ferrous porphyrin adducts lose solvent when heated *in vacuo*, weight loss experiments were carried out to determine the number of solvent molecules attached. The results are listed in Table XIV along with the microanalytical data. A typical experiment is as follows. A thoroughly ground sample (usually about 0.5 g) of the solvated compound was weighed in a small weighing bottle. This bottle was placed in a tube (fitted with a B45 cone and socket and a stopcock) which was then attached to a vacuum line equipped with a cold trap. The sample was then heated *in vacuo* to 150° -180°, and weighed at half-hourly intervals until constant weight was obtained. The Mössbauer spectrum was recorded, and the sample was redissolved in the appropriate solvent to obtain the original adduct. The Mössbauer spectrum was recorded again to confirm the reversibility of the process.

General Discussion

Octamethyltetrabenzporphyrin Complexes

The method used to prepare the Fe(OTBP) compounds follows closely Bonnett's route to the corresponding magnesium compound[110,111]. However, the 20% yield obtained is lower than that of the magnesium

TABLE XIV

Analytical and Magnetic Data for the Ferrous Porphyrin Complexes

COMPOUND	MICROANALYSIS C	H	N	COLOUR & MAGNETIC PROPERTY	WT. LOSS
$Fe(OTBP)(py)_2$	77.50	5.41	10.30	Purple (dia)	1 hr 180°C 19.0%
(Calc.	77.70	5.52	10.10)		(Calc. 18.9%)
$Fe(OTBP)(py)_4$	77.3	5.75	11.00	Purple	1 hr 180°C
(Calc.	77.4	5.65	11.30)	(dia)	31.4% (Calc. 31.8%)
$Fe(OTBP)(THF)_2$	76.23	6.24	6.71	Purple	1 hr 130°C 17.7%
(Calc.	76.10	6.34	6.81)	(μ_{eff}=5.5 B.M.)	(Calc. 17.6%)
$Fe(OTBP)(3\text{-pic})_2$	78.30	5.58	9.63	Purple	1 hr 180°C 21.8%
(Calc.	77.80	5.80	9.30)	(dia)	(Calc. 21.6%)
$Fe(OTBP)(4\text{-pic})_4$	77.60	6.42	10.14	Purple	1 hr 180°C 35.0%
(Calc.	77.70	6.13	10.34	(dia)	(Calc. 35.4%)
$Fe(OTBP)(IQ)_4$	81.00	5.32	9.11	Purple	1 hr 200°C 43.5%
(Calc.	80.50	5.37	9.40)	(dia)	(Calc. 43.3%
Fe(OTBP)	78.40	5.57	8.50	Blue	
(Calc.	78.10	5.35	8.28	(μ_{eff}=5.95 B.M.)	
$[Fe(OTBP)]_n$	78.24	5.40	8.13	Black	0%
(Calc.	78.10	5.35	8.28)	(variable)	
$Fe(OEP)(py)_2$	74.00	7.24	11.25	Orange	2½ hr 150°C 21.3%
(Calc.	73.70	7.19	11.19)	(dia)	(21.2%)
Fe(OEP)	73.58	7.59	9.44	Brown	
(Calc.	73.46	7.49	9.53)	(μ_{eff}=4.7 B.M.)	

porphyrin, reported to be 81%.[111] Our lower yield may be due to the presence of side reactions which are absent in the magnesium case. Secondly, due to the high solubility of the $Fe(OTBP)(py)_2$ in pyridine, precipitation from this solvent is far from quantitative. Attempts to increase the yield by alternative routes such as refluxing iron powder and the isoindole in chloronaphthalene showed that only a very small amount of the porphyrin was formed. An attempt to convert the magnesium compound into the free porphyrin with trifluoroacetic acid, followed by insertion of iron was equally unsuccessful.

In order to characterize this ferrous porphyrin system more completely, n.m.r., electronic and mass spectral measurements were made. The I.R. spectra of these compounds are very diffuse and cannot be interpreted easily.

The ^1H n.m.r. spectrum of $Fe(OTBP)(py)_2$ was obtained in both pyridine and DMSO-d_6 solutions, and data are given in ppm downfield from internal TMS. In both solvents the spectra arising from the methyl and methine (bridge) protons are identical, consisting of two singlets at 3.8 (area 6) and 11.8 (area 1). The OTBP ring protons are masked in pyridine solution, but in DMSO-d_6 there is a poorly defined multiplet centred at 7.9 [In Fe(Pc) this multiplet is seen at 7.6 in the same solvent.] The coordinated pyridines give rise to two doublets at 8.6 and 7.8, and a triplet at 7.5 (area ratio 2:2:1), only slightly shifted from their positions in neat pyridine (8.5, 7.6, 7.2).

The n.m.r. spectrum leaves no doubt as to the existence of Fe(OTBP). The bridge proton resonance at 11.8 ppm is very strongly shifted downfield from the usual aromatic absorption region of about

7 ppm, indicating a very large ring current. The deshielding of the methyl protons is somewhat less, although even here there is a downfield shift of nearly 2.5 ppm from the usual position of about 1.5 ppm.

The mass spectrum of Fe(OTBP) shows a prominent parent peak (P^+) at m/e = 676, and an even stronger peak at m/e = 338 which can be assigned to the doubly-charged P^{++} species. This type of mass spectrum is characteristic of porphyrin systems[114]. Due to the very high melting point of Fe(OTBP), it was necessary to heat the sample to about 450° in order to obtain a sufficiently high vapour pressure for the mass spectrometer, and at lower m/e values there is evidence of some decomposition.

The solution electronic spectrum of $Fe(OTBP)(py)_2$ in spectrograde pyridine provides definitive evidence of a porphyrin chromaphore (see Figure 26). There is a split band at 395 and 433 nm (ε_{max} = 8 x 10^4, 1.7 x 10^5), which is the unique Soret band of the porphyrins[115] and has the largest extinction coefficient known. Two further absorptions are seen at 560 nm (ε_{max} = 2 x 10^4) and 603 nm (ε_{max} = 9 x 10^4). These bands are in good agreement, both in positions and intensities, with those observed by Linstead[115] for the tetrabenzporphyrin (TBP) compound $Fe(TBP)(py)_2$.

All the adducts are purple in colour and (exoept for the THF complex) diamagnetic. The square planar Fe(OTBP) compound, on the other hand, is blue and has a room temperature magnetic moment of 5.95 B.M. indicating a high spin ground state. The large μ_{eff} value suggests a large orbital contribution, as in the case of the phthalocyánine iron compound[105]. The THF adduct has a room temperature moment of 5.5 B.M., quite typical of high spin octahedral ferrous complexes.

FIGURE 26

Electronic Spectrum of $Fe(OTBP)(py)_2$ in Pyridine at 25°

FIGURE 26

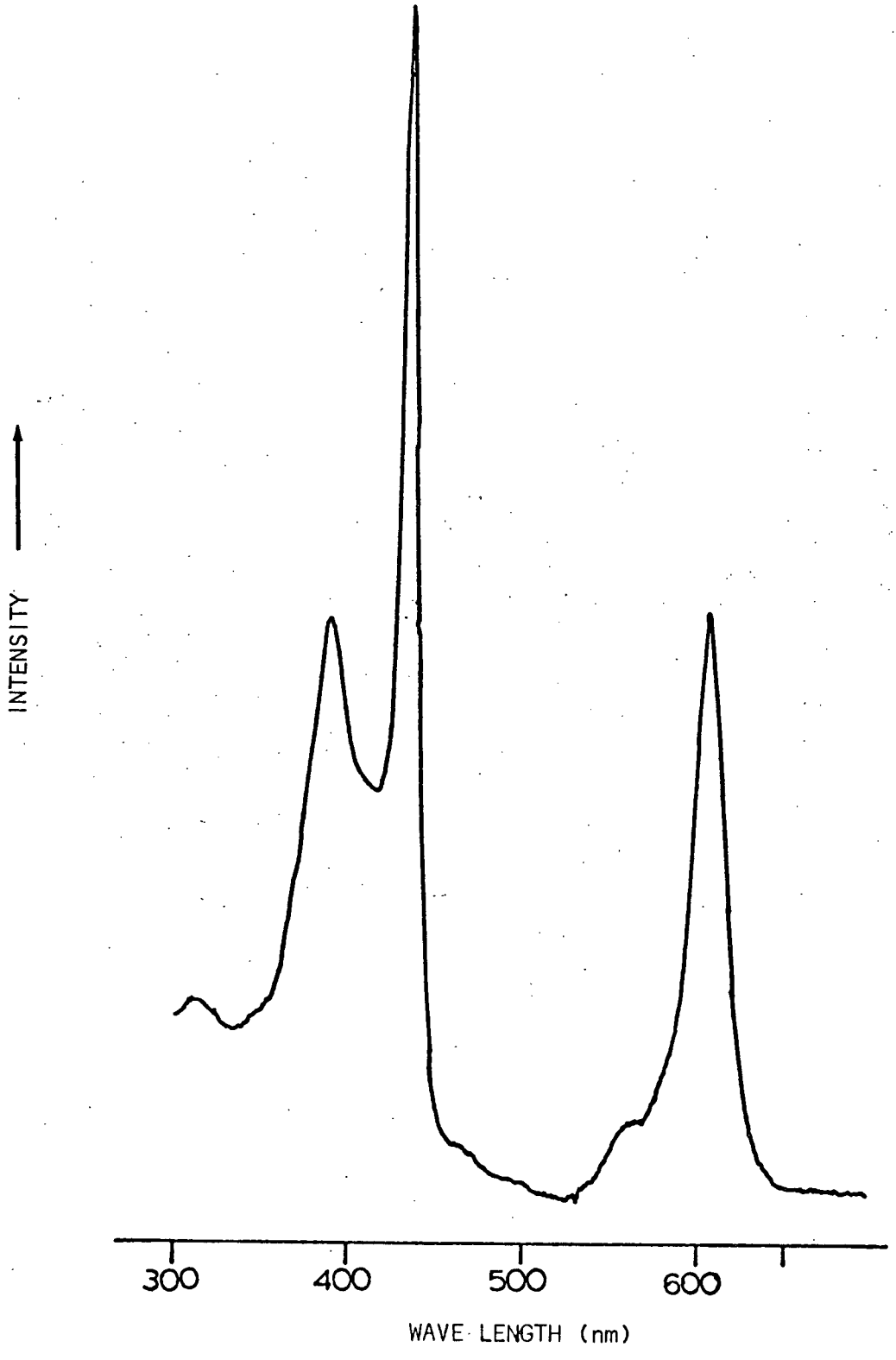

The Fe(OTBP) adducts with amine bases are remarkably stable in air. For example, the bispyridine complex showed no sign of decomposition after standing on the bench for two weeks. However on very long exposure to the atmosphere it gradually changes colour due to loss of pyridine. The THF adduct shows much lower air stability. Even when kept under nitrogen this adduct slowly loses THF to form a black compound which analyses for Fe(OTBP). A discussion of the properties of this black material is given at the end of this chapter.

The square planar Fe(OTBP) compound obtained by pyrolysis of the adducts also appears to be quite stable in air. Identical Mössbauer spectra and analytical data were obtained before and after exposure to the atmosphere for more than a week. However, it was noticed that over long periods of time in air, the blue colour of this compound gradually darkens.

Octaethylporphyrin Complexes

Since octaethylporphyrin has been characterized previously,[113] only n.m.r. and electronic spectra (in pyridine) of the $Fe(OEP)(py)_2$ compound were obtained for identification purposes. The n.m.r. spectrum differs little from that of the protonated ligand H_2OEP. The methyl protons absorb at 1.9 ppm and the methylene protons at 4.0 ppm, exactly the same positions as in H_2OEP. However, the methine bridge hydrogen resonance is shifted slightly from 10.2 ppm in H_2OEP to 10.0 ppm in the iron complex. The electronic spectrum (Fig. 27) shows a Soret band at 409 nm ($\varepsilon_{max} = 1.2 \times 10^5$) and two more bands at 520 nm and 549 nm. ($\varepsilon_{max} = 1.5 \times 10^4$, 2.5×10^4). The diamagnetic orange $Fe(OEP)(py)_2$

FIGURE 27

Electronic Spectrum of $Fe(OEP)(py)_2$ in Pyridine at 25°

FIGURE 27

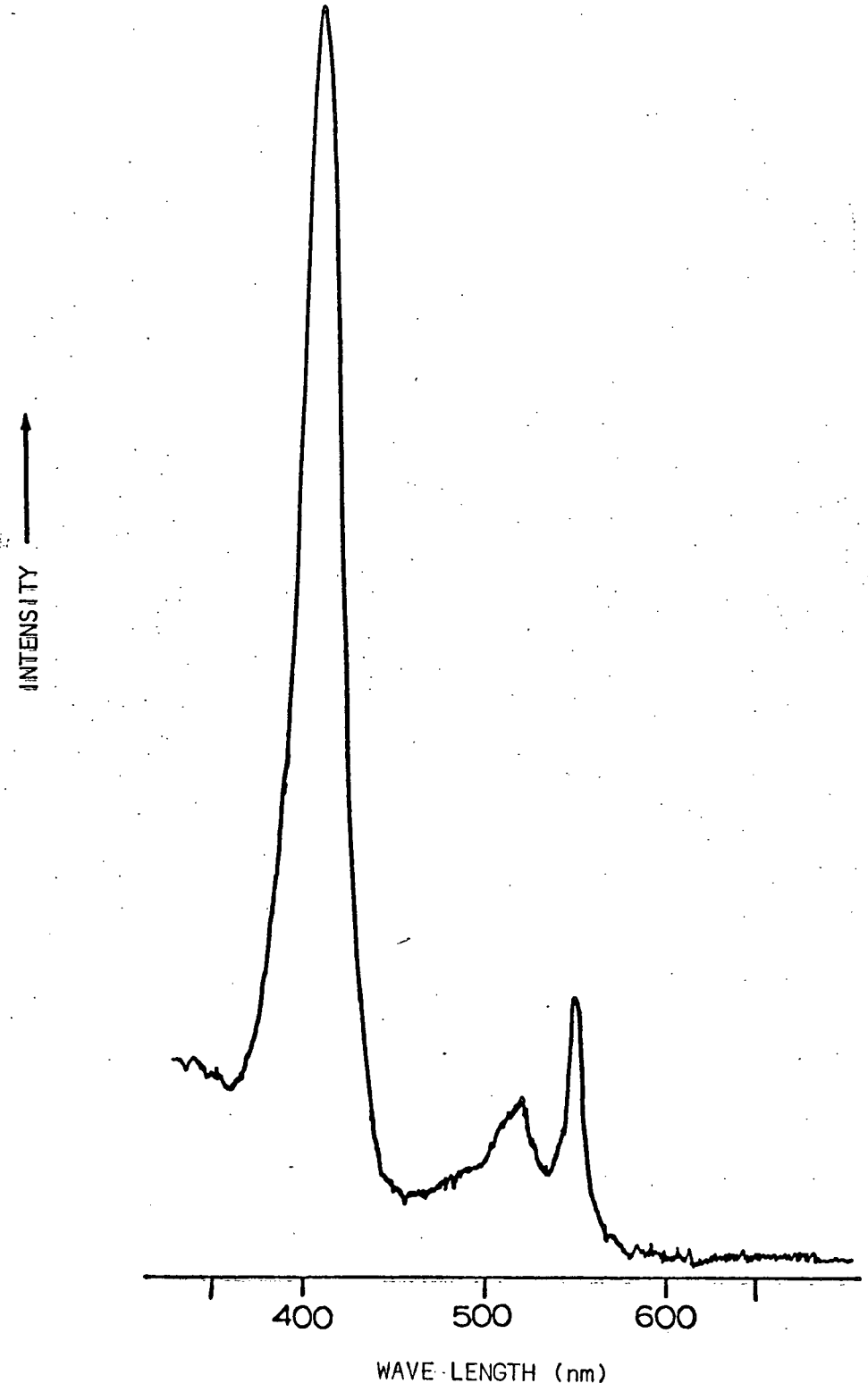

adduct is considerably more air sensitive than the corresponding OTBP complex. When $Fe(OEP)(py)_2$ was left in air for one day, its Mössbauer spectrum showed that it had suffered decomposition.

The dark brown square planar Fe(OEP) complex is extremely air sensitive and most operations on this compound were carried out in vacuo to prevent decomposition. A weighed sample of $Fe(OEP)(py)_2$ was loaded into a calibrated Gouy tube under a dry nitrogen atmosphere, and placed on the vacuum line. After heating the sample at 150° to constant weight (2.5 hr) the weight loss corresponded to the removal of 2 moles pyridine per mole $Fe(OEP)(py)_2$. The Gouy tube was then sealed in vacuo and room temperature susceptibility measurements indicated a magnetic moment of 4.7 B.M. This is slightly lower than the spin-only value of 4.9 B.M. expected for a high-spin ferrous complex, but similar to the value 4.75 B.M. found for Fe(TPP)[101,116].

Attempts were made to obtain $Fe(OEP)(THF)_2$ by two routes. In the first, Fe(OEP) was dissolved in deoxygenated THF and the solution was evaporated to dryness in vacuo at room temperature. This procedure afforded only Fe(OEP). The second route involved the attempted reduction of Fe(OEP)Cl in THF rather than pyridine, but yielded an oily product which could not be crystallized.

Discussion of the Mössbauer Data

Mössbauer parameters for the OTBP and OEP complexes are given in Table XV along with relevant data for some related compounds. A few general comments on the data should be made.

TABLE XV

^{57}Fe Mössbauer Parameters for the Ferrous Porphyrin Complexes

Compound	T(°K)	δ(mm s^{-1})	ΔE_Q(mm s^{-1})	Γ_1 (mm s^{-1})	Γ_2 (mm s^{-1})	n	Ref.
Fe(OTBP)	295	0.94	0.56	.30	.23		
	115	1.04	+0.61	.27	.28	~ 0	
	83	1.05	0.62	.27	.28		
	8.6	1.06	+0.63	.27	.28	~ 0	
Fe(TPP)	77	0.78	1.32				(101)
Fe(OEP)	295	0.81	1.49	.25	.20		
	115	0.88	+1.60	.31	.26	~ 0	
	4.2	0.86	1.60	.28	.27		
Fe(Pc)	293	0.66	2.62				(104-108)
	77	0.77	2.69				
	4	0.75	+2.70			~ 0	
Fe(OTBP)py$_2$	295	0.69	0.73	.25	.26		
	115	0.73	0.70	.28	.31		
	84	0.77	+0.68	.28	.31	~ 0	
	8.8	0.77	0.67	.28	.32		
Fe(TPP)py$_2$	300	0.62	1.22				(101)
	77	0.67	1.15				
Fe(OEP)py$_2$	295	0.65	1.21	.27	.26		
	115	0.72	1.17	.31	.30		
	85	0.73	+1.14	.31	.30	~ 0	
	8.25	0.73	1.13	.36	.36		
Fe(PP)py$_2$	77	0.72	1.21				(99) Frozen Solution
Fe(Pc)py$_2$	293	0.52	2.02				(104-108)
	77	0.59	1.97				
	4	0.58	+1.96				
Fe(OTBP)(3-pic)$_2$	295	0.69	0.81	.29	.27		
	115	0.78	+0.76	.28	.27	~ 0	
Fe(OTBP)py$_4$	295	0.67	0.85	.29	.26		
	115	0.72	+0.82	.29	.28	~ 0	
Fe(OTBP(4-pic)$_4$	295	0.70	0.79	.27	.25		
	115	0.76	+0.74	.28	.25	~ 0	
Fe(OTBP)(1Q)$_4$	295	0.65	0.92	.27	.27		
	115	0.72	+0.87	.31	.29	~ 0	
Fe(OTBP)(THF)$_2$	295	1.18	2.21	.34	.29		
	250	1.22	2.29	.26	.26		
	220	1.22	2.47	.24	.25		
	190	1.25	2.54	.26	.24		
	160	1.26	2.61	.24	.23		
	130	1.28	2.64	.24	.23		
	115	1.27	2.66	.24	.23		
	105	1.29	2.66	.24	.23		
	83	1.29	+2.67	.24	.23	~ 0	
	60	1.30	2.69	.24	.21		
	30	1.30	2.72	.24	.22		
	7.75	1.30	2.74	.25	.22		

Firstly, for the square planar complexes it is seen that each one has a distinctive set of δ and $|\Delta E_Q|$ parameters. Fe(OTBP) and Fe(Pc) lie at opposite ends of the scale with Fe(OEP) and Fe(TPP) having intermediate values. Similar behaviour is found for the bispyridine adducts except that the intermediate OEP, TPP and PP complexes have nearly identical Mössbauer parameters. An attempt will be made below to relate these differences to the σ and π bonding strengths of the tetradentate ligands.

Secondly, the isomer shifts for Fe(OTBP) and its THF adduct are fairly typical of high-spin (s = 2) ferrous systems, whereas the other complexes all have δ values close to 0.7 mm s^{-1}, the value usually considered to be the empirical dividing line between high-spin and low-spin ferrous derivatives. Indeed, for most of these compounds a positive assignment of spin state cannot be made on the basis of δ values alone, and one must rely on magnetic moment data. Moreover, one sees that in going from a tetracoordinate high-spin compound to a hexacoordinate low-spin one there is only a small change in δ, in contrast to the very large changes found in Chapter IV.

Thirdly, the $|\Delta E_Q|$ values vary widely, ranging from about 0.6 mm s^{-1} for Fe(OTBP) to 2.7 mm s^{-1} for Fe(Pc) and $Fe(OTBP)(THF)_2$. For this last complex the temperature dependence of $|\Delta E_Q|$ is characteristic of octahedral high-spin ferrous compounds (see Chapter III), but for all the other derivatives $|\Delta E_Q|$ is nearly independent of temperature.

Finally, magnetic perturbation Mössbauer measurements show that for all the OTBP and OEP derivatives [as well as for Fe(Pc),[106] and $Fe(Pc)(py)_2$,[104]], V_{zz} is positive and η is essentially zero. This indicates

a concentration of charge in the porphyrin (or phthalocyanine) plane and shows the equivalence of the x and y directions within that plane. We shall assume $V_{zz}>0$ also for Fe(TPP), although this has yet to be confirmed experimentally.

Before discussing the Mössbauer parameters in relation to the bonding in these complexes, it is important to consider in general the structural characteristics of the tetradentate ligands and the differences expected in their σ and π bonding properties.

The four porphyrins OTBP, OEP, TPP and PP are all expected to have very similar ring sizes, and in the ferrous complexes the Fe-N bond distances should be nearly identical. Thus, one does not expect any significant differences in N→Fe σ-donor strength amongst the porphyrins. On the other hand, phthalocyanine has a substantially smaller ring size[117-122] due to the =N- rather than =CH- bridge, and the Fe-N distance should be significantly shorter in Fe(Pc) than in the porphyrins. This should have the effect of making Pc the strongest σ donor of the ligands considered here.

The nitrogen bridging atoms in Pc are also expected to influence the π bonding strength of this ligand. Simple Hückel π electron calculations[123] on such ring systems have shown that the total electronic charge at the bridge atoms is lower than at the other ring atoms. That is, the formation of an aromatic π electron system favours removal of a certain amount of electron density from the bridge atoms. Since nitrogen is more electronegative than carbon, the ring current system with a methine bridge will be inherently stronger than with a nitrogen bridge. On the other hand, the fused benzene rings in Pc

should contribute additional resonance energy which will probably more than compensate for any weakening of the π system induced by the bridging nitrogens. It therefore seems reasonable to suggest that OTBP will have the greatest π bonding strength of the ligands under discussion, with Pc probably second.

Of the remaining porphyrins, TPP should have the next highest π bonding strength because of the electron releasing phenyl groups in the four meso positions. However, these phenyl groups are oriented perpendicular to the plane of the porphyrin[122] so that the phenyl π system will not contribute directly to the ring current. Protoporphyrin (PP) is expected to be the weakest π bonding ligand because of the electron withdrawing vinyl and acidic side chains on the pyrrole rings. Thus, the suggested order of π bonding strengths is OTBP>Pc>TPP>OEP>PP. This order has been partially verified by the n.m.r. spectra of $Fe(OTBP)(py)_2$ and $Fe(OEP)(py)_2$, since the position of the methine proton resonance is directly related to and is a good indication of the strength of the π electron system. As we saw above this resonance occurs 1.8 ppm further downfield in the OTBP compound, indicating a stronger deshielding of this proton.

With these qualitative considerations in mind we turn to a more detailed examination of the Mössbauer data. For a paramagnetic ferrous ion in a square planar environment there are four possible electronic ground states, namely $^5B_{2g}$ and ^5E_g for the S = 2 case, and ^3E_g and $^3B_{2g}$ for the S = 1 case. These ground states are illustrated schematically in Figure 28. From Table I and the estimate of ~ 4 mm s^{-1} for the quantity $\frac{4}{7}e(1-R)\langle r^{-3}\rangle$ as discussed in Chapter III, simple crystal field model

FIGURE 28

Possible Ground States for Ferrous Porphyrins under D_{4h}

b_{1g} $(d_{x^2-y^2})$

a_{1g} (d_{z^2})

e_g (d_{xz}, d_{yz})

b_{2g} (d_{xy})

FIGURE 28

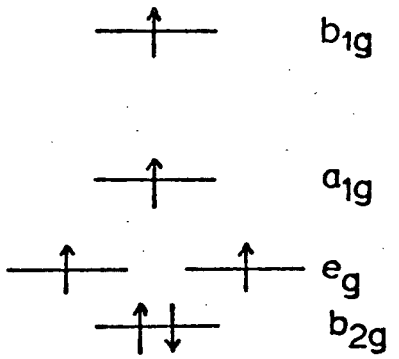

$^5B_{2g}$

$V_{zz}/e = \frac{4}{7}\langle r^{-3}\rangle$

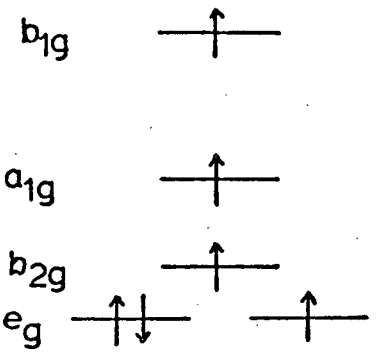

^5E_g

$V_{zz}/e = -\frac{2}{7}\langle r^{-3}\rangle$

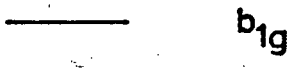

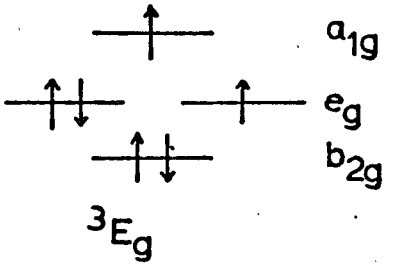

^3E_g

$V_{zz}/e = -\frac{2}{7}\langle r^{-3}\rangle$

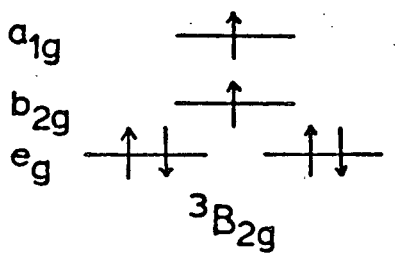

$^3B_{2g}$

$V_{zz}/e = -\frac{8}{7}\langle r^{-3}\rangle$

estimates for the sign and magnitude of ΔE_Q for each of these ground states can be obtained, and these are included in Figure 28. The extended Hückel MO calculations of Gouterman and co-workers[124,125] predict a ^3E_g ground state if the ferrous ion lies in the plane of the cyclic ligand, whereas if it lies 0.492 Å out of the porphyrin plane the predicted ground state is $^5B_{2g}$. For all three ferrous porphyrins which have been isolated, susceptibility data indicate spin quintet ground states. In view of Gouterman's calculations[124] and the observed positive values of V_{zz} in these compounds it might seem reasonable to assume that the ground states are in fact $^5B_{2g}$.

However, results for Fe(Pc) indicate that one should be very cautious about assigning the ground states in systems such as these on the basis of crystal field predictions of the sign of the efg. Low temperature susceptibility measurements show that Fe(Pc) is an intermediate-spin complex, but there appears to be some uncertainty about the exact nature of the ground state. Johnson and co-workers[105,106] have assigned the ground state as ^3E_g, but Barraclough, et al.[109] suggest it is $^3B_{2g}$. In either case ΔE_Q is predicted to be negative, whereas the measured value is large and positive. Johnson[106] has suggested that the most likely explanation of this sign reversal is that the effects of covalency are so great as to completely swamp the negative contribution from the iron's own valence electrons, thus rendering the crystal field approximation completely inadequate. Note that the in-plane N→Fe σ donation will be into the iron $3d_{x^2-y^2}$, $4p_x$ and $4p_y$ orbitals (assuming iron uses dsp^2 hybrids for σ bonding), all of which make positive contributions to V_{zz}.

The effect of strong σ bonding is also reflected to some extent in the orbital occupancies calculated by Gouterman[124] for the ^3E_g ground state of a ferrous porphyrin. These calculations indicate the presence of about 0.9 electron in the iron $b_{1g}(d_{x^2-y^2})$ orbital instead of zero. Using these orbital occupancies the calculated ΔE_Q becomes +1.13 mm s^{-1}. It is clear that this approximate MO calculation is an improvement over the crystal field approach, since the predicted sign of V_{zz} is at least correct. However, the magnitude of ΔE_Q is still very much smaller than the measured value, indicating that at least for Fe(Pc) the effects of covalency are still grossly underestimated. This is not too surprising, since as we have suggested above phthalocyanine should be a much stronger σ donor than the porphyrins.

In view of these results we think it would be unwise to make a definite choice between $^5B_{2g}$ and ^5E_g as the ground state of iron in the ferrous porphyrins. As we shall see below, Fe(OTBP)$(THF)_2$ does in fact have an orbital singlet ($^5B_{2g}$) ground state, and if one assumes that the only perturbation introduced by these weak axial ligands is an increase in the energy of the iron $a_{1g}(d_{z^2})$ orbital, this would imply a $^5B_{2g}$ ground state in the neat ferrous porphyrins as well. Although we consider this the more likely ground state, the choice must still be regarded as tentative.

Despite the uncertainties concerning the exact nature of the ground states in these complexes, Gouterman's calculations[124,125] suggest an important difference between Fe(Pc) and the ferrous porphyrins: only if the iron atom lies in the plane of the macrocyclic ligand is a spin triplet ground state predicted. This may indicate that the very strong σ bonding in Fe(Pc) is able to keep the iron atom in the

plane, while in the porphyrins a more stable configuration is achieved with the iron atom slightly out of the plane. A possible mechanism for stabilizing an out-of-plane configuration is the increase in π bonding which could be achieved. Under D_{4h} the π orbitals of the planar porphyrin span e_g, a_{2u} and b_{2u},[126] so that only the $e_g(d_{xz},d_{yz})$ orbitals on iron have appropriate symmetry to overlap with the porphyrin π system in the in-plane configuration. In the out-of-plane configuration the transformation properties of d_{z^2} are altered and this orbital is then able to mix with ligand π orbitals transforming as a_{2u},[124] an interaction which is symmetry forbidden for the in-plane case.

For the $^5B_{2g}$ ground state of ferrous porphyrin, Gouterman's[124] orbital occupancy numbers lead to a predicted E_Q of + 3.81 mm s^{-1}, which does not differ appreciably from the simple crystal field estimates but is much larger than the observed splittings (see Table XV). The most probable explanation of the small positive ΔE_Q values found for all three porphyrins is the occurrence of strong <u>forward</u> ligand→metal π bonding. If the iron atom is in an out-of-plane configuration as suggested above, some degree of σ bonding with the $d_{x^2-y^2}$ orbital will be lost, and this will tend to make ΔE_Q less positive. At the same time however, the three d orbitals, d_{xz}, d_{yz} and d_{z^2}, can participate in π bonding with filled e_g and a_{2u} orbitals on the porphyrin rings. The resulting increase in electron density in these orbitals will give a negative contribution to V_{zz}, leading to a reduction in the magnitude of ΔE_Q. Since we expect the σ bonding in the three porphyrins to be very similar, the extent to which $|\Delta E_Q|$ is reduced

should be a direct measure of the strength of the π bonding in the complex.

On this basis we would conclude that of the three porphyrins studied OTBP is the strongest π donor and OEP the weakest. The order obtained is exactly the same as that suggested on structural grounds above. The isomer shift data are in at least qualitative agreement with these ideas of strong σ bonding and strong (but variable) forward π bonding. The very low δ values for the Fe(TPP) and Fe(OEP) complexes probably reflect a substantial augmentation of 4s electron density of iron arising from the σ donation. The ΔE_Q values suggest that the difference in π bonding strengths of TPP and OEP is not large, and the δ values are also similar. For Fe(OTBP) on the other hand, there is a large decrease in ΔE_Q indicating an increase in the donor strength of the ligand. The extra electron density introduced into the iron d orbitals would increase the shielding of the 4s electrons and raise the isomer shift as observed.

One further point of interest concerning the ΔE_Q values of the ferrous porphyrins is the very small temperature dependence observed. In the usual octahedral high-spin ferrous complexes there will always be at least one low-lying excited state which can be thermally populated at room temperature, and the $|\Delta E_Q|$ value observed is a thermal average of the values for the ground and excited states. Lowering the temperature depletes the excited state (s) and produces the usual temperature-dependent $|\Delta E_Q|$. The lack of temperature dependence found here indicates that there are no thermally accessible excited states in these complexes, and that $|\Delta E_Q|$ measured at any temperature reflects the true value of $|\Delta E_Q|$ for the ground state. We estimate that the b_{2g}-e_g separation in these complexes is greater than 1000 cm^{-1}.

With the introduction of two THF molecules in the axial positions of Fe(OTBP), there is a very large increase in $|\Delta E_Q|$. The

magnitude and temperature dependence of $|\Delta E_Q|$ and the positive V_{zz} found from a magnetic perturbation measurement indicate that the ground state is the |xy> orbital singlet. The principal effect of the axial field introduced by the THF ligands is to raise substantially the energy of the iron d_{z^2} orbital[101,124] and this must be largely responsible for the sharp (positive) increase in $|\Delta E_Q|$ compared to Fe(OTBP) itself. However, the strong temperature dependence of $|\Delta E_Q|$ shows that the $b_{2g} - e_g$ separation has also been narrowed. A satisfactory fit of the E_Q vs T data with a crystal field model as described in Chapter III could not be obtained, probably because of the strong covalency in the porphyrin plane. However, a very rough estimate gives a $b_{2g} - e_g$ splitting of $\sim 400\ cm^{-1}$. The fact that $\eta \simeq 0$ indicates that d_{xz} and d_{yz} remain degenerate (or very nearly so). This degeneracy can be maintained in the hexacoordinate case only if the iron atom lies in the porphyrin plane[124], so that our results appear to favour an in-plane configuration in $Fe(OTBP)(THF)_2$. The significantly greater δ value for this compound is also consistent with the lack of involvement of the d_{z^2} orbital in π bonding with the porphyrin.

Turning now to the diamagnetic hexacoordinate bispyridine adducts, one sees from Table XV that $Fe(OTBP)(py)_2$ has the smallest $|\Delta E_Q|$, $Fe(Pc)(py)_2$ the largest, and that the other three porphyrin complexes have intermediate and nearly identical values. The Mössbauer spectrum of $Fe(OTBP)(py)_2$ at 84°K in a 50 kG applied magnetic field is shown in Figure 29, and V_{zz} is clearly positive. The only possible ground state for an octahedral low-spin ferrous system is $^1A_{1g}$, and in the "pure" crystal field limit this state has zero quadrupole splitting. However, differences in bonding interactions with axial and equatorial ligands can produce a non-zero efg.

FIGURE 29

Mössbauer Spectrum of $Fe(OTBP)(py)_2$ at 84° K in an applied magnetic field of 50 kG. The full curve is the theoretical spectrum calculated for the parameters $\delta = 0.77$, $\Delta E_Q = +0.68$, $\Gamma = 0.29$ (all in mm s^{-1}) and $\eta = 0$.

FIGURE 29

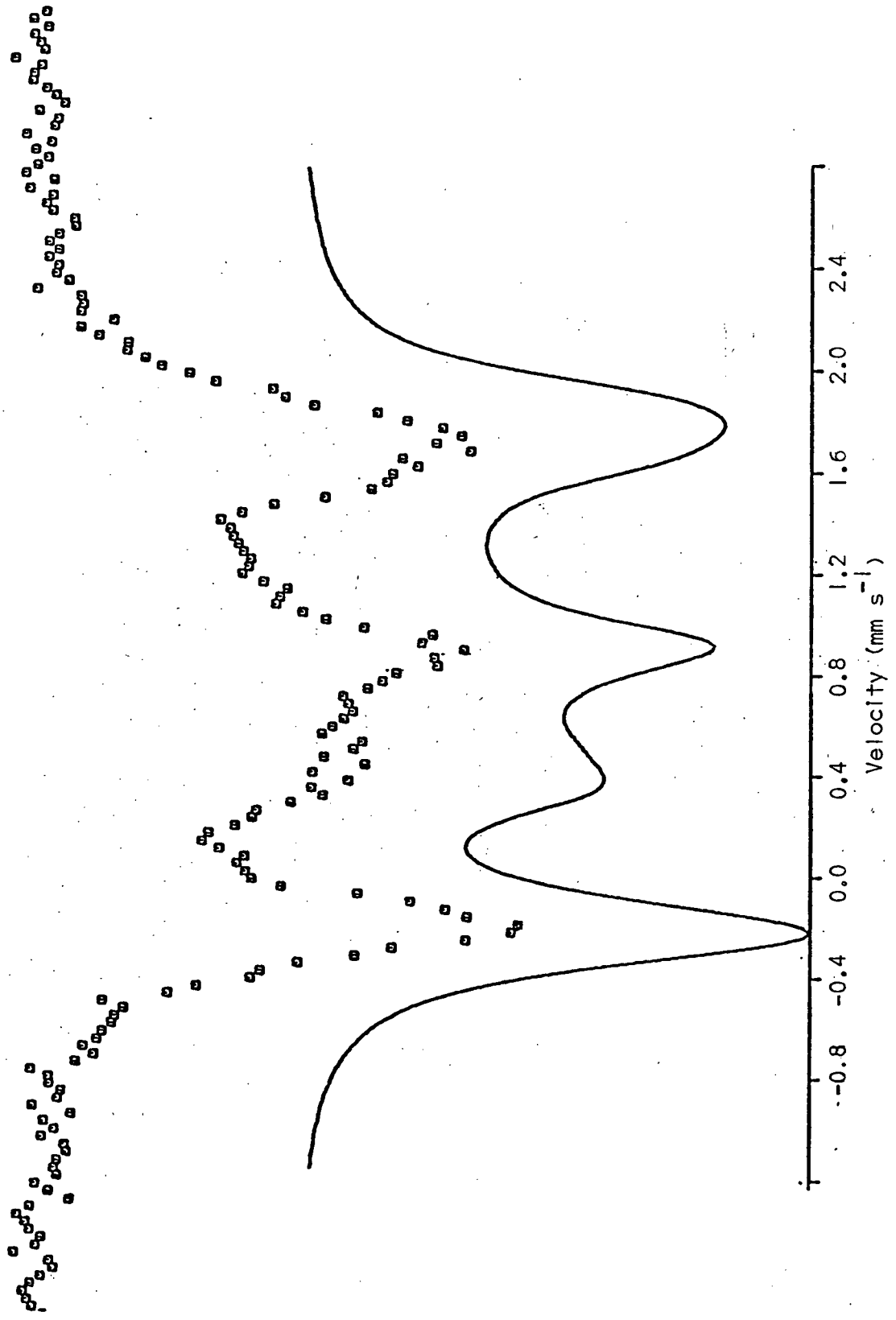

Gouterman and co-workers[124] have also carried out MO calculations for the ferrous porphyrin bisaquo adduct. Using their d orbital populations the predicted value of ΔE_Q is +1.10 mm s^{-1}, remarkably close to the values found for the bispyridine adducts of ferrous TPP, OEP and PP. Their calculations[124] suggest that the major contribution to V_{zz} comes from the imbalance in electron densities in the $d_{x^2-y^2}$ and d_{z^2} orbitals. That is, the covalent bonding to the planar porphyrin is stronger than that to the axial ligands.

The fact that the phthalocyanine derivative shows the largest ΔE_Q presumably reflects very strong σ donation into the iron $3d_{x^2-y^2}$ orbital in this case ($4p_x$ and $4p_y$ may also contribute). Since the porphyrins should be poorer σ donors than Pc there will be smaller imbalances in $d_{x^2-y^2}$ and d_{z^2} charge densities, and smaller ΔE_Q values. The very small splitting for the OTBP complex can be attributed to the great π donor strength of this ligand, which will increase the d_{xz}, d_{yz} populations. For the other three porphyrins the data suggest there are only modest differences in their overall σ and π bonding characteristics.

The isomers shifts for the bispyridine adducts behave quite similarly to those of the tetracoordinate compounds, with the OTBP complex having the highest δ and the Pc one the lowest, and the explanation of this trend is presumably similar to the one given above. As we have already mentioned, these δ values lie at the upper end of the usual range for low-spin ferrous compounds, indicating that the 3d (and possibly 4p) orbital charge densities and the resultant shielding of the s electron density are greater than normally encountered

in such systems.

Since the major contribution to the quadrupole splitting in the bispyridine complexes comes from different electron densities in the $d_{x^2-y^2}$ and d_{z^2} orbitals, it seemed of interest to study the effect of other axial ligands on the Mössbauer parameters for the Fe(OTBP) system. Therefore attempts were made to prepare the 2:1 adducts of this complex with 2-, 3- and 4-picoline and isoquinoline. Only with 3-picoline were we able to isolate the desired 2:1 adduct. As seen from Table XV this complex has a ΔE_Q value similar to that of the bispyridine derivative, suggesting only a slight effect on the efg at iron.

The inability to obtain an adduct with 2-picoline is probably the result of steric hindrance due to the ortho-methyl group. However, with 4-picoline and isoquinoline, instead of the expected 2:1 adducts we obtained 4:1 adducts. A 4:1 adduct with pyridine could also be prepared when the crude Fe(OTBP) was extracted with neat pyridine replacing the pyridine/petroleum ether mixture used to prepare $Fe(OTBP)(py)_2$. There have been no previous reports of such 4:1 adduct formation with any metalloporphyrin or phthalocyanine complex, and attempts to prepare a 4:1 adduct of 4-picoline with Fe(Pc) were unsuccessful.

Interestingly, the 4:1 complexes appear to be at least as stable as the 2:1 adducts with respect to loss of base molecules, either at room temperature or on heating, suggesting that the two "extra" ligands are reasonably strongly bound. The fact that $Fe(OTBP)(py)_4$ shows a larger quadrupole splitting than $Fe(OTBP)(py)_2$ could indicate a weakening of the porphyrin→iron π bonding due to involvement of the

third and fourth pyridine groups with the rich π system of OTBP. The alternative explanation of a weakening of the axial ligand σ donation due to steric interference seems less likely in view of the stability of the 4:1 adducts. Because of the uncertainty concerning the nature of the bonding in the 4:1 complexes it is difficult to know how to interpret the small differences in their Mössbauer parameters.

Magnetic Perturbation Measurements on the High-Spin Ferrous Porphyrins

In view of the unusual effects which can be observed when paramagnetic Fe^{2+} complexes are subjected to applied magnetic fields at low temperatures, we should comment briefly on the behaviour of the high-spin ferrous porphyrins under these conditions.

In zero field, the three compounds Fe(OEP), Fe(OTBP) and $Fe(OTBP)(THF)_2$ all show simple two-line Mössbauer spectra at liquid helium temperature, with no indication of line broadening. Thus, under these conditions, spin relaxation is fast compared to the nuclear precession frequency. The THF adduct was not studied in an applied field at 4.2° K, but at 83° K in a longitudinal magnetic field of 50 kG, the Mössbauer spectrum consisted of a simple triplet-doublet pattern with $H_{eff} \sim H_{ext}$.

For Fe(OTBP) at 4.2° K, an applied field of 50 kG induces a small magnetization, and H_{eff} is estimated to be ∿ 80 kG under these conditions. However, as shown in Figure 30, despite this augmentation of the applied field the spectrum resembles much more closely that of a diamagnetic compound than those of the $FeL_6(ClO_4)_2$ solvates discussed in Chapter III (see Figures 13-15), and the sign of V_{zz} is clearly positive. At 115° K with a 50 kG applied field the spectrum is

FIGURE 30

Mössbauer Spectrum of Fe(OTBP) at 4.2° K in an applied magnetic field of 50 kG. V_{zz} is positive and the effective field at the ^{57}Fe nucleus is estimated to be $\sim$ 80 kG.

FIGURE 30

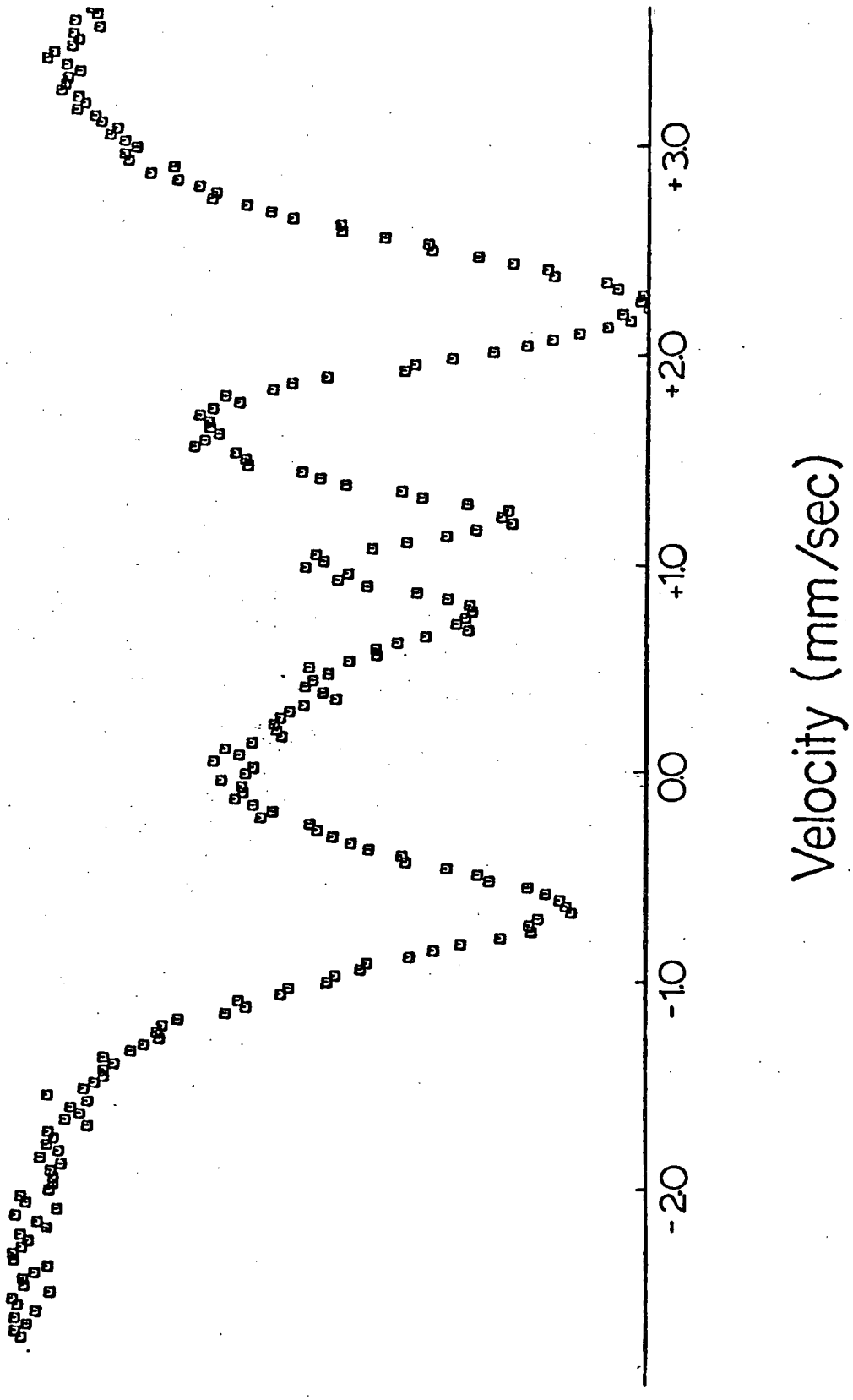

"normal" and there is no apparent internal field. These results imply very fast spin relaxation at all temperatures. This is particularly interesting since one of the few examples of slow-relaxing Fe^{2+} ions is gillespite, in which iron is also in a square planar environment.

Fe(OEP) behaves somewhat differently in applied fields. At 115° K with H_{ext} = 50 kG we estimate $H_{eff} \simeq 67$ kG from the observed Zeeman splitting. At 4.2° K the behaviour of this complex in a magnetic field is much more complicated, the spectral shape depending on the magnitude of the applied field, but being quite different from those shown in Figs. 13-15. The lines are broad and the spectra diffuse and ill-defined (see Figure 31), which will render any theoretical treatment extremely difficult. However, from the large number of spectra calculated in different relaxation limits for $Fe(PyNO)_6(ClO_4)_2$, it seems likely that Fe(OEP) represents an example of intermediate relaxation, in which the spin relaxation rate and the nuclear Larmor frequency have comparable time scales.

Poly[octamethyltetrabenzporphyriniron(II)]

When the crude Fe(OTBP) from the sealed tube reaction is extracted either with 2-picoline, aniline or quinoline and the product dried *in vacuo* at room temperature, a black material invariably results which analyses correctly for Fe(OTBP). This product can also be obtained by leaving either a solution of the THF adduct in THF, or a solution of the pyridine adduct in 1:50 pyridine/petroleum ether to stand overnight in a nitrogen atmosphere. Since oxygen was excluded

FIGURE 31

Mössbauer Spectrum of Fe(OEP) at 4.2° K in an Applied Magnetic Field of 25kG

FIGURE 31

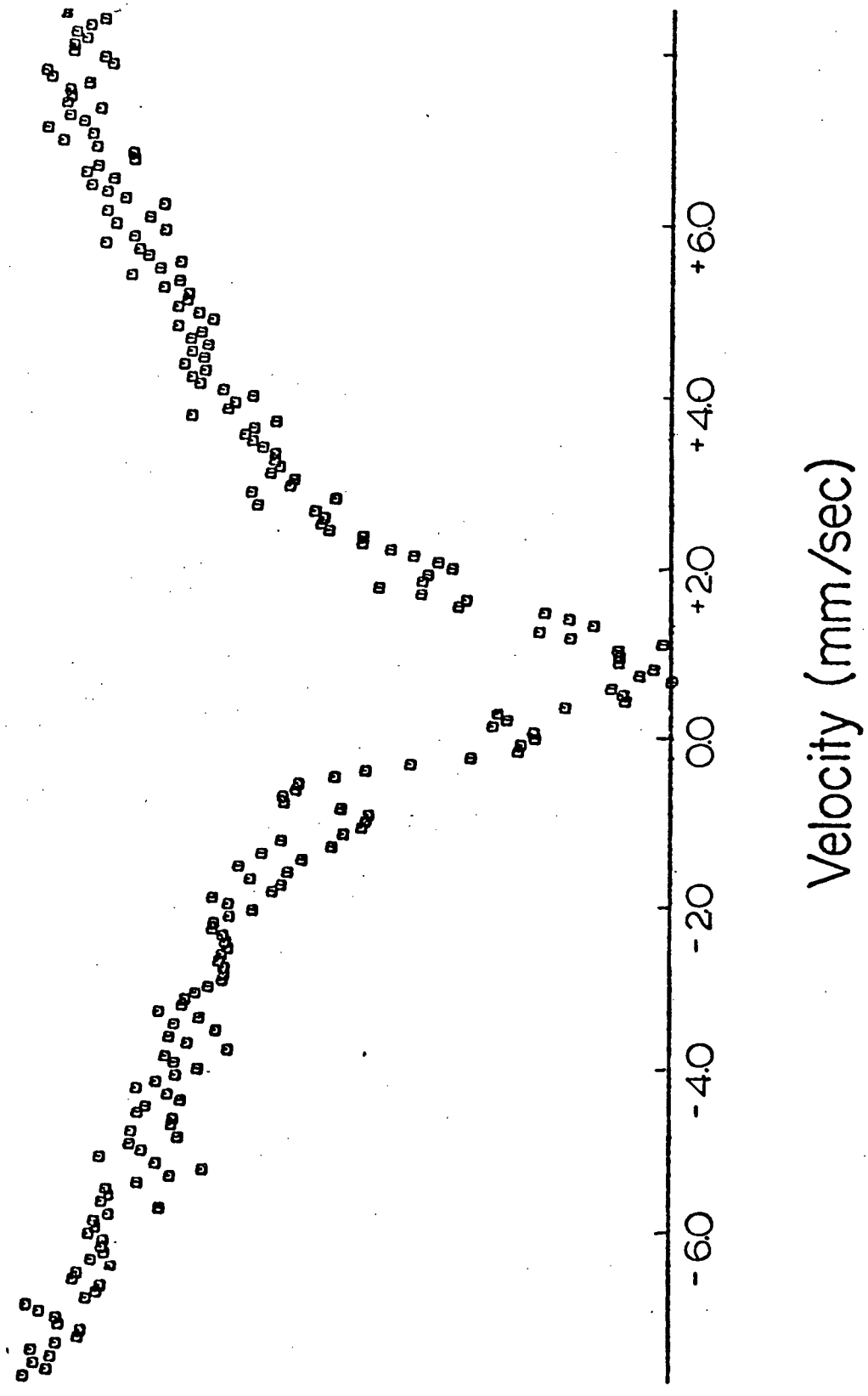

from these systems, it is unlikely that Fe(OTBP) has been converted to an oxo-bridged ferric dimer, as is common with ferrous porphyrins. We shall designate this black compound as $[Fe(OTBP)]_n$ to distinguish it from the blue Fe(OTBP), and because there is considerable evidence pointing to a polymeric form for this compound.

Evidence against $[Fe(OTBP)]_n$ being an oxidation product is quite substantial. Firstly, analytical data for all the black $[Fe(OTBP)]_n$ compounds obtained agree accurately with an Fe(OTBP) formulation. (Data for the compound obtained from 2-picoline solution appear in Table XIV.) The calculated carbon content for μ-O$[Fe(OTBP)]_2$ is 77.1%, and in no case did the microanalyses show less than 78.1% carbon. Secondly, the blue Fe(OTBP) can be left in air for several weeks without showing any conversion to either the black compound or an oxo-bridged dimer. Analytical data, Mössbauer and electronic spectra (the latter in pyridine solution) of Fe(OTBP) are unchanged after three weeks' exposure of the compound to the atmosphere. We feel this evidence is very convincing that the black material is not μ-O$[Fe(OTBP)]_2$.

When $[Fe(OTBP)]_n$ is dissolved in pyridine it first forms a dark olive green solution. The electronic spectrum of this solution contains a Soret band at 417 nm ($\varepsilon_{max} = 1 \times 10^5$) and two other bands at 485 nm ($\varepsilon_{max} = 1 \times 10^4$) and 660 nm ($\varepsilon_{max} = 5 \times 10^4$). This spectrum is very different from that of $Fe(OTBP)(py)_2$ shown in Figure 26 above. However, after two hours the solution has become deep apple green in colour. In addition to the 417, 485 and 660 nm bands, the electronic spectrum now contains bands due to $Fe(OTBP)(py)_2$ which strengthen with time at the expense of the original spectrum. Complete conversion to

the $Fe(OTBP)(py)_2$ spectrum requires one or two days, depending on the particular sample, but after this time evaporation of the solution to dryness at room temperature affords pure $Fe(OTBP)(py)_2$. This behaviour is suggestive of a polymeric structure which is gradually broken down in solution.

Further indication of the polymeric nature of $[Fe(OTBP)]_n$ is provided by magnetic susceptibility measurements at room temperature. The susceptibility varies from sample to sample and is field dependent, suggesting the presence of exchange interactions typical of molecular aggregates[127]. The effective magnetic moments range from 6 to 14 B.M., values which are abnormally high for monomeric systems.

Althoughthe blue Fe(OTBP) is quite stable and shows no conversion to the black compound under normal conditions, samples of Fe(OTBP) subjected to pressures of 10-13 kbar on an hydraulic press do show partial conversion to $[Fe(OTBP)]_n$. The Mössbauer parameters of Fe(OTBP) and $[Fe(OTBP)]_n$ are quite different (see below), and spectra of the pressed products showed lines corresponding to both species. However, complete conversion could not be affected at these pressures, even when the sample was left under pressure for several days.

In view of the unusual magnetic moments observed, it was decided to study the solid state electrical conductivities of these compounds. Pellets made on the hydraulic press were coated with silver paint and connected to a vacuum-tube voltmeter. The dimensions of the pellets were determined with a micrometer gauge. The sensitivity of the voltmeter was such that conductivities of about 10^{-10} Ω^{-1} cm^{-1} or greater could be detected. Several samples of $[Fe(OTBP)]_n$ obtained

TABLE XVI

^{57}Fe Mössbauer Parameters for Fe(OTBP) and $[Fe(OTBP)]_n$

Compound	T(°K)	δ(mm s^{-1})	ΔE_Q(mm s^{-1})	Γ_1 (mm s^{-1})	Γ_2 (mm s^{-1})	η
Fe(OTBP)	295	0.94	0.56	.30	.23	
	115	1.04	+0.61	.27	.28	≈ 0
	83	1.05	0.62	.27	.28	
	8.6	1.06	+0.63	.27	.28	≈ 0
$[Fe(OTBP)]_n$	295	0.58	0.48	.26	.24	
	84	0.68	-0.49	.30	.31	≈ 0
	8.25	0.69	0.50	.29	.32	

from different solvents were studied at room temperature, and all showed conductivities of $\sim 10^{-6}\ \Omega^{-1}\ cm^{-1}$. This value is quite typical of those found for polymeric organic semiconductors[127], and can be taken as an indication that bonds are formed between neighbouring molecules which are considerably stronger than the crystal packing forces that exist in normal covalent crystals. A sample of the partially converted blue Fe(OTBP) gave a conductivity of $\sim 10^{-8}\ \Omega^{-1}\ cm^{-1}$, whereas no conductivity could be detected with pellets of $Fe(OTBP)(py)_2$ and μ-O[Fe(OEP)]$_2$. (The last compound was kindly provided by Dr. D. Dolphin.) These results provide additional evidence that $[Fe(OTBP)]_n$ is not an oxo-bridged ferric dimer.

The Mössbauer parameters for samples of $[Fe(OTBP)]_n$ are independent of the solvent from which the material was isolated. These parameters are compared with those of the blue Fe(OTBP) in Table XVI. The isomer shift of $[Fe(OTBP)]_n$ is considerably lower than that of Fe(OTBP), indicating a greater effective s electron density at the iron nucleus in the polymer. Although the magnitudes of ΔE_Q are quite similar in the two compounds, V_{zz} is found to be negative for $[Fe(OTBP)]_n$ rather than positive. For every other ferrous porphyrin and phthalocyanine derivative studied to date, $V_{zz}>0$. This sign reversal indicates that there is now an excess of electron density at iron in the axial direction over that in the porphyrin plane. In view of the evidence in favour of a polymeric structure, a likely explanation of the negative V_{zz} is the involvement of the d_{z^2} orbital in the formation of an iron-iron σ bond.

Summary

The data we have obtained for the ferrous OTBP and OEP complexes, together with previous results on other ferrous porphyrins and ferrous phthalocyanine, show that the electronic structure of iron is very sensitive to changes in σ and π bonding properties of the planar ring systems. This is particularly true in the high-spin tetracoordinate species, and indicates that it is advantageous to study the neat ferrous porphyrins without axial ligands. Furthermore, although theoretical analysis of the applied field Mössbauer spectra obtained at 4.2° K for Fe(OTBP) and Fe(OEP) has not yet been attempted (and it is expected that such an analysis will be very difficult), there is potentially a great deal more information to be obtained on these complexes. The development of a satisfactory theoretical framework to explain these results is an obvious extension of the present study. Because of the very small temperature dependence of $|\Delta E_Q|$ for these derivatives, it may be possible to base such a theory on the spin Hamiltonian formalism, but some account will have to be taken of the strong covalency effects which are present.

It would also be very interesting to study additional ferrous porphyrins in which there are less drastic changes in the porphyrin structure than the ones examined here. Again, this will not be easy. Although Fe(OTBP) has remarkable stability, Fe(OEP) is an extremely sensitive compound and required very careful handling in obtaining physical measurements. Several attempts have been made to isolate Fe(PP) in the solid state without success, and other ferrous porphyrins closely related to haeme are likely to be equally difficult to obtain.

The introduction of ligands in the axial coordination sites almost invariably leads to a $^1A_{1g}$ ground state for iron, and tends to mask the differences between the various complexes studied. However, the positive V_{zz} observed in all cases is in agreement with the intuitive concept that bonding to the porphyrin nitrogens is stronger than that to the axial ligands, and the differences in Mössbauer parameters which do remain are consistent with the bonding properties deduced from the square planar complexes.

The properties of $[Fe(OTBP)]_n$ are unusual and interesting, particularly its semiconducting behaviour and the negative V_{zz} found. We have suggested that the polymeric nature of this material may be due to Fe-Fe bonding between adjacent planar molecules, but the mechanism of formation remains unclear.

Although the work reported in this chapter is only the first phase in the development of a more general study of ferrous porphyrins, it shows the great potential of the Mössbauer effect in such systems and suggests that further efforts along these lines are likely to be fruitful.

BIBLIOGRAPHY

1. N.N. Greenwood and T.C. Gibb, "Mössbauer Spectroscopy", Chapman and Hall Ltd., London, 1971, Chaps. 6, 7.
2. Ref. 1, Chap. 5.
3. R.L. Collins and J.C. Travis in "Mössbauer Effect Methodology", Vol. 3, I.J. Gruverman, Ed., Plenum Press, New York, 1967, p.123.
4. J. Reedijk and A.M. van der Kraan, Rec. Trav. Chim., 88, 828 (1969).
5. M.H. Cohen and F. Reif, Solid State Phys., 5, 321 (1967).
6. V.I. Gol'danskii and E.F. Makarov in "Chemical Applications of Mössbauer Spectroscopy", V.I. Gol'danskii and R.H. Herber, Eds., Academic Press, New York, 1968, Chap. 1.
7. H. Watanabe, "Operator Methods in Ligand Field Theory", Prentice-Hall, Englewood Cliffs, N.J., 1966, Chap. 2.
8. G.M. Bancroft, Chem. Phys. Letters, 10, 449 (1971), and references.
9. Ref. 1, Chap. 3.
10. M.E. Rose, "Elementary Theory of Angular Momentum", Wiley, New York, 1957.
11. C.E. Johnson, Proc. Phys. Soc., 92, 748 (1967).
12. H.H. Wickman and G.K. Wertheim in "Chemical Applications of Mössbauer Spectroscopy", V.I. Gol'danskii and R.H. Herber, Eds., Academic Press, New York, 1968, Chap. 11.
13. H.H. Wickman in "Mössbauer Effect Methodology", Vol. 2, I.J. Gruverman, Ed., Plenum Press, New York, 1966, p.39.

14. M. Blume, Phys. Rev. Letters, 14, 96 (1965).

15. R. Zimmermann, H. Spiering and G. Ritter, Chem. Phys.,4, 133 (1974).

16. J. Lewis and R.G. Wilkins, "Modern Coordination Chemistry. Principles and Methods", Interscience Publishers Inc., New York, 1960, Chap. 6.

17. G. Lang, J. Chem. Soc. (A), 3245 (1971).

18. R. Ingalls, Phys. Rev., 133, A787 (1964).

19. I. Dézsi and L. Keszthelyi, Solid State Commun., 4, 511 (1966).

20. J.M.D. Coey, I. Dézsi, P.M. Thomas and P.J. Ouseph, Phys. Letters, 41A, 125 (1972).

21. J. Reedijk and A.M. van der Kraan, Rec. Trav. Chim., 88, 828 (1969).

22. J. Reedijk, personal communication to J.R. Sams.

23. J. Selbin, W.E. Bull and L.H. Holmes, J. Inorg. Nucl. Chem., 16, 219 (1961).

24. W.F. Currier and J.H. Weber, Inorg. Chem. 6, 1539 (1967).

25. J. Reedijk, P.W.N.M. van Leeuwen and W.L. Groeneveld, Rec. Trav. Chim., 87, 1073 (1968).

26. C.P. Prabhakaran and C.C. Patel, J. Inorg. Nucl. Chem., 32, 1223 (1970).

27. P.A. Yeats, J.R. Sams and F. Aubke, Inorg. Chem., 9, 740 (1970), and references therein.

28. R.S. Randall, B.V. Liengme and J.R. Sams, Can. J. Chem., 50, 3212 (1972).

29. G.K. Wertheim, "Mössbauer Effect: Principles and Applications", Academic Press, New York, 1964, Chap. 3.

30. C.J. Ballhausen, "Introduction to Ligand Field Theory", McGraw-Hill, New York, 1962, Chap. 4.

31. J.N.R. Ruddick and J.R. Sams, J. Chem. Soc. Dalton Trans., 470 (1974).

32. J.R. Sams and J.C. Scott, J. Chem. Soc. Dalton Trans., 2265 (1974).

33. E.A. Blom, B.R. Penfold and W.T. Robinson, J. Chem. Soc. (A), 939 (1969).

34. N.W. Isaacs and C.H.L. Kennard, J. Chem. Soc. (A), 1257 (1970).

35. M.J. Bennett, F.A. Cotton and D.L. Weaver, Acta Cryst., 23, 581 (1967).

36. T.C. Gibb, J. Chem. Soc. (A), 1439 (1968).

37. R.M. Golding, "Applied Wave Mechanics", Van Nostrand, Princeton, 1969, Chap. 9.

38. B.N. Figgis, J. Lewis, F.E. Mabbs and G.A. Webb, J. Chem. Soc. (A), 442 (1967).

39. B.N. Figgis, "Introduction to Ligand Fields", Interscience, New York, 1966, Chap. 10.

40. Ref. 30, Chap. 1.

41. R. Ingalls, K. Ono and L. Chandler, Phys. Rev., 172, 295 (1968).

42. U. Gonser and R.W. Grant, Phys. Stat. Sol., 21, 381 (1967).

43. R.H. Herber and S. Chandra, J. Chem. Phys., 52, 6045 (1970).

44. V.I. Gol'danskii, E.F. Makarov and V.V. Khrapov, Phys. Letters, 3, 344 (1963).

45. P.A. Flinn, S.L. Ruby and W.L. Kehl, Science, 143, 1434 (1964).

46. A.N. Buckley, G.V.H. Wilson and K.S. Murray, Solid State Commun., 7, 471 (1970).

47. A.N. Buckley, B.D. Rumbold, G.V.H. Wilson and K.S. Murray, J. Chem. Soc. (A), 2298 (1970).

48. A.N. Buckley, I.R. Herbert, B.D. Rumbold, G.V.H. Wilson and K.S. Murray, J. Phys. Chem. Solids, 31, 1423 (1970).

49. B.W. Fitzsimmons and C.E. Johnson, Chem. Phys. Letters, 6, 267 (1970).

50. M. Blume, Phys. Rev. Letters, 18, 305 (1967).

51. M. Cox, B.W. Fitzsimmons, A.W. Smith, L.F. Larkworthy and K.A. Rogers, Chem. Commun., 183 (1969).

52. M.G. Clark, G.M. Bancroft and A.J. Stone, J. Chem. Phys., 47, 4250 (1967).

53. M.G. Clark, J. Chem. Phys. 48, 3246 (1968).

54. J.S. Griffith, Phys. Rev., 132, 316 (1963).

55. J.S. Griffith, "The Theory of Transition Metal Ions", Cambridge University Press, Cambridge, 1964, pp. 355-360.

56. M.G. Clark, personal communication to J.R. Sams.

57. Ref. 55, p.330.

58. Ref. 39, p.164.

59. E.K. Barefield, D.H. Busch and S.M. Nelson, Quart. Rev., 22, 457 (1968).

60. E. König and K. Madeja, Chem. Commun., 61 (1966).

61. E. König and K. Madeja, Inorg. Chem., 6, 48 (1967).

62. I. Dézsi, B. Molnar, T. Tarnoczi and K. Tompa, J. Inorg. Nucl. Chem., 29, 2486 (1967).

63. D.C. Fisher and H.G. Drickamer, J. Chem. Phys., 54, 4825 (1971).

64. E. König, K. Madeja and K.J. Watson, J. Amer. Chem. Soc., 90, 1146 (1968).

65. E. König and K.J. Watson, Chem. Phys. Letters, 6, 457 (1970).

66. J.P. Jesson, S. Trofimenko and D.R. Eaton, J. Amer. Chem. Soc., 89, 3158 (1967).

67. J.P. Jesson, J.F. Weiher and S. Trofimenko, J. Chem. Phys., 48, 2058 (1968).

68. E. König, G. Ritter, H. Spiering, S. Kremer, K. Madeja and R. Rosenkranz, J. Chem. Phys., 56, 3139 (1972).

69. E. König, G. Ritter, B. Braunecker, K. Madeja, H.A. Goodwin and F.E. Smith, Ber., Phys. Chem., 76, 393 (1972).

70. E. König and S. Kremer, Theor. Chim. Acta., 20, 143 (1971).

71. D.M.L. Goodgame and A.A.S.C. Machado, Chem. Commun., 1420 (1969).

72. D.M.L. Goodgame and A.A.S.C. Machado, Inorg. Chem., 8, 2031 (1969).

73. R.J. Dosser, W.J. Eilbeck, A.E. Underhill, P.R. Edwards and C.E. Johnson, J. Chem. Soc. (A), 810 (1969).

74. T.R. Harkins and H. Freiser, J. Amer. Chem. Soc., 78, 1143 (1956).

75. B. Chiswell, F. Lions and B.S. Morris, Inorg. Chem., 3, 110 (1964).

76. W.J. Geary, Coord. Chem. Rev., 7, 81 (1971).

77. M.A. Robinson and D.H. Busch, Inorg. Chem., 2, 1171 (1963).

78. T.J. Lane, I. Nakagawa, J.L. Walter and A.J. Kandathil, Inorg. Chem., 1, 267 (1962).

79. J.H.S. Green, W. Kynaston and H.M. Paisley, Spectrochim. Acta., 19, 549 (1963).

80. K. Nakamoto, "Infrared Spectra of Inorganic and Coordination Compounds", Wiley, New York, 1963.

81. B.J. Hathaway and A.E. Underhill, J. Chem. Soc., 3091 (1961).

82. E. König and K. Madeja, Spectrochim. Acta., 23A, 45 (1967).

83. N.N. Greenwood, J. Chem. Soc., 3811 (1959).

84. M.A. Bennett, R.J.H. Clark and A.D.J. Goodwin, Inorg. Chem., 6, 1625 (1967).

85. G. Costa, A. Camus, N. Marich and L. Gatti, J. Organometal. Chem., 8, 339 (1967).

86. K.B. Harvey and G.B. Porter, "Introduction to Physical Inorganic Chemistry", Addison-Wesley, Reading, Mass., 1963, pp.22, 135.

87. Y. Sasaki and T. Shigematsu, Bull. Chem. Soc. Japan, 46, 3438 (1973).

88. Ref. 39, Chap. 9.

89. D.H. Busch and J.C. Bailar, J. Amer. Chem. Soc., 78, 1137 (1956).

90. E. König and S. Kremer, Theor. Chim. Acta., 22, 45 (1971).

91. L. Pauling, "The Nature of the Chemical Bond", 2nd. ed., Cornell University Press, Ithaca, N.Y., 1948, p.333.

92. J.R. Sams, Prog. Surf. Membrane Sci., 8, 1 (1974), and references therein.

93. G.M. Bancroft, M.J. Mays and B.E. Prater, Discuss.Faraday Soc., 47, 136 (1969).

94. G.M. Bancroft, M.J. Mays and B.E. Prater, J. Chem. Soc. (A), 956 (1970).

95. B.W. Fitzsimmons, R.J. Seeley and A.W. Smith, J. Chem. Soc. (A), 143 (1969).

96. G.M. Bancroft and R.H. Platt, Advan. Inorg. Chem. Radiochem., 15, 59 (1972).

97. J.R. Sams, MTP Int. Rev. Sci.: Phys. Chem., Ser. One, 4, 85 (1972).

98. G. Lang, Quart. Rev. Biophys., 3, 1 (1970).

99. L.M. Epstein, D.K. Straub and C. Maricondi, Inorg. Chem., 6, 1720 (1969).

100. H. Kobayashi, Y. Maeda and Y. Yanagawa, Bull.Chem. Soc. Japan, 43, 2342 (1970).

101. H. Kobayashi and Y. Yanagawa, Bull. Chem. Soc. Japan, 45, 450 (1972).

102. J.P. Collman and C.A. Reed, J. Amer. Chem. Soc., 95, 2048 (1973).

103. M.A. Torrens, D.K. Straub and L.M. Epstein, J. Amer. Chem. Soc., 94, 4160 (1972).

104. B.W. Dale, R.J.P. Williams, P.R. Edwards and C.E. Johnson, Trans. Faraday Soc., 64, 3011 (1968).

105. B.W. Dale, R.J.P. Williams, C.E. Johnson and T.L. Thorp, J. Chem. Phys., 49, 3441 (1968).

106. B.W. Dale, R.J.P. Williams, P.R. Edwards and C.E. Johnson, J. Chem. Phys., 49, 3445 (1968).

107. I. Dézsi, A. Balazs, B. Molnar, V.D. Gorobchenko and I.I. Lukashevich, J. Inorg. Nucl. Chem., 31, 1661 (1969).

108. B.W. Dale, R.J.P. Williams, P.R. Edwards and C.E. Johnson, Trans. Faraday Soc., 64, 620 (1968).

109. C.G. Barraclough, R.L. Martin, S. Mitra and R.C. Sherwood, J. Chem. Phys., 53, 1643 (1970).

110. C.O. Bender, R. Bonnett and R.G. Smith, Chem. Commun., 345 (1969).

111. C.O. Bender, R. Bonnett and R.G. Smith, J. Chem. Soc. (C), 1251 (1970).

112. H. Fletcher, Tetrahed., 22 2481 (1966).

113. M.J. Dimsdale, Ph.D. thesis, University of London (1968).

114. D. Dolphin, personal communication.

115. P.A. Barrett, R.P. Linstead, F.G. Rundall and G.A.P. Tuey, J. Chem. Soc., 1079 (1940).

116. S.M. Husain and J.G. Jones, Inorg. Nucl. Chem. Letters, 10, 105 (1974).

117. J.M. Robertson and I. Woodward, J. Chem. Soc., 219 (1937).

118. J.M. Robertson, J. Chem. Soc., 1195 (1936).

119. M.B. Crute, Acta. Cryst., 12, 24 (1959).

120. E.B. Fleischer, J. Amer. Chem. Soc., 85, 146 (1963).

121. B.M.L. Chen and A. Tulinsky, J. Amer. Chem. Soc., 94, 4144 (1972).

122. L.J. Radonovich, A. Bloom and J.L. Hoard, J. Amer. Chem. Soc., 94, 2073 (1972).

123. H.C. Longuet-Higgins, C.W. Rector and J.R. Platt, J. Chem. Phys., 18, 1174 (1950).

124. M. Zerner, M. Gouterman and H. Kobayashi, Theor. Chim. Acta., 6, 363 (1966).

125. A.M. Schaffer, M. Gouterman and E.R. Davidson, Theor. Chim. Acta., 30, 9 (1973).

126. A.B.P. Lever, J. Chem. Soc., 1821 (1965).

127. Ya. M. Paushkin, T.P. Vishnyaicova, A.J. Lunin and S.A. Nizova, "Organic Polymeric Semiconductors", Wiley Inc., New York, 1974, Chap. 4.

APPENDIX I

In order to compute the theoretical Mössbauer spectrum, transition probabilities have to be calculated. The procedure used is outlined here.

The unpolarized γ radiation contains equal numbers of right-handed and left-handed circularly polarized quanta. These can be represented by S=1 angular momentum functions $|1,1\rangle'$ and $|1,-1\rangle'$, respectively, along the axis of propagation. The $|1,0\rangle$ state is not used due to the absence of longitudinally polarized γ-rays. Since it is convenient to calculate the γ absorption process along the principal axis of the efg which lies at an angle (θ,ϕ) with respect to the γ propagation axis, it is necessary to transform into the efg axis representation via the equations[3]

$$|1,\pm1\rangle' = \pm\frac{1}{2}(1\pm\cos\theta)e^{i\phi}|1,1\rangle \mp \frac{1}{2}(1\mp\cos\theta)e^{-i\phi}|1,-1\rangle$$

$$- \frac{1}{2}\sqrt{2}\sin\theta|1,0\rangle \qquad \text{(A-1)}$$

In order to simplify further equations, the coefficients will be denoted by

$$A_{\pm}(1) = \pm\frac{1}{2}(1\pm\cos\theta)e^{i\phi}$$

$$A_{\pm}(0) = -\frac{\sqrt{2}}{2}\sin\theta$$

$$A_{\pm}(-1) = \mp\frac{1}{2}(1\mp\cos\theta)e^{-i\phi} \qquad \text{(A-2)}$$

The intensities will be related to overlap integrals of the type

$$\langle \tfrac{1}{2},m|\langle 1,M|\tfrac{3}{2},m'\rangle \tag{A-3}$$

where $|\frac{1}{2},m\rangle$ are the nuclear ground state basis kets, $|1,M\rangle$ the photon basis kets, and $|\frac{3}{2}m'\rangle$ the nuclear excited state basis ket vectors. The integrals (A-3) are in fact the Clebsh-Gordan Coefficients connecting the $I = \frac{3}{2}$ and $I = \frac{1}{2}$ nuclear states and are tabulated[10].

The intensity of the spectrum for the unpolarized beam will be given by the equation[3].

$$I(\theta,\phi) = T_+^2 + T_-^2 \tag{A-4}$$

where T_+^2 is the intensity contributed by the right-handed circularly polarized light and T_-^2 the contribution from the left-handed component.

$$T_+ = \begin{bmatrix} b_1^* & b_2^* \end{bmatrix} \begin{bmatrix} C_+(\frac{1}{2},\frac{3}{2}) & C_+(\frac{1}{2},\frac{1}{2}) & C_+(\frac{1}{2},-\frac{1}{2}) & 0 \\ 0 & C_+(-\frac{1}{2},\frac{1}{2}) & C_+(-\frac{1}{2},-\frac{1}{2}) & C_+(-\frac{1}{2},-\frac{3}{2}) \end{bmatrix} \begin{bmatrix} a_1 \\ a_2 \\ a_3 \\ a_4 \end{bmatrix} \tag{A-5}$$

$$T_- = \begin{bmatrix} b_1^* & b_2^* \end{bmatrix} \begin{bmatrix} C_-(\frac{1}{2},\frac{3}{2}) & C_-(\frac{1}{2},\frac{1}{2}) & C_-(\frac{1}{2},-\frac{1}{2}) & 0 \\ 0 & C_-(-\frac{1}{2},\frac{1}{2}) & C_-(-\frac{1}{2},-\frac{1}{2}) & C_-(-\frac{1}{2},-\frac{3}{2}) \end{bmatrix} \begin{bmatrix} a_1 \\ a_2 \\ a_3 \\ a_4 \end{bmatrix} \tag{A-6}$$

Where

$$C_{\pm}(m_1,m_2) = \langle \tfrac{1}{2}, 1, m_1, (m_2-m_1) \mid \tfrac{3}{2}, m_2 \rangle \; A_{\pm}(m_2-m_1)$$

$\langle \frac{1}{2}, 1, m_1, (m_2-m_1) \mid \frac{3}{2}, m_2 \rangle$ are Clebsch-Gordan coefficients,

$\begin{bmatrix} b_1 \\ b_2 \end{bmatrix}$ are eigenfunctions for the $I = \frac{1}{2}$ ground state,

$\begin{bmatrix} a_1 \\ a_2 \\ a_3 \\ a_4 \end{bmatrix}$ are eigenfunctions for the $I = \frac{3}{2}$ excited state.

The above result is for specific θ and ϕ angles. The powder averaged spectrum should then be an integrated spectrum over all values of θ and ϕ. Due to the fact that the efg has mirror symmetry about its principal planes, only values of θ and ϕ lying in one octant need be integrated[17]. The computer simulates the integration process by a sum of elements $d(\cos\theta)d\phi$ over the first octant where ten increments of θ and ϕ are normally computed.

APPENDIX II

Hamiltonian Matrix of Tetragonal Distortion

$$|A\rangle = \frac{1}{\sqrt{2}}(|2,2\rangle - |2,-2\rangle) \quad |B\rangle = |2,1\rangle \quad |C\rangle = |2,-1\rangle$$

	$\|A\rangle\|2\rangle$	$\|A\rangle\|1\rangle$	$\|A\rangle\|0\rangle$	$\|A\rangle\|-1\rangle$	$\|A\rangle\|-2\rangle$	$\|B\rangle\|2\rangle$	$\|B\rangle\|1\rangle$	$\|B\rangle\|0\rangle$	$\|B\rangle\|-1\rangle$	$\|B\rangle\|-2\rangle$	$\|C\rangle\|2\rangle$	$\|C\rangle\|1\rangle$	$\|C\rangle\|0\rangle$	$\|C\rangle\|-1\rangle$	$\|C\rangle\|-2\rangle$
$\langle 2\|\langle A\|$	$2D_s-2D_\sigma$											$+\sqrt{2}\lambda$			
$\langle 1\|\langle A\|$		$2D_s+D_\sigma$				$-\sqrt{2}\lambda$							$+\sqrt{3}\lambda$		
$\langle 0\|\langle A\|$			$2D_s+2D_\sigma$				$-\sqrt{3}\lambda$							$+\sqrt{3}\lambda$	
$\langle -1\|\langle A\|$				$2D_s+D_\sigma$				$-\sqrt{3}\lambda$							$+\sqrt{2}\lambda$
$\langle -2\|\langle A\|$					$2D_s-2D_\sigma$				$-\sqrt{2}\lambda$						
$\langle 2\|\langle B\|$		$-\sqrt{2}\lambda$				$-D_s-2\lambda-2D_\sigma$					$6D_r$				
$\langle 1\|\langle B\|$			$-\sqrt{3}\lambda$				$-D_s-\lambda+D_\sigma$					$6D_r$			
$\langle 0\|\langle B\|$				$-\sqrt{3}\lambda$				$-D_s+2D_\sigma$					$6D_r$		
$\langle -1\|\langle B\|$					$-\sqrt{2}\lambda$				$-D_s+\lambda+D_\sigma$						
$\langle -2\|\langle B\|$										$-D_s+2\lambda-2D_\sigma$				$6D_r$	
$\langle 2\|\langle C\|$						$6D_r$					$-D_s+2\lambda-D_\sigma$				$6D_r$
$\langle 1\|\langle C\|$	$+\sqrt{2}\lambda$						$6D_r$					$-D_s+\lambda+D_\sigma$			
$\langle 0\|\langle C\|$		$+\sqrt{3}\lambda$						$6D_r$					$-D_s+2D_\sigma$		
$\langle -1\|\langle C\|$			$+\sqrt{3}\lambda$						$6D_r$					$-D_s-\lambda+D_\sigma$	
$\langle -2\|\langle C\|$				$+\sqrt{2}\lambda$						$6D_r$					$-D_s-2\lambda-2D_\sigma$

Hamiltonian Matrix of Trigonal Distortion

$$|A\rangle = |2,0\rangle \quad |B\rangle = \sqrt{\tfrac{2}{3}}\,|2,-2\rangle + \sqrt{\tfrac{1}{3}}\,|2,1\rangle \quad |C\rangle = \sqrt{\tfrac{2}{3}}\,|2,2\rangle - \sqrt{\tfrac{1}{3}}\,|2,-1\rangle$$

	$\|A\rangle\|2\rangle$	$\|A\rangle\|1\rangle$	$\|A\rangle\|0\rangle$	$\|A\rangle\|-1\rangle$	$\|A\rangle\|-2\rangle$	$\|B\rangle\|2\rangle$	$\|B\rangle\|1\rangle$	$\|B\rangle\|0\rangle$	$\|B\rangle\|-1\rangle$	$\|B\rangle\|-2\rangle$	$\|C\rangle\|2\rangle$	$\|C\rangle\|1\rangle$	$\|C\rangle\|0\rangle$	$\|C\rangle\|-1\rangle$	$\|C\rangle\|-2\rangle$
$\langle 2\|\langle A\|$	$-2D_s-2D\sigma$					4Dr	$-\sqrt{2}\,\lambda$				4Dr				
$\langle 1\|\langle A\|$		$-2Ds+D\sigma$					4Dr	$-\sqrt{3}\,\lambda$			$\sqrt{2}\,\lambda$	4Dr			
$\langle 0\|\langle A\|$			$-2Ds+2D\sigma$					4Dr	$-\sqrt{3}\,\lambda$			$\sqrt{3}\,\lambda$	4Dr		
$\langle -1\|\langle A\|$				$-2Ds+D\sigma$					4Dr	$-\sqrt{2}\,\lambda$			$\sqrt{3}\,\lambda$	4 Dr	
$\langle -2\|\langle A\|$					$-2Ds-2D\sigma$					4Dr				$\sqrt{2}\,\lambda$	4Dr
$\langle 2\|\langle B\|$	4Dr					$Ds+2\lambda-2D\sigma$					$-2Dr$				
$\langle 1\|\langle B\|$	$-\sqrt{2}\,\lambda$	4Dr					$Ds+\lambda+D\sigma$					$-2Dr$			
$\langle 0\|\langle B\|$		$-\sqrt{3}\,\lambda$	4Dr					$Ds+2D\sigma$					$-2Dr$		
$\langle -1\|\langle B\|$			$-\sqrt{3}\,\lambda$	4Dr					$Ds-\lambda+D\sigma$					$-2Dr$	
$\langle -2\|\langle B\|$				$-\sqrt{2}\,\lambda$	4Dr					$Ds-2\lambda-2D\sigma$					$-2Dr$
$\langle 2\|\langle C\|$	4Dr	$\sqrt{2}\,\lambda$				$-2Dr$					$Ds-2\lambda-2D\sigma$				
$\langle 1\|\langle C\|$		4Dr	$\sqrt{3}\,\lambda$				$-2Dr$					$Ds-\lambda+D\sigma$			
$\langle 0\|\langle C\|$			4Dr	$\sqrt{3}\,\lambda$				$-2Dr$					$Ds+2D\sigma$		
$\langle -1\|\langle C\|$				4Dr	$\sqrt{2}\,\lambda$				$-2Dr$					$Ds+\lambda+D\sigma$	
$\langle -2\|\langle C\|$					4Dr					$-2Dr$					$Ds+2\lambda-2D\sigma$